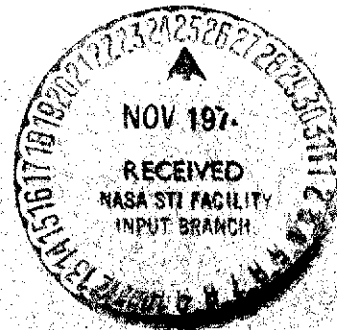


(NASA-CR-140806) PLANETARY QUARANTINE:
SPACE RESEARCH AND TECHNOLOGY Semiannual
Review, 1 Jan. - 30 Jun. 1974 (Jet
Propulsion Lab.) 126 p HC \$5.75

N75-10707

Unclas

CSCCL 06M G3/54 02251



JET PROPULSION LABORATORY
 CALIFORNIA INSTITUTE OF TECHNOLOGY
 PASADENA, CALIFORNIA

900-675

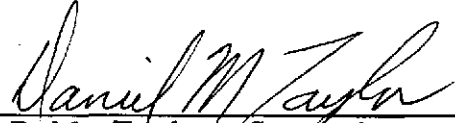
PLANETARY QUARANTINE

Semi-Annual Review
Space Research and Technology

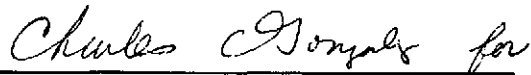
1 January - 30 June 1974

September 30, 1974

APPROVED, Sections
I, II, III, and IV



D.M. Taylor, Supervisor
Life Sciences Research



A.R. Hoffman, Supervisor
Planetary Quarantine Analysis



D.S. Hess, Manager
Environmental Requirements
Section

APPROVED, Section V



J.R. Puleo, Supervisor
Planetary Quarantine Laboratory



D. Alcorn, Manager
Systems Test and Launch
Operations Section

JET PROPULSION LABORATORY
CALIFORNIA INSTITUTE OF TECHNOLOGY
PASADENA, CALIFORNIA

DISTRIBUTION

Alcorn, D.	179-203
Caird, H.	111-118
Craven, C.	180-703
Flitton, D.D. (2)	111-208
Hess, D.S.	233-208
Hoffman, A.R. (2)	233-206
Puleo, J.R. (14)	179-203
Small, J.G. (3)	180-703
Taylor, D.M. (75)	233-206

PRECEDING PAGE BLANK NOT FILMED

PRECEDING PAGE BLANK NOT FILMED

PREFACE

This document contains a report on Research and Advanced Development at the Jet Propulsion Laboratory during the period 1 January 1974 to 30 June 1974, sponsored by the Planetary Quarantine branch of the NASA Office of Space Science and Applications.

PRECEDING PAGE BLANK NOT FILMED

CONTENTS

I.	PLANETARY QUARANTINE STRATEGIES FOR ADVANCED MISSIONS (NASA No. 193-58-61-01)	
1.1	STRATEGIES FOR SATELLITE ENCOUNTER	1-1
	1.1.1 Subtask A Introduction	1-1
	1.1.2 Significant Accomplishments	1-1
	1.1.3 Future Activities	1-5
	1.1.4 Presentations	1-5
1.2	OUTER PLANET ENTRY ANALYSIS	1-6
	1.2.1 Subtask B Introduction	1-6
	1.2.2 Significant Accomplishments	1-6
	1.2.3 Future Activities	1-8
	1.2.4 Presentations	1-11
	1.2.5 References	1-11
II.	NATURAL SPACE ENVIRONMENT STUDIES (NASA No. 193-58-61-02)	
2.1	EFFECT OF PLANETARY TRAPPED RADIATION BELT ON MICROORGANISMS	2-1
	2.1.1 Subtask A Introduction	2-1
	2.1.2 Significant Accomplishments	2-1
	2.1.3 Future Activities	2-1
2.2	EFFECT OF SOLAR WIND RADIATION ON MICROORGANISMS	2-3
	2.2.1 Subtask B Introduction	2-3
	2.2.2 Significant Accomplishments	2-3
2.3	EFFECT OF SPACE VACUUM ON MICROORGANISMS	2-4
	2.3.1 Subtask C Introduction	2-4
	2.3.2 Significant Accomplishments	2-4
	2.3.3 Future Activities	2-9
	2.3.4 Presentations	2-9
	2.3.5 References	2-9
2.4	PROBABILITY OF GROWTH IN PLANETARY ATMOSPHERES AND SATELLITES	2-10
	2.4.1 Subtask D Introduction	2-10
	2.4.2 Significant Accomplishments	2-10

CONTENTS (contd)

	2.4.3	Future Activities	2-11
	2.4.4	Presentations	2-11
2.5		EFFECT OF SOLAR ELECTROMAGNETIC RADIATION ON MICROORGANISMS	2-12
	2.5.1	Subtask E Introduction	2-12
	2.5.2	Approach	2-12
	2.5.3	Significant Accomplishments	2-13
	2.5.4	References	2-32
	2.5.5	Presentations and Publications	2-32
III.		POST LAUNCH RECONTAMINATION STUDIES (NASA No. 193-58-62-03)	
	3.1	POST LAUNCH RECONTAMINATION STUDIES	3-1
	3.1.1	Introduction	3-1
	3.1.2	Significant Accomplishments	3-1
	3.1.3	Future Activities	3-6
	3.1.4	References	3-7
IV.		SPACECRAFT CLEANING AND DECONTAMINATION TECHNIQUES (NASA No. 193-58-63-02)	
	4.1	PHYSICAL REMOVAL OF SPACECRAFT MICROBIAL BURDEN	4-1
	4.1.1	Subtask A Introduction	4-1
	4.1.2	Approach	4-2
	4.1.3	Significant Accomplishments	4-7
	4.1.4	Summary and Conclusions	4-19
	4.1.5	Future Activities	4-20
	4.1.6	Open Areas	4-22
	4.2	EVALUATION OF PLASMA CLEANING AND DECONTAMINATION TECHNIQUES	4-23
	4.2.1	Subtask B Introduction	4-23
	4.2.2	Approach	4-24
	4.2.3	Significant Accomplishments	4-31
	4.2.4	Summary and Conclusions	4-58
	4.2.5	Future Activities	4-59
	4.2.6	References	4-59

CONTENTS (contd)

V.	PLANETARY QUARANTINE LABORATORY - RESEARCH ACTIVITIES (NASA No. 193-58-63-06)	
5.1	TEFLON RIBBON EXPERIMENTS	5-1
5.1.1	Subtask A Introduction	5-1
5.1.2	Significant Accomplishments	5-1
5.1.3	Future Activities	5-8
5.1.4	Presentations	5-8

FIGURES

1-B.1	Sterilization profiles for small particles released at various atmospheric density levels -- Titan nominal atmosphere	1-9
1-B.2	Late release sterilization density for the model atmospheres of Jupiter, Saturn, and Titan -- parent body ballistic coefficient of 10 and 100 kg.m ⁻²	1-10
2-C.1	Viking solar panel temperature profile during missions A and B	2-5
2-C.2	Effect of vacuum temperature on survival of spacecraft spore isolates	2-8
2-E.1	Solar cell fixture for population collection	2-14
2-E.2	Viking solar panel temperature profile during missions A and B	2-15
2-E.3	Schematic of solar electromagnetic radiation system	2-16
2-E.4	JPL planetary quarantine chamber	2-17
2-E.5	JPL planetary quarantine solar simulator	2-18
2-E.6	Control panel of solar electromagnetic radiation source	2-20
2-E.7	Cone radiometer measurement of the solar electromagnetic beam	2-23
2-E.8	Irradiation side of the pure cultered organism test fixture	2-25
2-E.9	Dark side of the pure cultered organism test fixture (shown with thermocoupled stages)	2-26
2-E.10	Gaseous nitrogen transport case for pure cultured organism test fixture	2-27
2-E.11	Pure cultured organism test fixture mounted in vacuum chamber	2-28
3-A.1	Typical spacecraft cross-sectional geometry with cone spacecraft model superimposed	3-2
3-A.2	Conceptual view of cone spacecraft model in the first octant (x, y, z all positive) with illuminated and shaded areas indicated	3-4

FIGURES (contd)

3-A.3	Conceptual block diagram of the recontamination software	3-5
4-A.1	Schematic of rotary mask test set up	4-3
4-A.2	Rotary mask pulse generator assembly	4-3
4-A.3	Pulse blow test set up (shown with 12 inch transfer tube installed between pulse generator and sample)	4-4
4-A.4	Pulse blow nozzle arrangement as viewed through sample plate. Left: vacuum nozzle; Right: transfer tube from generator	4-4
4-A.5	Schematic of ultrasonic generator set up	4-5
4-A.6	Schematic of oscillating rod set up	4-6
4-A.7	Oscillating rod set up. In experiment shown, hypodermic needle is used as the rod.	4-7
4-A.8A	Schematic seeding apparatus	4-8
4-A.8B	Dust seeding apparatus	4-8
4-A.9	Pulse frequency vs sound pressure level, 5 mm from mask	4-10
4-A.10	Effect of pulse frequency on removal efficiency	4-11
4-A.11	Effect of plenum pressure on removal efficiency comparison of 4 and 48 sector mask at breakway RPM	4-11
4-A.12	Effect of pulse frequency on impingement pressure	4-12
4-A.13	Removal efficiencies vs plenum pressure and particle size	4-13
4-A.14	Typical pressure characteristics of test apparatus without transfer tube	4-13
4-A.15	Removal efficiency vs particle size with and without transfer tube	4-14
4-A.16	Removal efficiency vs particle size for practically dry surface	4-15

FIGURES (contd)

4-A.17	Flow rates and dynamic behavior of spray-rod vs nozzle pressure	4-16
4-A.18	Flow pattern of liquid surface film during oscillating spray-rod test	4-18
4-A.19	Concept for a rotary self cleaning brush	4-21
4-A.20	Concept for an intermittently cleanable vacuum brush	4-21
4-A.21	Concept of a pulsating blow - vacuum, spot cleaning tool	4-22
4-B.1	Test configuration	4-26
4-B.2	Test sample arrangement	4-27
4-B.3	Electrode placement and design	4-30
4-B.4	<u>Bacillus subtilis</u> var. <u>niger</u> spores exposed to argon plasma, 9000X	4-37
4-B.5	<u>Bacillus subtilis</u> var. <u>niger</u> spores exposed to argon plasma, 9000X	4-38
4-B.6	<u>Bacillus subtilis</u> var. <u>niger</u> spores, 8000X	4-39
4-B.7	<u>Bacillus subtilis</u> var. <u>niger</u> spores exposed to helium plasma, 8000X	4-40
4-B.8	<u>Bacillus subtilis</u> var. <u>niger</u> spores, 10,000X	4-41
4-B.9	<u>Bacillus subtilis</u> var. <u>niger</u> spores, 140, 220, 340, nanometers	4-42
4-B.10	Nitrogen plasma probe curve	4-50
4-B.11	Helium plasma probe curve	4-51
4-B.12	Helium plasma probe curve	4-54
4-B.13	Helium plasma probe curve	4-54
4-B.14	Argon plasma probe curve	4-55
4-B.15	Helium plasma probe curve	4-55
4-B.16	Helium plasma probe curve	4-56
4-B.17	Argon plasma probe curve	4-56

TABLES

1-A.1	Pair Values of $P_{C/I}$ and P_{MM}	1-3
2-C.1	Effect of Vacuum-Temperature on Survival of Spacecraft Isolates ^a Test Duration	2-6
2-E.1	Spectral Analysis of the Solar Electromagnetic Beam	2-21
2-E.2	Percent Survival of Pure Culture Populations Exposed to Solar Electromagnetic Radiation at 0.1 Sun Irradiance	2-30
4-B.1	Test Organisms	4-25
4-B.2	Operating Parameters	4-25
4-B.3	Test Matrix	4-28
4-B.4	Operating Parameters	4-28
4-B.5	Operating Parameters	4-29
4-B.6	Mean Number of Microorganisms Surviving Helium Plasma Exposure	4-31
4-B.7	Percent Survival of Microorganisms After Exposure to Helium Plasma	4-32
4-B.8	Mean Number of Spores Surviving Helium Plasma Exposure	4-33
4-B.9	Mean Percent Survival of Spores to Helium Plasma	4-34
4-B.10	Total Number of <i>Bacillus subtilis</i> var. <i>niger</i> Spores Surviving Helium Plasma Exposure	4-34
4-B.11	Mean Number of <i>Bacillus subtilis</i> var. <i>niger</i> Spores Protected from Plasma Environment with Filters	4-36
4-B.12	Percent Survival of <i>Bacillus subtilis</i> var. <i>niger</i> Spores Protected from Plasma Environment with Filters	4-36
4-B.13	Percent Survival <i>Bacillus subtilis</i> var. <i>niger</i> Spores Exposed to Mixed Gas Plasma	4-43
4-B.14	Mean Percent Survival of <i>Bacillus subtilis</i> Spores in Helium Plasma	4-57
4-B.15	Mean Percent Survival of <i>Bacillus subtilis</i> Spores in Plasma	4-58

TABLES (contd)

4-B. 16	Comparison of Plasma Environment with Spore Survival	4-60
5-A. 1	Thermal Resistance of Spores Collected on Teflon Ribbons - VAB - KSC	5-2
5-A. 2	Thermal Resistance of Spores Collected on Teflon Ribbons - VAB - KSC	5-3
5-A. 3	Thermal Resistance of Spores Collected on Teflon Ribbons - VAB - KSC	5-3
5-A. 4	Summary of Thermal Teflon Ribbon Experiments Conducted in MSOB and VAB	5-5
5-A. 5	Biochemical Test Reactions of Heat-Stressed Environmental Isolates	5-5
5-A. 6	Biochemical Test Reactions of Heat-Stressed Environmental Isolates	5-7

SECTION I

PLANETARY QUARANTINE STRATEGIES
FOR
ADVANCED MISSIONS
(NASA NO. 193-58-61-01)

<u>Contents</u>	<u>Title and Related Personnel</u>
Subtask A para. 1.1	STRATEGIES FOR SATELLITE ENCOUNTER Cognizance: C. Gonzalez Associate Personnel: W. Stavro
Subtask B para. 1.2	OUTER PLANET ENTRY ANALYSIS Cognizance: C. Gonzalez Associate Personnel: W. Jaworski A. McRonald

1.1 STRATEGIES FOR SATELLITE ENCOUNTER

1.1.1 Subtask A Introduction

The objectives of this task are to determine the impact of satisfying satellite quarantine constraints on current outer planet mission and spacecraft designs; and to develop tools required to perform trajectory and navigation analyses for determining satellite impact probabilities.

1.1.2 Significant Accomplishments

1.1.2.1 Jupiter Satellite Tour Orbiter Mission

1. Maneuver Reliability Implications on PQ/SQ Considerations for a Jupiter Satellite Tour Orbiter Mission. Since control of the trajectory of a spacecraft is mainly dependent on "maneuver reliability," the interrelation between this reliability and PQ/SQ parameters becomes of vital importance. The reliability problem was considered in connection with the ability of the Orbiter to reach a long lived terminal orbit which would be required in order to satisfy the PQ lifetime constraints.

The general formula for P_C (probability of contamination) for large impactables is:

$$P_C = P_{C/I} P_{Imp} Q_{MM} \quad (1)$$

and applying this equation only to the operation of attempting to achieve terminal orbit, the symbols become:

- P_C = the probability of contaminating a planet or satellite.
- $P_{C/I}$ = the probability of contamination given impact of a planet or satellite.
- P_{Imp} = the probability of impact by a large impactable.
- Q_{MM} = the probability of not being able to perform the necessary maneuver(s) to place the spacecraft into its terminal orbit, where lifetime requirements can be satisfied.

A spacecraft in a low inclination orbit about Jupiter will have to be considered to have a probability of impact of one in a time period equivalent to present PQ/SQ lifetime requirements. This conclusion is based on the fact that the many perturbations on the orbit due to the satellites will make it virtually impossible to design a low inclination orbit not having this characteristic.

The effect of the value of $P_{C/I}$ selected on the required maneuver reliability was investigated. Let

$$P_{MM} = 1 - Q_{MM}$$

where P_{MM} is the maneuver "reliability."

Therefore, in terms of the requirement of maneuver "reliability," Eq. (1) becomes

$$P_{MM} \geq 1 - P_C/P_{C/I}$$

in order to satisfy the PQ or SQ constraint. The above equation simply says that at all times during the mission (until terminal orbit attainment), the probability of being able to perform the necessary maneuvers to place the spacecraft into a terminal orbit must be greater than or equal to $(1 - P_C/P_{C/I})$.

Table 1-A.1 shows pair values of $P_{C/I}$ and P_{MM} for two values of P_C . The P_C values are representative of present P_C constraints used for outer planet missions. Present values of $P_{C/I}$ for spacecraft in flyby outer planet missions are:

	Jupiter	Saturn	Satellites
$P_{C/I}$	10^{-3}	10^{-2}	10^{-1}

It can be concluded from the above values that very high reliabilities are required for the maneuvers if the $P_{C/I}$ of satellites was to remain at 10^{-1} . If further analysis shows that this value can be reduced to 10^{-3} (similar to Jupiter), then the reliabilities (0.94 to 0.97) are reasonable and probably can be achieved.

Table 1-A.1. Pair Values of $P_{C/I}$ and P_{MM}

$P_C = 3 \times 10^{-5}$		$P_C = 6 \times 10^{-5}$	
$P_{C/I}$	P_{MM}	$P_{C/I}$	P_{MM}
10^{-1}	0.9997	10^{-1}	0.9994
10^{-2}	0.997	10^{-2}	0.994
10^{-3}	0.97	10^{-3}	0.94
10^{-4}	0.7	10^{-4}	0.4

The main conclusion derived from the above analysis is that if $P_{C/I}$ for outer planet satellites was 10^{-3} and the probability of being able to place the spacecraft in a terminal orbit can remain at a value higher than 0.94 during the mission duration, then the PQ/SQ constraints are satisfied.

2. Analysis of the Impact of Advanced Mission Concepts on PQ and SQ. There are a number of characteristics and concepts of the satellite tour orbiter missions which are very different from missions planned for the 70s, characteristics which will have a tremendous impact on the approach to satisfying PQ.

One of the most significant advanced concepts is an adaptive mission sequence and encounter strategy for the orbit phase. With this strategy, one prelaunch fixed mission sequence would not exist. The adaptive strategy results from the multitude of options available to mission planners resulting from multiple satellite encounters and techniques for achieving given orbits. The adaptive strategy calls for an assessment of options once the mission is in progress. This allows a choice of the satellite, which will be encountered, the altitude of closest approach, the period and periapsis of the orbit, etc. These may be used in order to meet desired scientific objectives or in order to respond appropriately to engineering requirements such as those which may arise from the radiation belts. This means that demonstration of the satisfying of PQ constraints can not proceed as it has in past missions using a fixed suballocation

for each maneuver when performing the prelaunch analysis. An adaptive suballocation strategy will have to be used since the mission sequence will involve a number of options after the orbit insertion.

Another characteristic of the satellite tour orbiter missions is the potential close encounter distance (equal to or less than 1000 km) required in order to achieve the degree of control of the orbital parameters desired. This type of encounter will require advanced navigation techniques in order to effect the precise control needed. Such techniques as optical tracking and autonomous navigation are included. Use of such techniques will remove the earth based control leading to another element of uncertainty which will have to be taken into account in a PQ analysis.

The above mission characteristics will impact the method of determining whether PQ constraints are satisfied in several ways:

- 1) First, in order to respond to an adaptive mission sequence plan, an adaptive suballocation strategy must be applied. The current practice of developing a suballocation model for the prelaunch analysis documentation which then remains fixed after launch must be altered. Instead, an adaptive suballocation strategy is required which incorporates the results of prior decisions in the mission sequence at a particular decision point.
- 2) The probability of impact may increase significantly relative to the results obtained in our earlier studies of satellite encounters because of the close encounter distance of equal or less than 1000 km. They may result in a requirement for more maneuvers and increased ΔV .
- 3) Autonomous navigation with its removal of earth based control will, of course, require an adaptive mission sequence. It will also mean depending on a predetermined set of maneuvers independent of earth based control in satisfying the PQ constraints. The reliabilities involved will have a very significant impact on the difficulty in satisfying PQ.

1.1.3 Future Activities

The following future activities will be undertaken with reference to outer planet orbiters:

- 1) An investigation of the determination of the probability of impact and strategies required to satisfy the SQ constraints for a Jupiter Satellite Tour Orbiter Mission.
- 2) An investigation of the problem of achieving a terminal orbit which will satisfy the PQ and SQ lifetime requirements for a Jupiter Satellite Tour Orbiter Mission.
- 3) An extension of the analysis cited in 1) and 2) to cover Saturn Satellite Tour Orbiter Mission.
- 4) An investigation of the PQ implications of outer planet probes.

1.1.4 Presentations

Stavro, W., "Strategies for Satellite Encounter," presented at NASA Spacecraft Sterilization Technology Seminar, San Francisco, California, February, 1974.

1.2 OUTER PLANET ENTRY ANALYSIS

1.2.1 Subtask B Introduction

The objective of the outer planet atmospheric entry analysis subtask is to develop and use the tools to determine the thermal response characteristics of a typical spacecraft and related debris upon entry into the atmospheres of Jupiter, Saturn or Titan.

1.2.2 Significant Accomplishments

1.2.2.1 Large Impactable Analyses. The results of the analytical studies performed on effects of Jupiter atmospheric entry heating on components and materials (see reference) were evaluated in terms of their significance to the satisfying PQ for Jupiter. The evaluation revealed that experimental tests need to be performed in order to clarify the results of the analytical studies which have led to conclusions which may be overly conservative. This testing includes:

- 1) Testing the teflon cabling in an atmospheric entry simulation facility where entry shock is produced in order to assess the side flow heating effects due to external flow along the side of the cable and the entry configuration of the cable. This test would also show the effectiveness of this type of heating in causing disintegration of the teflon jacket exposing the interior wires. The test should also provide information on the possible "brooming" effects (wire spreading) on the cable front due to high pressure behind the shock and its contribution to disintegration of the cabling during entry.
- 2) Testing of other cable insulating materials in addition to teflon in combination with other tests described above in an entry simulation facility if time and expense warrant it.
- 3) Testing of a component such as the UVS under conditions in which the hot gases evolved from plastic components are able to circulate through the structure. Instrumenting the component with thermocouples will allow a determination of the effectiveness of the hot gases in heating materials throughout the component. Also,

the potential disintegration of the cable jacket and penetration of the gases into the interior wires can be evaluated.

Work also continued on the large impactable analyses in preparation for analysis similar to those performed for Jupiter for a Titan entry. To perform entry heating calculations for the major parts of a spacecraft or another body entering a planetary atmosphere, one needs details of the equilibrium plasma formed in the shock layer ahead of the body. This knowledge is particularly basic to the calculation of radiative heating. The shock layer thermochemical information has been generated for the three Titan gases likely to give substantial radiative heating, viz., the two alternative compositions predicted for the nominal atmospheres [(A) 100% methane, (B) 30% hydrogen, 40% methane, 30% nitrogen; and the Titan heavy gas (30% methane, 70% nitrogen)].

Modifications have been made to the JPL Plasma Radiation Program* including the capability to accept three constituent gases simultaneously in order to accommodate the Titan Model atmosphere. In addition, the new approach allows computation of the continuum at the basic wavelength points as before, but now interpolates it only where required, i. e., where a strong line rises into the optically thick region and must be represented at a number of wavelengths. Further, the waveband values are determined by integral formulas which give the true areas. The new process is simultaneously more accurate and economical of computer storage and time.

1.2.2.2 Small Impactable Analyses. The small particle analyses for Jupiter and Saturn have shown that there is a point in the atmosphere (depending on particle size, entry angle, and the atmospheric density at particle release), such that any debris liberated after that will not contain viable organisms. These results come from analyses for the initial entry phase and did not apply to the post-peak heating regions. These results have been studied and the following conclusions reached. Debris is completely sterilized if liberated only slightly into the atmosphere (at about $100 \mu\text{g}/\text{cm}^3$ of density) which is about the early continuum for large impactables for Jupiter. This means that most of the debris liberated will be sterilized. However, some disintegration

*An acknowledgement is made to Dr. Peter Poon of JPL for his valuable assistance in this effort.

and break up will occur at or slightly before the beginning of the continuum where there is some probability of survival at these lower densities. Although large impactable analyses have not been completed for Saturn, the same general conclusion is expected.

Survival entry corridors were investigated for Titan and the results are shown in Fig. 1-B.1. Referring to Fig. 1-B.1, the survival entry corridor is the triangular area bounded on the left by the nearly vertical hyperbolic skipout lines, on the bottom by the minimum organism size, and bounded above by the lines pertaining to atmospheric density at particle release. It can be seen that the corridor rapidly contracts as the density at release increases through the levels 1 to $64 \times 10^{-9} \text{ kg/m}^3$ shown. At the same time the skipout boundaries on the left move upwards and to the left. These densities pertain to very high levels of the atmosphere so that particles for which survival corridors exist are those released early and thus necessarily pre-existing, entrained with the spacecraft or absorbed on its surface.

Analyses were also performed to determine analogous survival boundaries for late release of small particles, assumed to have been sheltered inside a major part of the spacecraft during peak entry heating for Jupiter, Saturn and Titan. The results, shown in Fig. 1-B.2, indicate that the boundaries are independent of particle size (at least in the range 1 to 100 μ of interest) and depend mainly on the entry angle and effective ballistic coefficient of the major spacecraft part from which the particle escapes. The results in Fig. 1-B.2 give the atmospheric density boundary (in absolute value or density) above which survival occurs for a parent body $M/C_D A$ of 10 and 100 kg/m^2 (which is believed to represent the expected range for a typical spacecraft), as a function of entry angle. The boundary falls generally in the range 1 to $100 \times 10^{-3} \text{ kg/m}^3$. This means that in the case of Jupiter and Saturn, viable organisms released just prior or at the region of biological significance will not be killed by the entry heating.

1.2.3 Future Activities

The following future activities are planned for the large impactable analyses:

- 1) Perform experimental tests needed to clarify the large impactable analyses for Jupiter.

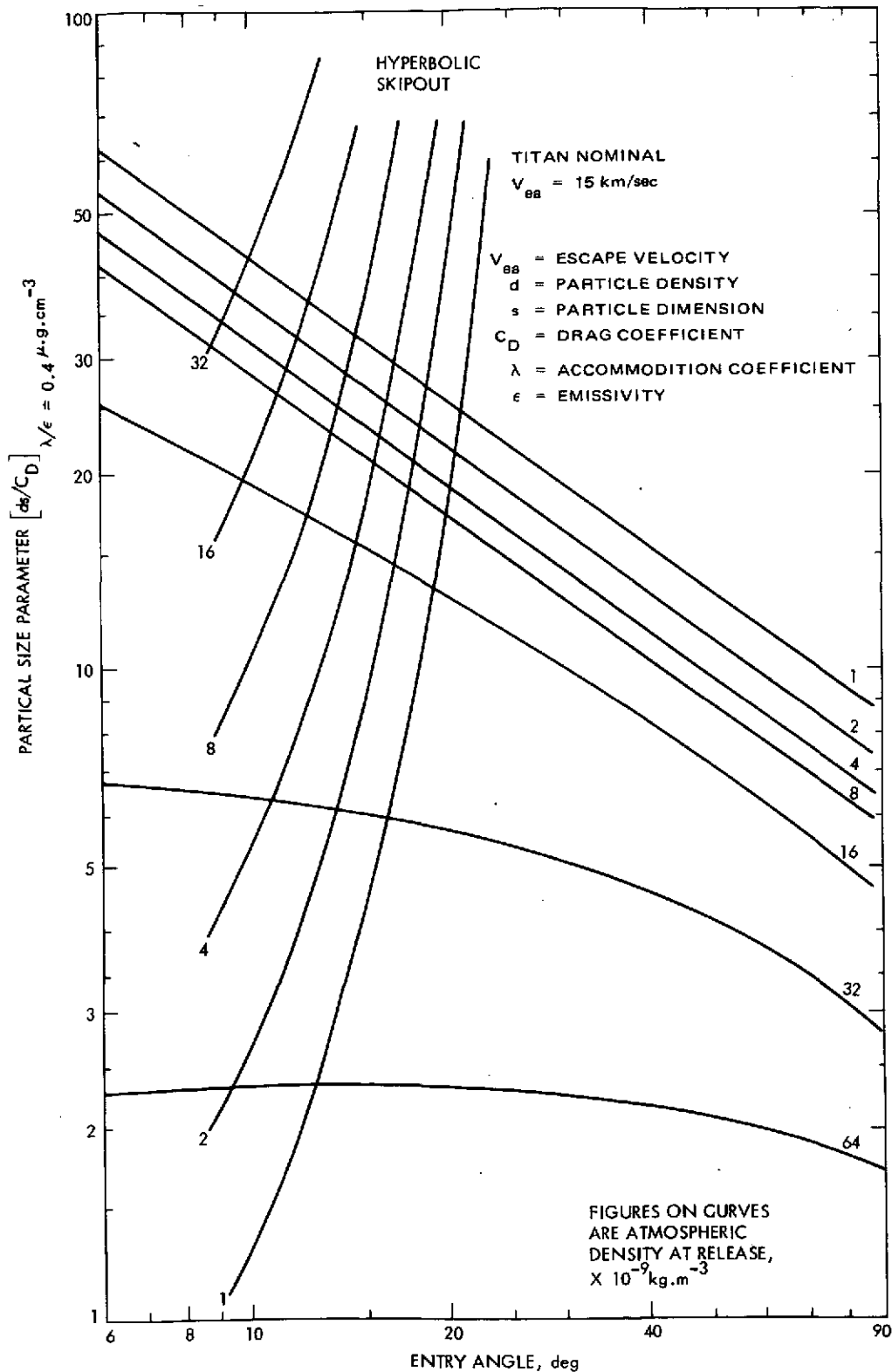


Fig. 1-B.1. Sterilization profiles for small particles released at various atmospheric density levels -- Titan nominal atmosphere

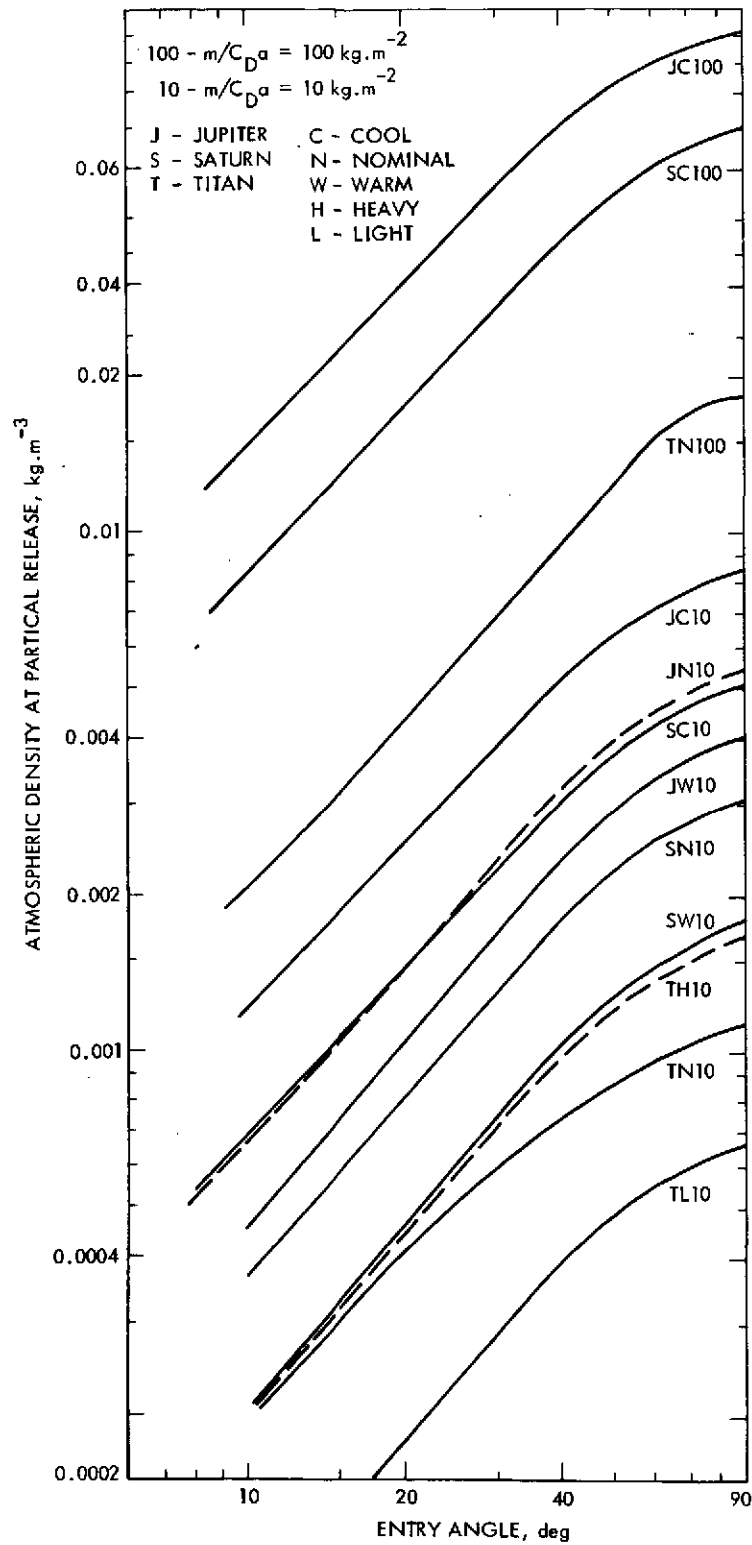


Fig. 1-B.2. Late release sterilization density for the model atmospheres of Jupiter, Saturn, and Titan -- parent body ballistic coefficient of 10 and 100 kg.m^{-2}

- 2) Complete Saturn and Titan large impactable analyses.
- 3) Consider large impactable entries from circular orbit for Jupiter and Saturn.
- 4) Perform a preliminary survey into Uranus to scope the aerothermal effects in relation to the prior planetary cases.

One further future activity is planned for the small particle analyses and that is to assess the impact of "skip up" of the parent body on the results of study of late released particles described above.

1.2.4 Presentations

Jaworski, W., "Jupiter Entry Analysis," presented at NASA Spacecraft Sterilization Technology Seminar, San Francisco, California, February, 1974.

Hoffman, A. R., Jaworski, W., McRonald, A. D., "Status of Outer Planet Entry Heating Analysis," Videotape recording prepared for NASA PQ Officer February, 1974.

Hoffman, A. R., Jaworski, W., Taylor, D. M., "Self Sterilization of Bodies During Outer Planet Entry," paper presented at the 17th Planetary Meeting of COSPAR, Sao Paulo, Brazil, June 17 - July 1, 1974.

1.2.5 References

Planetary Quarantine: Semi-Annual Review Space Research and Technology, 1 July - 31 December, 1973, JPL Document 900-655, April, 1974.

SECTION II

NATURAL SPACE ENVIRONMENT STUDIES
(NASA No. 193-58-61-02)

<u>Contents</u>	<u>Title and Related Personnel</u>
Subtask A para. 2.1	EFFECT OF PLANETARY TRAPPED RADIATION BELT ON MICROORGANISMS Cognizance: D. Taylor C. Hagen (Bionetics) Associate Personnel: J. Barengoltz J. Yelinek (Bionetics)
Subtask B para. 2.2	EFFECT OF SOLAR WIND ON MICROORGANISMS Cognizance: J. Barengoltz
Subtask C para. 2.3	EFFECT OF SPACE VACUUM ON MICROORGANISMS Cognizance: C. Hagen (Bionetics) D. Taylor Associate Personnel: G. Simko (Bionetics) C. Smith (Bionetics) J. Yelinek (Bionetics)
Subtask D para. 2.4	PROBABILITY OF GROWTH IN PLANETARY ATMOSPHERE AND SATELLITES Cognizance: D. Taylor Associate Personnel: R. Berkman N. Divine
Subtask E para. 2.5	EFFECT OF SOLAR ELECTROMAGNETIC RADIATION ON MICROORGANISMS Cognizance: M. Wardle D. Taylor Associate Personnel: C. Hagen (Bionetics) D. Ross J. Smith

2.1 EFFECT OF PLANETARY TRAPPED RADIATION BELT ON MICROORGANISMS

2.1.1 Subtask A Introduction

The objective of this subtask is to determine the effect of planetary trapped radiation belts on the survival of microorganisms associated with an unsterile spacecraft.

With flyby missions now planned for Jupiter and Saturn and possible Jupiter orbiters and probes, the trapped radiation belts may represent an environment lethal to microorganisms and thereby reduce the requirement for decontamination of spacecraft before launch.

The major components of planetary trapped radiation belts are electrons and protons. The approach of the present task is to evaluate possible biological effects of these belts by subjecting spacecraft microbial isolates to different energies, exposures and dose rates of those particles.

2.1.2 Significant Accomplishments

During this report period the effort to model the electron data on the radiation sensitivity of microbial populations has continued. This data includes the data on 0.6, 2, 12 and 25 MeV electrons previously reported in JPL Document No. 900-655, April, 1974.

2.1.3 Future Activities

The future activities of this task will be involved with the analyses of data and subsequent modeling of the radiation sensitivity of microbial populations that would allow evaluation of radiation environments, encountered by future spacecraft missions, for the survival of spacecraft surface microbial populations. Additional activities will be to evaluate the effect of secondary radiation on the survival of microorganisms. This activity could become an important factor for future orbiter-type missions because, if it is found that forms of secondary radiation effectively reduce the internal microbial burden of spacecraft, then the orbiter lifetime required to avoid violating planetary quarantine constraints for a particular mission could be proportionately reduced. Both the evaluation of external radiation environments in terms of

the electron data and the evaluation of the effect of secondary radiation will be conducted with the use of updated Jupiter electron radiation belt models currently being prepared inhouse. Finally, a statement of work will be formulated for the procurement of a high energy proton facility for the purpose of investigating the effects of high energy protons similar to those present in planetary trapped radiation belts.

2.2 EFFECT OF SOLAR WIND RADIATION ON MICROORGANISMS

2.2.1 Subtask B Introduction

The objective of this subtask is to determine the effect of solar wind radiation on microorganisms associated with nonsterile spacecraft.

This study is directed towards determining the reduction in spacecraft associated microbial burden attributable to solar wind radiation.

The approach does not attempt a simulation of the total radiation environment, but rather an examination of the effect of low energy electrons and protons as a function of fluence and energy. The data acquired would apply to all missions.

2.2.2 Significant Accomplishments

During this report period a conceptual design of an electron source and vacuum system for use in the investigation of the effect of low energy electrons in the range 1 to 5 KeV on the survival of microbial populations has been completed. A contract for the electron source has been let, with an expected delivery date of late October this year. The required modifications of an existing vacuum system are also in progress. Another future activity will be an analogous study with naturally occurring organisms. The final future activity planned is to define and conduct a solar wind proton test program.

2.3 EFFECT OF SPACE VACUUM ON MICROORGANISMS

2.3.1 Subtask C Introduction

This study was designed to examine the combined effects of space vacuum and spacecraft temperatures on the survival of microorganisms. The scope of study was modified to include in the test matrix the higher temperatures that will be experienced by the Viking solar panels (Ref. 1). The Viking solar panel temperature profile is shown in Fig. 2-C.1. In addition, the number of MM71 spacecraft isolates normally used in the Natural Space Environment studies were reduced to five sporeformers and one nonsporeformer. The sporeformer, Bacillus subtilis var. niger and the nonsporeformer, Staphylococcus epidermidis ATCC 17917, were included in the tests for comparative purposes.

2.3.2 Significant Accomplishments

2.3.2.1 Description of Study. During this report period the test matrix for cultured spacecraft microbial isolates was completed. The microbial subpopulation from MM71 spacecraft was exposed to simulated space vacuum of 10^{-7} torr at temperatures of 55, 65, and 75°C for periods of 7, 14, and 28 days.

2.3.2.2 Experimental Conditions.

1. Microbiology. The test organisms, isolated from MM71 spacecraft, were the same organisms that were used in the launch pressure profile study, the space particle radiation study, and are presently being used in the solar electromagnetic radiation study. The derivation, culture, and assay procedures for the isolates were previously described in para. 3.2.1.2 of the Annual Report (JPL Doc. No. 900-597, February, 1973).

2. Vacuum Equipment. Photographs, together with a description of the test facility, were presented in para. 3.2.1.2 of the Annual Report (JPL Doc. No. 900-597, February, 1973).

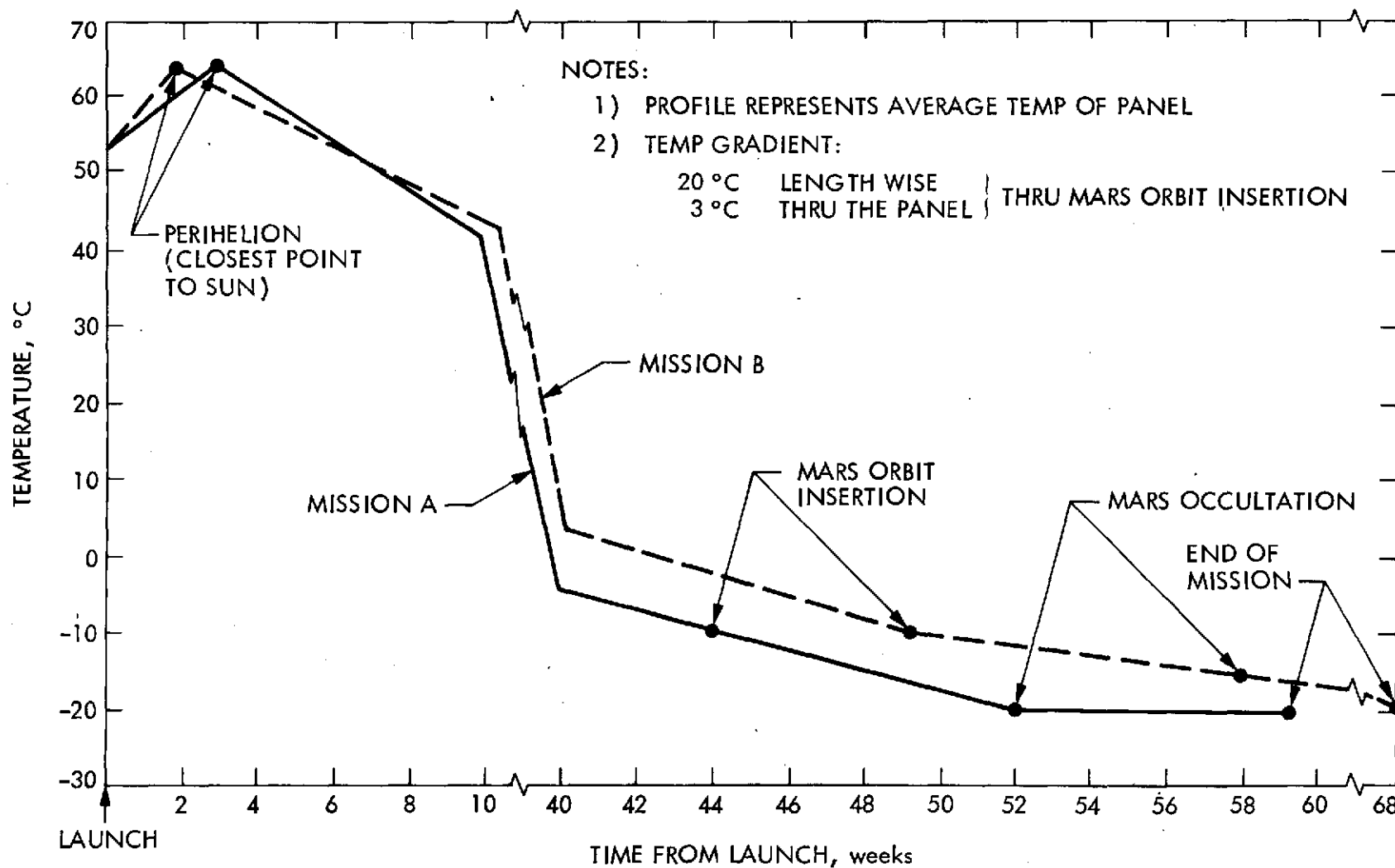


Fig. 2-C.1. Viking solar panel temperature profile during missions A and B

2.3.2.3 Results. All reported data, expressed as geometric mean survival fraction, are based on data obtained from the microbial recovery from four planchets for each isolate and each test condition. In addition, the data from a single planchet is the geometric mean of three plate counts.

The mean survival fractions of sporeformers and nonsporeformers are shown in Table 2-C. 1. The sporeformers present similar survival fraction patterns as previously reported for lower temperatures up to and including 55°C (Ref. 2). The survival fraction pattern has been referred to as a trough effect: That is, in general, the survival fraction after 7 and 28 days vacuum-temperature exposure were lower than survival fractions after a 14-day exposure. This trend apparently continues for most of the sporeforming isolates even at the higher temperatures of 65 and 75°C used in the currently reported tests.

The reason for the trough effect is not known but the implication is that of possible cell membrane injury with subsequent recovery, or repair, as the vacuum-temperature exposure time is increased.

Table 2-C. 1. Effect of Vacuum-Temperature on Survival of Spacecraft Isolates^a Test Duration

ISOLATE	TEMP	7 days			14 days			28 days		
		55°C	65°C	75°C	55°C	65°C	75°C	55°C	65°C	75°C
SPORES	1	0.248	0.090	0.025	0.526	0.295	0.029	0.303	0.092	0.004
	2	0.097	0.052	0.0002	0.065	0.014	0.0002	0.039	0.005	0.0003
	9	0.023	0.009	0.00004	0.117	0.027	0.0003	0.017	0.002	0.00008
	13	0.036	0.003	0.0003	0.159	0.036	0.001	0.093	0.006	0.00009
	16	0.109	0.137	0.020	0.227	0.085	0.013	0.201	0.093	0.002
	BSN	0.022	0.010	0.0002	0.028	0.009	0.0003	0.029	0.00006	0.00001
VEGETA-TIVES	5	0.137	0.064	0.012	0.141	0.179	0.005	0.026	0.009	0.001
	SE	0.021	NS ^b	NS	0.002	0.0006	NS	0.006	0.004	NS
a. Data expressed as survival fraction										
b. No viable cells detected.										

With few exceptions, the B. subtilis var. niger spores were less resistant to the vacuum-temperature environments than spores of the spore-forming spacecraft isolates. In addition, the nonsporeforming isolate number 5 exhibited a greater resistance to the test environments than B. subtilis var. niger spores.

In studies of this nature a consideration of the resistance of the spacecraft total microbial population, and not the resistance of an individual isolate, is more helpful to the area of Planetary Quarantine. The resistance of the sporeforming spacecraft isolates were, for this reason, considered as a group. Similar treatment of the survival data from the nonsporeforming isolates was not possible because only a single spacecraft isolate was tested from the non-sporeforming group.

Figure 2-C. 2 presents survival data expressed as the mean of the sporeforming spacecraft isolates. Survival data of B. subtilis var. niger are included for purposes of comparison. The clustering of survival fractions at the temperature points of 55, 65, and 75°C for the 7-, 14-, and 28-day exposures indicates that little difference exists for survival fractions at the three exposure durations. The most significant effect, by far, is that of temperature and that as the temperature is increased from 55°C to 75°C a larger portion of the initial populations is rendered nonviable. In general, a one log reduction occurred after a 7-, 14-, or 28-day exposure to 55°C and a 1.5 and 3.0 log reduction occurred after exposure to 65 and 75°C, respectively, during the 7-, 14-, and 28-day exposures. Spores of B. subtilis var. niger, the comparative organism, exhibited a marked duration effect at 65 and 75°C with the 28-day exposure.

In summary:

- 1) The spacecraft spore isolates were reduced 1 log at 55°C, 1.5 logs at 65°C, and 3 logs at 75°C irrespective of a 7-, 14-, or 28-day exposure;
- 2) The nonsporeforming isolate number 5 exhibited a resistance to the test environments similar to spores;
- 3) The comparative organisms were more sensitive to the test environments than the spacecraft isolates.

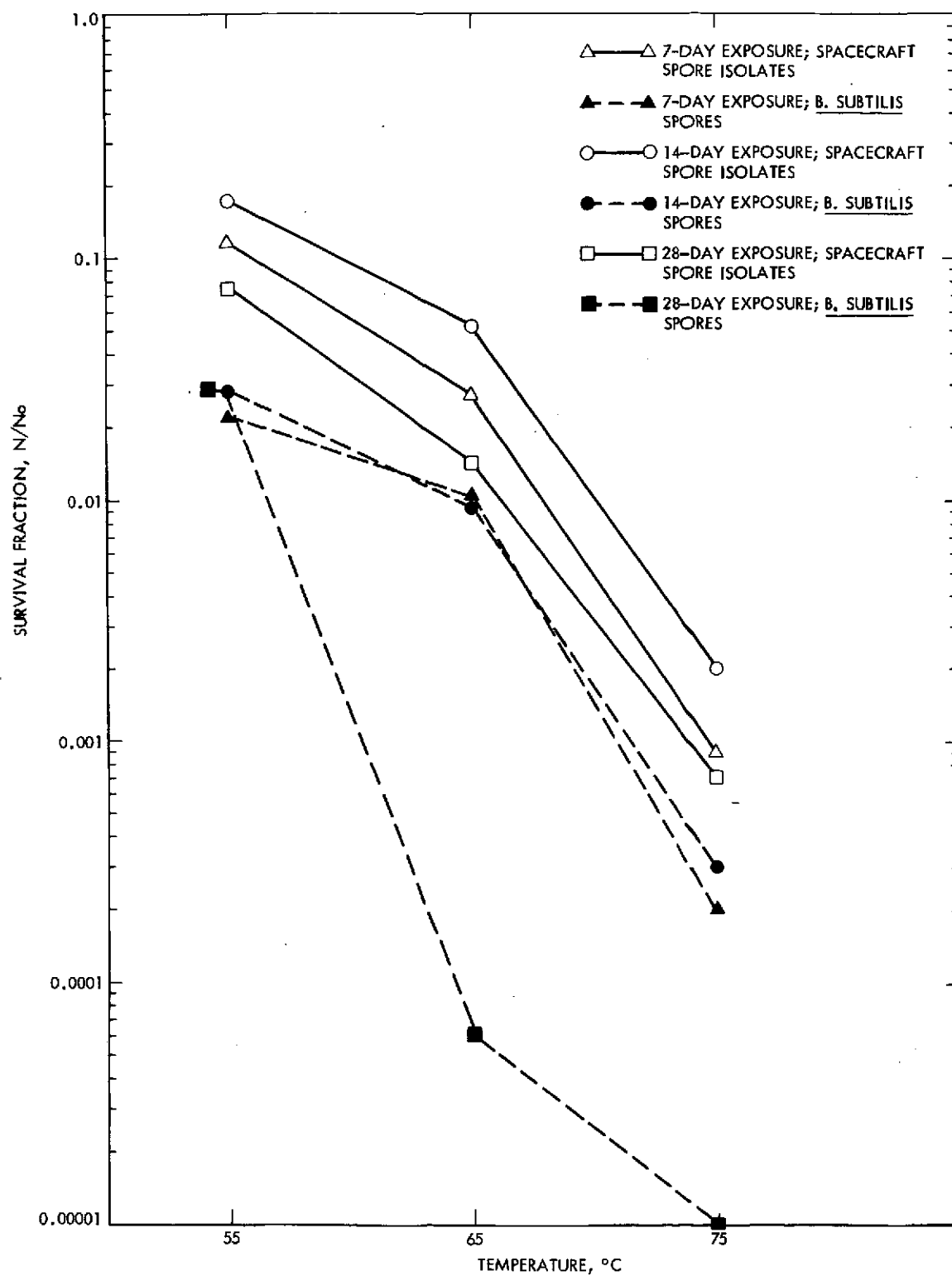


Fig. 2-C.2. Effect of vacuum temperature on survival of spacecraft spore isolates

2.3.3 Future Activities

Future activities of the vacuum-temperature task will be to initiate studies to investigate the thermal vacuum resistance of naturally occurring (uncultured) microbial populations present in spacecraft assembly areas.

2.3.4 Presentations

Taylor, D.M., "Effect of Space Vacuum on Microorganisms," presented at NASA Spacecraft Sterilization Technology Seminar, San Francisco, California, February, 1974.

2.3.5 References

Wang, J., private communication

Hagen, C. A., Semi-Annual Review Space Research and Technology, JPL Doc. No. 900-636, October, 1973, pp 11-20.

2.4 PROBABILITY OF GROWTH IN PLANETARY ATMOSPHERES AND SATELLITES

2.4.1 Subtask D Introduction

The objectives of this subtask are to relate environmental parameters affecting microbial growth to conditions present in the atmospheres of Jupiter and Saturn, and to identify and study satellites of Jupiter and Saturn having possible biological interest.

2.4.2 Significant Accomplishments

During the past six months no new work has been conducted on this task because of the need for data from Pioneer 10 to update the analyses accomplished to date. A paper was presented to COSPAR in Sao Paulo, Brasil and will be published in "Life Sciences and Space Research." The paper was a summary of the results published in the last four Semi-Annual Reports giving the results of the relative probability of growth for Jupiter, Saturn and their satellites. The summary from the paper is as follows:

"Absolute probability of growth values cannot be calculated reliably for the planetary bodies discussed here. On the basis of current knowledge, a relative rank ranging from high to nil probability of growth can be assigned to each body. Saturn has been assigned the highest probability of growth in the likelihood that liquid water and relatively high concentrations of nutrients are available. Jupiter has a somewhat lower probability of growth because there is only a 10 to 20% chance that water is present as a liquid. Titan has been ranked high on the basis of its atmosphere and the accompanying greenhouse effect. The actual surface temperature of Titan cannot be ascertained at this time because radiation measurements provide data on the upper atmosphere only. Hence, the ranking for Titan is tentative. The four Gallilean satellites of Jupiter have been ranked considerably lower than Titan, and can be considered to have a very low probability of growth. Smaller satellites including

the rings of Saturn, which are probably composed of ice or rock, up to a few km in diameter, have essentially a nil probability of growth. "

2.4.3 Future Activities

The future effort on this task will be to update the atmospheric model for Jupiter based on the data from Pioneer 10 and then conduct a reevaluation of the results of the present analysis. The Pioneer 10 data would suggest that the planet is warmer than originally thought, therefore, the zone where growth might occur would be at lower pressures, (present estimates are between 3-100 atms). Another effort to be conducted is the development of a dynamic model of the atmosphere in order to estimate the half-life of particles in such an atmosphere and in the temperature range where growth might occur.

2.4.4 Presentations

Taylor, D., "Consideration of Probability of Bacterial Growth for Jovian Planets and Their Satellites," at COSPAR, Sao Paulo, Brasil, June, 1974. .

2.5 EFFECT OF SOLAR ELECTROMAGNETIC RADIATION ON MICROORGANISMS

2.5.1 Subtask E Introduction

The objective of this task is to estimate the effect of solar electromagnetic radiation (SER) on the survival of microbial populations in a space environment. Efforts will be addressed to the investigation of the photobiological effect of SER in a fashion that permits direct transference of the results to considerations of planetary quarantine. Such information will enable the updating of probability constants in the assessment of applicable planetary quarantine constraints for a mission.

2.5.2 Approach

In line with the objective of this task, the initial approach will involve the subjection of test species to SER in a manner that will yield interpretive data on the response of spacecraft biocontaminants to the SER of space. Primarily, this will entail the high vacuum irradiation of microorganisms with broad spectrum SER (far ultraviolet to infrared).

The first stage of experimentation will involve the testing of pure cultured species to study the effect of solar electromagnetic radiation under different dose, dose rate, and temperature conditions. Seven MM71 isolates (5 sporeformers and 2 nonsporeformers), Staphylococcus epidermidis and spores of Bacillus subtilis var. niger will be tested as pure cultures. Irradiation of test species will be conducted at solar constants* (dose rates) of 0.1, 0.5 and 1.0 sun with temperatures at exposure of -125, -15 and +70°C, respectively. These conditions respectively correspond to representative, near Jupiter, Mars and Earth environments. In order to obtain survivor curves, organisms will be exposed to varying doses for each temperature-dose rate condition.

* For this task, 1.0 solar constant is defined as a beam intensity, at the plane of irradiance, of 0.54 mW cm^{-2} in the wavelength interval from 200 to 270 nanometers.

The second stage of experimentation will be directed to the testing of naturally occurring microbial populations. These populations will be collected on Viking-type solar cell fixtures (Fig. 2-E.1) and exposed to SER in a natural state; i. e., no laboratory treatment of the organisms will be instituted prior to their testing. As with the axenic culture tests, dose rate, dose and temperature will be imposed as experimental variables. The temperatures to be studied (-15°C and $+70^{\circ}\text{C}$) are those expected to nominally occur on the sun side surfaces of the Viking solar panels (Fig. 2-E.2 — Reference 1): dose rates will correspond as stated above.

Work to date has been comprised of pure culture tests at 0.1 and 0.5 sun and has been aimed at the checkout of the test system, definition of dose response curves, and initiation of the planned test matrix for pure cultured cells.

2.5.3 Significant Accomplishments

2.5.3.1 The Solar Electromagnetic Radiation Test System. A significant portion of the activity on this task during the present reporting period has been concerned with the preparation and testing of the SER system. The SER system (Figs. 2-E.3, .4, and .5) consists of two main elements: a nonionizing electromagnetic radiation source and a vacuum chamber; their integration provides for the exposure of microorganisms to a simulated space environment.

The radiant energy is produced by a 2.5 kW xenon arc lamp. The lamp is of a static gas fill design with a Suprasil quartz envelope to extend transmission through the UV spectrum. It has a rated life of 1000 hours, as stated by the manufacturer, and is cooled by a GN_2 blower (with filter) located at the base of the lamp mount.

The radiation is focused by an aluminized (with MgF_2 overcoating to enhance UV reflectivity), water-cooled reflector through an intensity modulator; turned by a water-cooled mirror (aluminized; MgF_2 overcoat) and passed through an integrator assembly and vacuum penetration lens en route to the target plane of the microbiological test fixture.

The SER source is designed to provide a uniform light intensity ($\pm 2\%$) of 0.1 to 1.0 solar constants over a 12 inch diameter target plane located

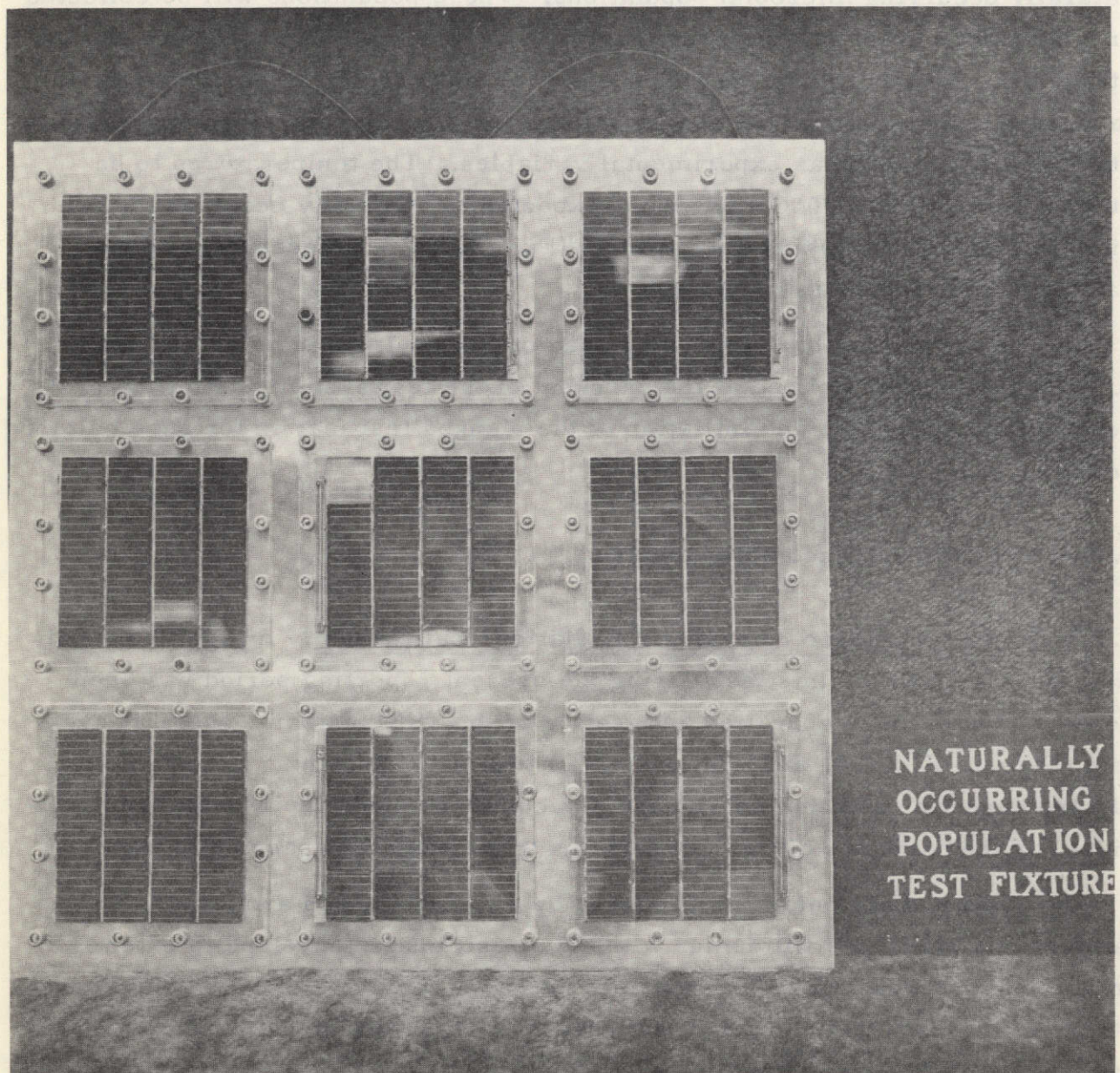


Fig. 2-E.1. Solar cell fixture for naturally occurring population collection

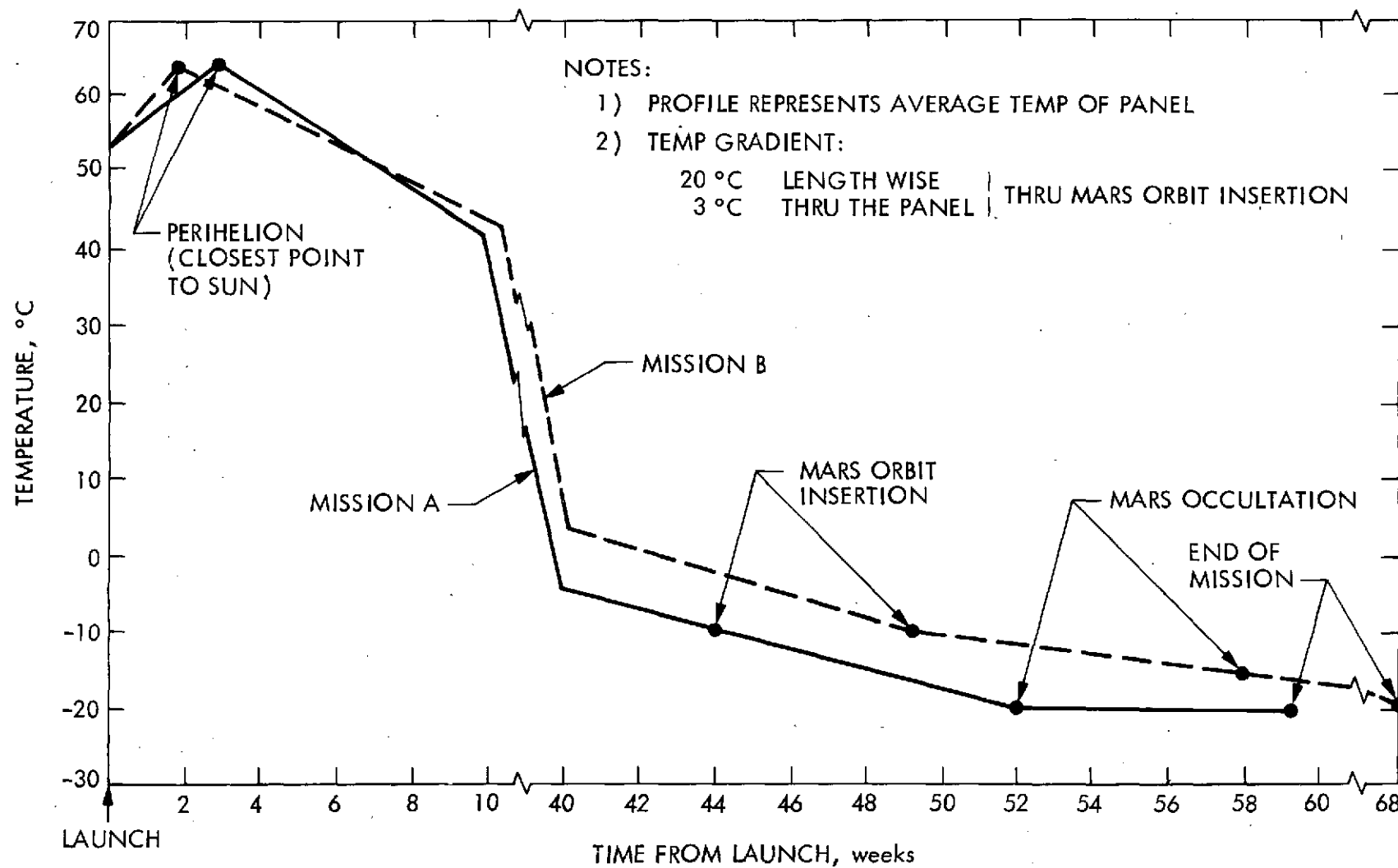


Fig. 2-E.2. Viking solar panel temperature profile during missions A and B

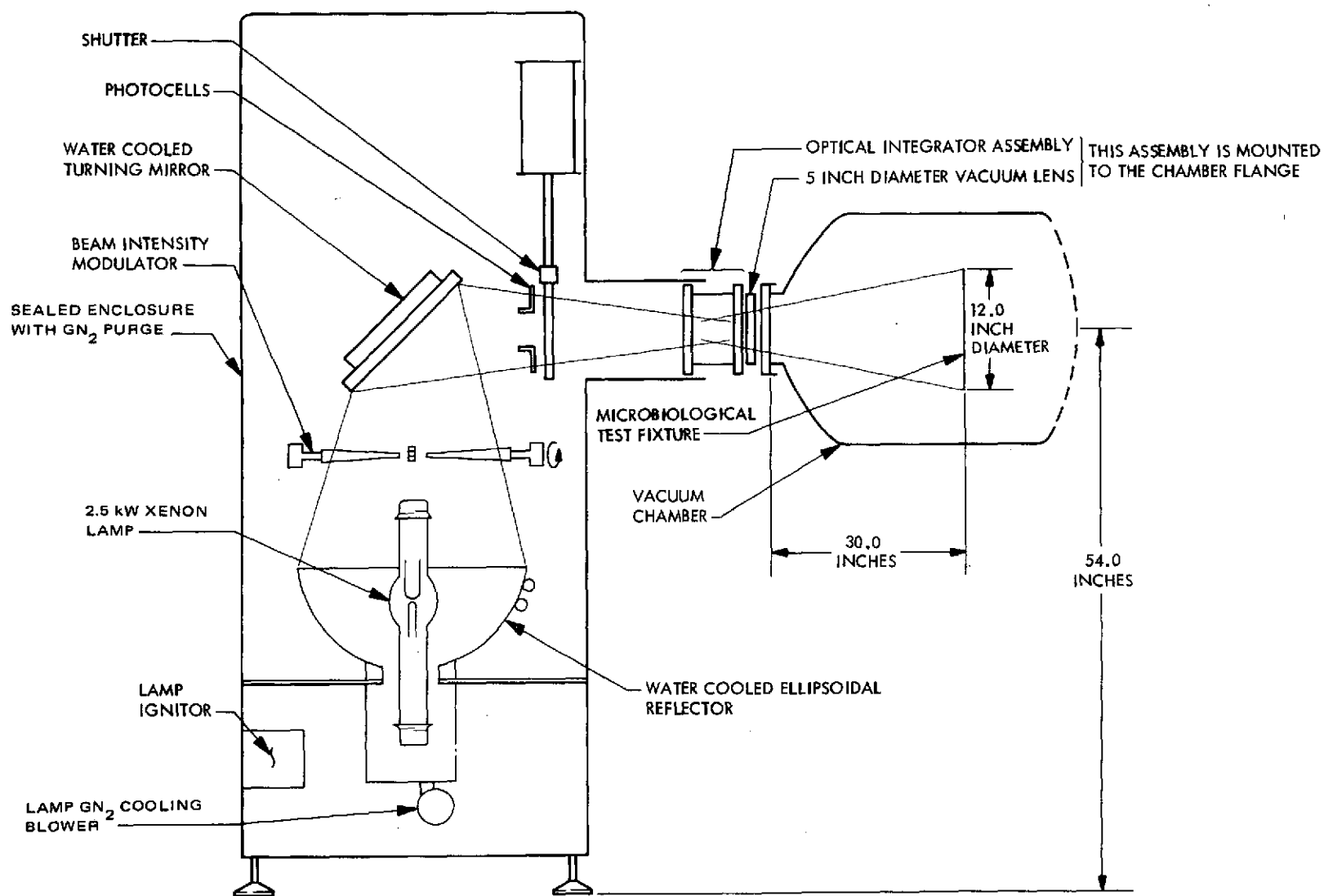


Fig. 2-E.3. Schematic of solar electromagnetic radiation system

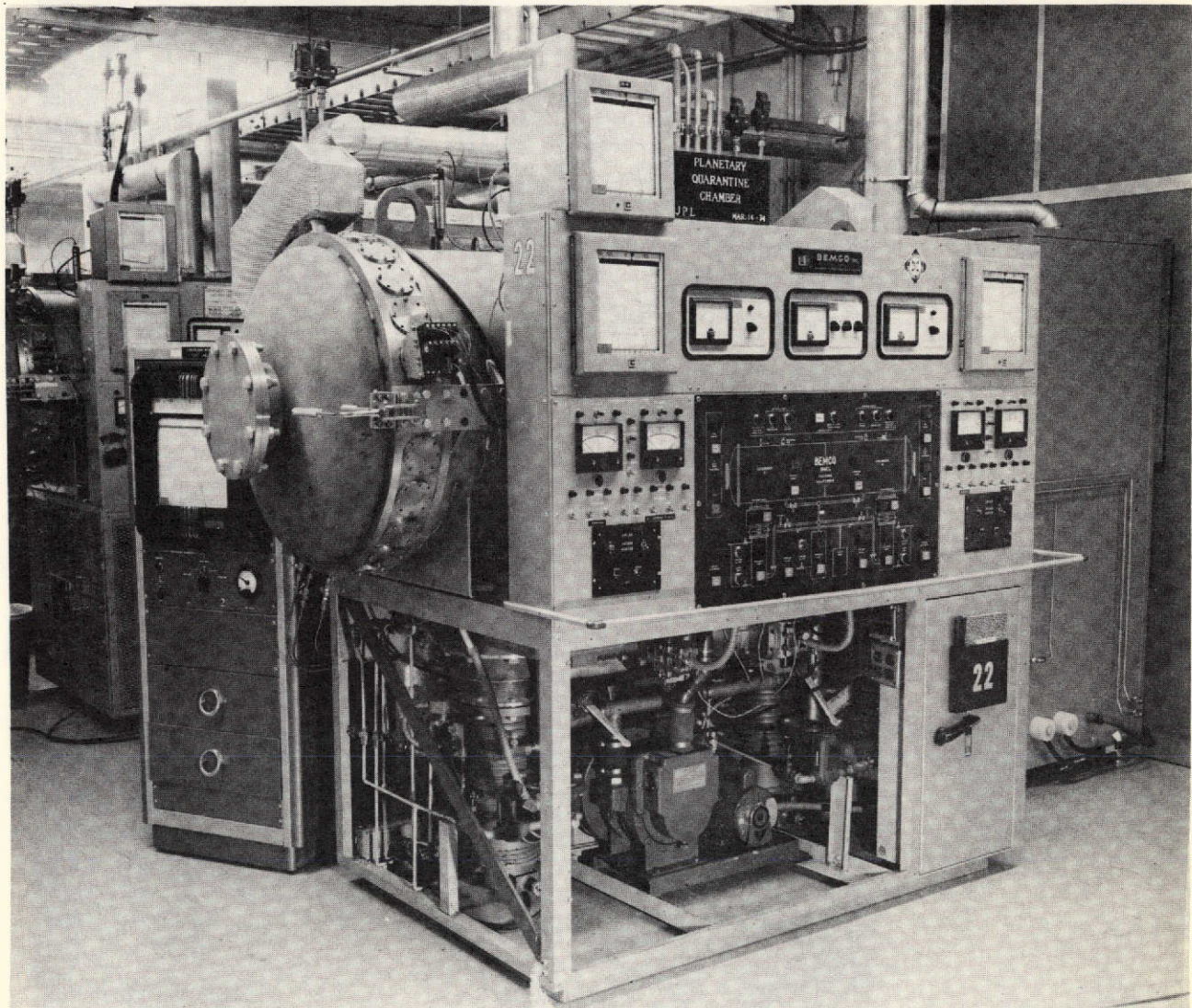


Fig. 2-E.4. Vacuum chamber element of solar electromagnetic radiation system

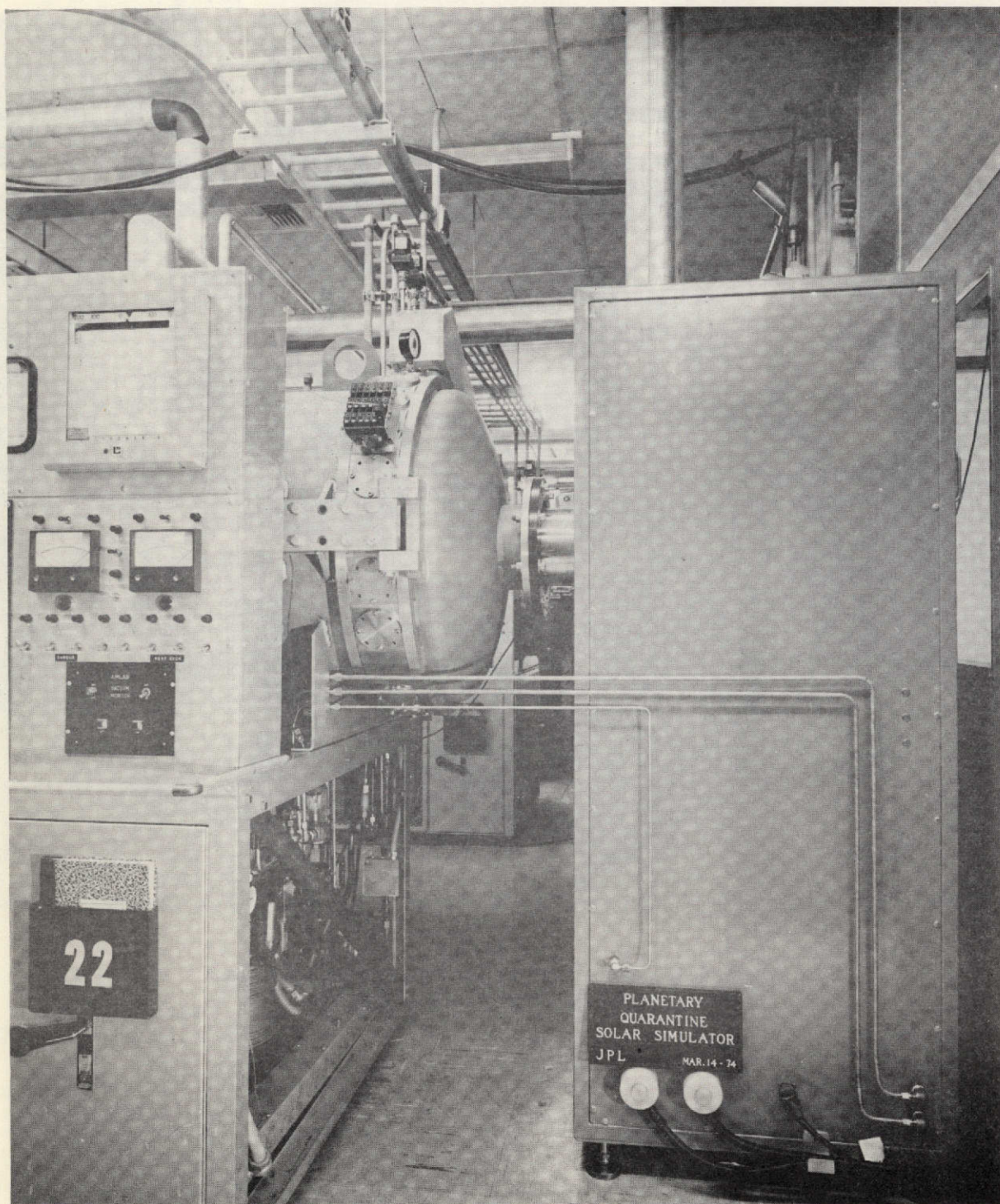


Fig. 2-E.5. Interface of vacuum chamber and solar electromagnetic radiation source.

30 inches from the vacuum penetration lens. This is made possible by two key elements in the system: the intensity modulator and the optical integrator assembly.

The intensity modulator is composed of 12 blades arranged in a circular configuration that resembles a sliced pizza. The rotation of the blades from horizontal to vertical permits intensity variation from minimum to maximum. The blades are geared to rotate simultaneously through a motor drive that is servo controlled by a photocell amplifier output setting located in the control panel (Fig. 2-E. 6). The photocells are mounted in the front plate of the integrator assembly. The servo control is used to set and monitor the output intensity, and to compensate for any small variations in lamp output.

A uniform beam intensity is accomplished by use of a dual, 19 element Suprasil quartz lens integrator assembly arranged in a hexagonal pattern. The quartz lenses are mounted in water-cooled, nickel-coated, brass plates. The two plates are adjustable to provide for beam focus and diameter control at the target plane.

2.5.3.2 Experimental Activities.

1. Spectral Analyses. Spectral distribution measurements were conducted at the plane of irradiance. The beam was collimated (six inches in diameter), and all measurements were made at an intensity of 1.0 solar constant. Optical readings were made with a scanning spectrometer which utilizes a 1200 line/mm grating blazed for $0.15 \mu\text{m}$ in the first order. This grating, along with the other reflecting optical elements within the spectrometer, is aluminized and overcoated with MgF_2 . The dispersion radiation was detected with photomultiplier tubes.

Table 2-E.1 shows the results of a typical spectral analysis of the solar electromagnetic beam. The integrated radiant flux density from 200 to 270 nm was used as a reference point in the definition of the required dose rates.

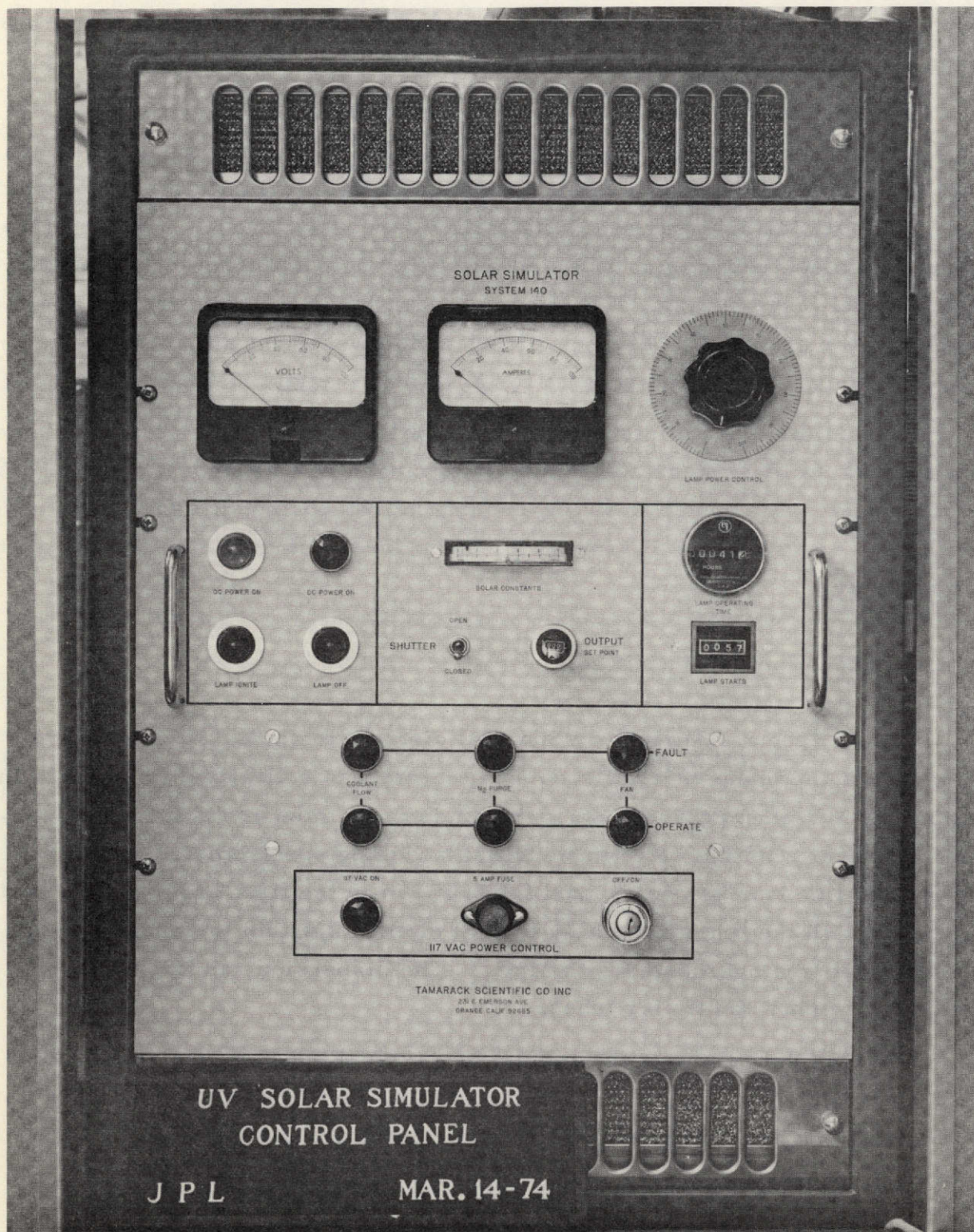


Fig. 2-E.6. Control panel of solar electromagnetic radiation source

Table 2-E. 1. Spectral Analysis of the Solar Electromagnetic Beam

Wavelength Interval, nm	Radiant Flux Density, $\mu\text{W cm}^{-2}$ (10 nm)	Wavelength Interval, nm	Radiant Flux Density, $\mu\text{W cm}^{-2}$ (10 nm)
200 - 210	14	350 - 360	549
210 - 220	19	360 - 370	566
220 - 230	37	370 - 380	557
230 - 240	59	380 - 390	590
240 - 250	108	390 - 400	646
250 - 260	167	400 - 410	677
260 - 270	217	410 - 420	659
270 - 280	263	420 - 430	680
280 - 290	317	430 - 440	687
290 - 300	377	440 - 450	728
300 - 310	407	450 - 460	789
310 - 320	438	460 - 470	864
320 - 330	488	470 - 480	986
330 - 340	522	480 - 490	891
340 - 350	533	490 - 500	898
Integrated radiant flux density (200 - 270 nm) = 0.62 mW cm^{-2} ($\pm 20\%$)			
Integrated radiant flux density (400 - 500 nm) = 7.9 mW cm^{-2} ($\pm 15\%$)			
Radiometer measurements made at the same distance indicated a total radiant flux density of 84.4 mW cm^{-2}			

In order to calibrate the intensity output necessary to achieve the required dose rates, a cone radiometer was used to measure total irradiance at the plane of the microbiological test fixture (Fig. 2-E. 7). A standard curve was then constructed to translate total irradiance (shown as variable output settings on the modulator system (Fig. 2-E. 6)) to solar constants.

Since the critical parameter in the definition of a solar constant was the irradiance interval from 200 to 270 nm, measurements of the beam were made on a routine basis with a UV dose-rate meter high in sensitivity to far UV and low, to infrared. Due to the small percentage of UV in the beam relative to the infrared, it was necessary to place a band-pass filter between the SER source and the detector when making UV measurements. Readings were taken in a manner analogous to the cone radiometer measurements (Fig. 2-E. 7). The routine use of the meter served to indicate any impairment in the system that may have led to a reduction or loss in the far UV portion of the SER.

2. Preparation of Pure Culture Test Samples. Pure cultures of MM71 Proof Test Module (PTM) isolates (see Section III, para. 3. 2. 1. 2 of Planetary Quarantine Semi-Annual Review, JPL Document 900-556, 1 Jan - 30 June 1971), Bacillus subtilis var. niger and Staphylococcus epidermidis (ATCC-17917) were prepared. Sporeforming organisms were sporulated in the liquid synthetic medium of Lazzarini and Santangelo (J. Bacteriol. 94: 125-130, 1967) modified by the addition of 25 mg of both L-methionine and L-tryptophan to one liter of medium. Mature spores were harvested and washed (7 times with sterile distilled water) by centrifugation (10 min at 9750 relative centrifugal force) with final suspension in distilled water. Nonsporeformers were maintained on Trypticase Soy Agar (TSA; BBL) slants. Lawns were prepared by resuspension of the slant growth in Trypticase Soy Broth (TSB; BBL) and inoculation of TSA plates with the suspension. Plates were incubated at 37°C for 48 h, and cells, harvested (on the day they were to be irradiated) by washing the plates with 20 ml of sterile distilled water. The resulting suspension was washed with sterile distilled water 4 times by centrifugation (10 min at 9750 relative centrifugal force).

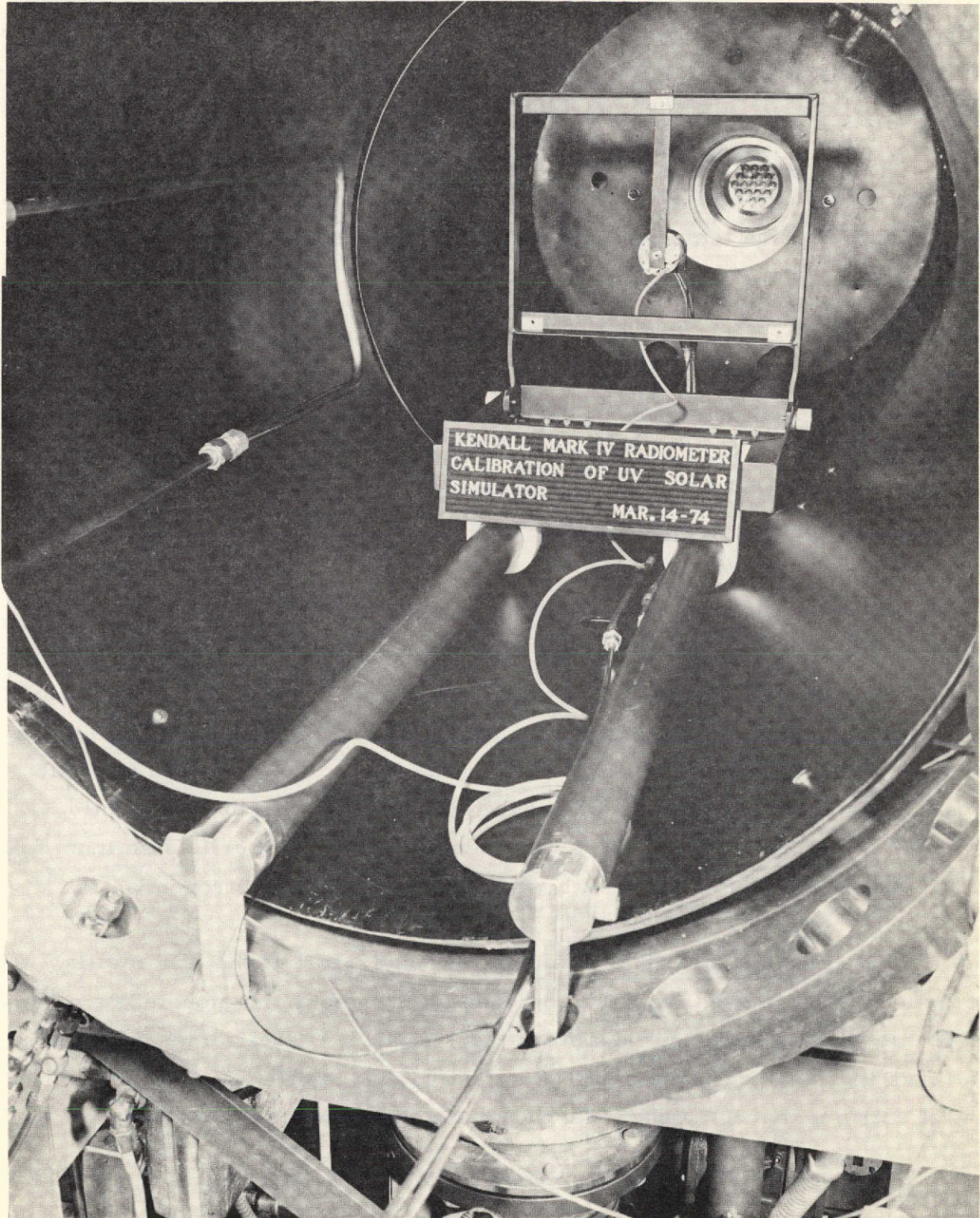


Fig. 2-E.7. Cone radiometer measurement of the solar electromagnetic beam

In order to provide for equivalent inoculums, vegetative cell concentrations were obtained by spectrophotometric means. Absorbance curves were acquired for each organism tested, and inoculum titers were adjusted to between 1 to 2×10^8 viable organisms/ml. Spore suspensions were titered prior to use.

A micropipette was used to inoculate polished (Ref. 2) 6061 aluminum stages with approximately 10^6 viable organisms. The inoculum was allowed to dry in a humidity and temperature controlled room (45^{+5}_{-0} % relative humidity, $21 \pm 2^\circ\text{C}$).

After drying, stages were loaded onto a polished (Ref. 2) 6061 aluminum test fixture (Fig. 2-E.8), per a randomized site selection scheme, and torqued to 15 in-lb. The opposite side of the fixture (Fig. 2-E.9), which during tests faced away from the SER, had film heaters bonded to it that were painted black to maximize emitted radiant energy to the vacuum chamber's LN_2 cold wall. For each organism tested, three inoculated stages were placed on the polished side (sun side) and three, on the painted side (dark side). These served as test and control samples, respectively. In addition, nine thermocoupled stages were torqued to the test fixture (Fig. 2-E.9).

Since the SER test facility was not proximally located to the microbiology laboratory, it was necessary to transport the fixture under controlled conditions. This was accomplished by placing the fixture (as prepared for SER exposure and after SER exposure) into a sealable case with inlet and outlet valves (Fig. 2-E.10). The fixture was then covered with sterile aluminum foil and the box, sealed and purged with extra high purity, dry nitrogen.

3. Irradiation of Test Samples. Upon arrival at the SER facility, the test fixture was removed from the nitrogen environment and mounted on a support frame within the vacuum chamber (Fig. 2-E.11). The frame was situated on a track that enabled placement of the test fixture exactly 30 inches from the point of entry of the light beam into the vacuum chamber.

The nine thermocoupled stages, placed in fixed locations on the test fixture, were then connected to a recorder that provided continuous readout of the fixture temperature throughout the test.

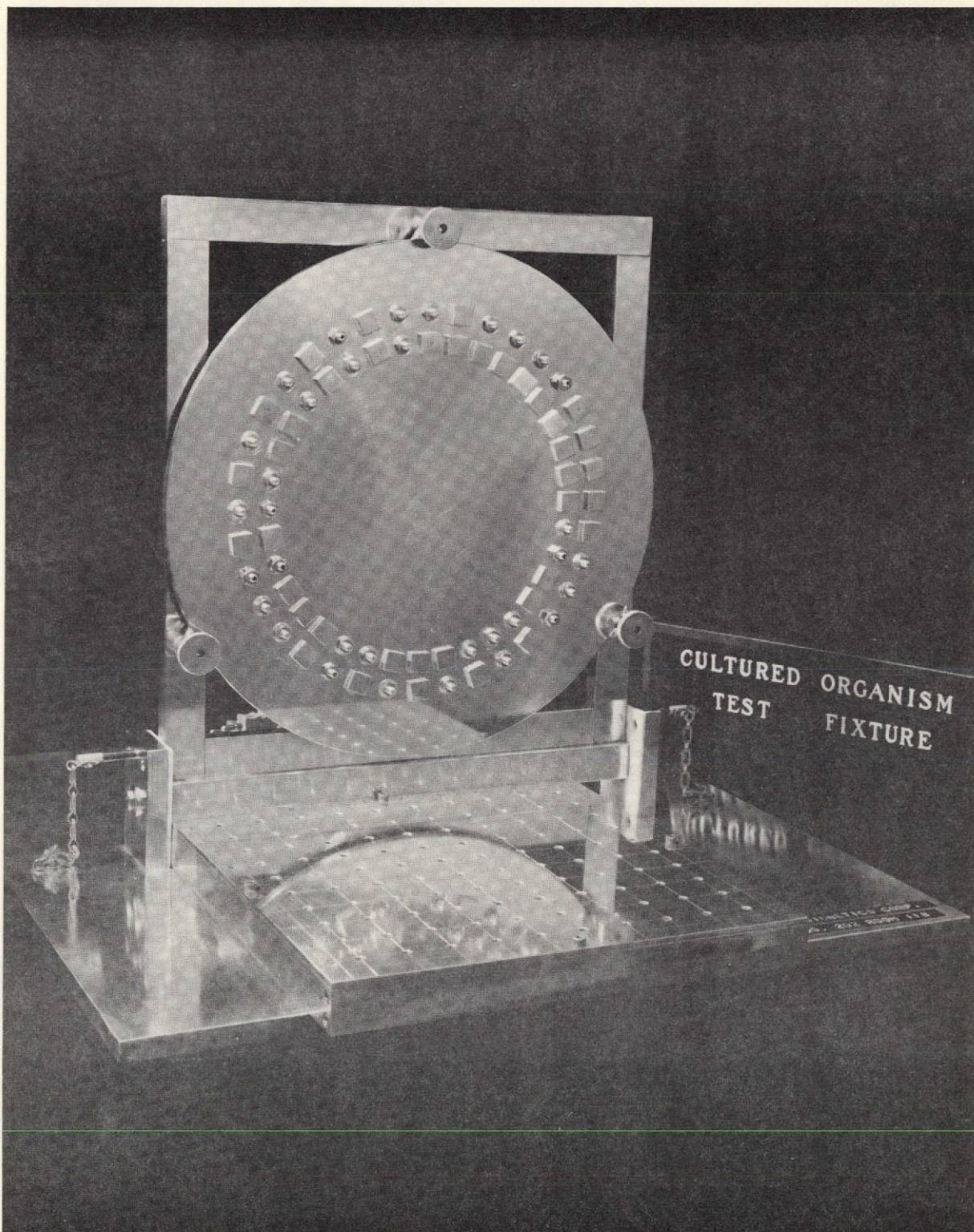


Fig. 2-E.8. Irradiation side of the pure cultured organism test fixture (with inoculation tray in foreground).

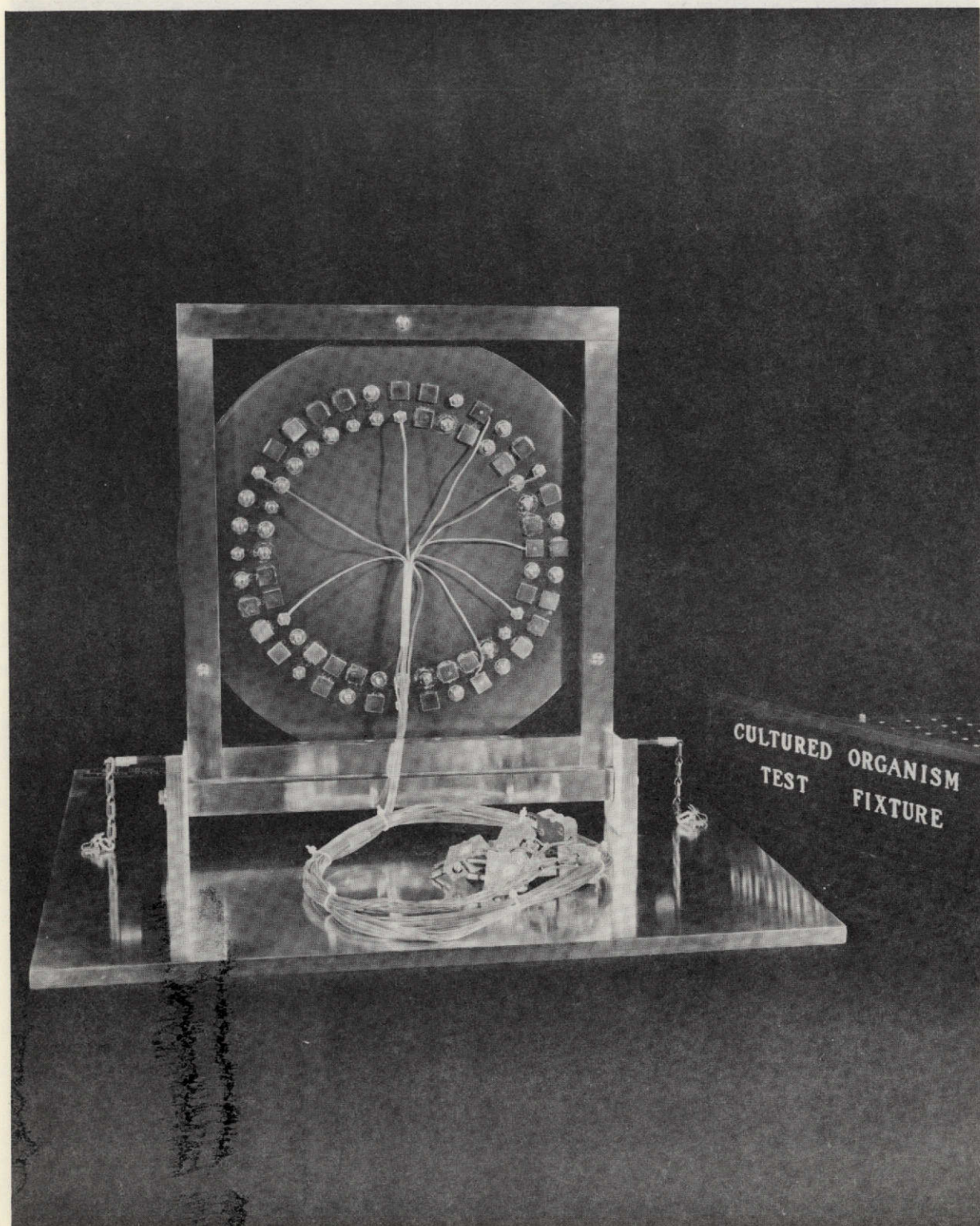


Fig. 2-E.9. Dark side of the pure cultured organism test fixture (shown with thermocoupled stages)



Fig. 2-E.10. Transport case for pure cultured organism test fixture

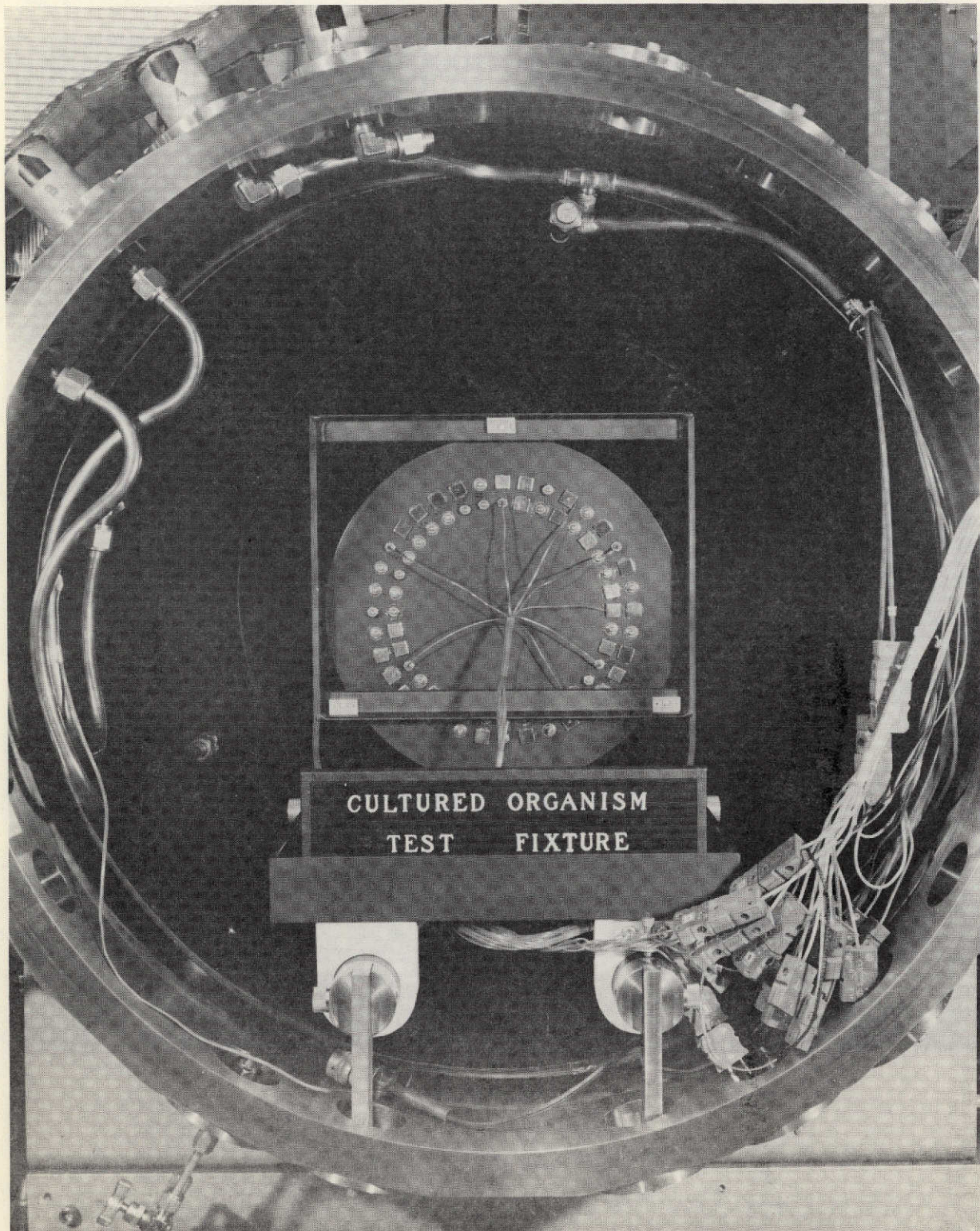


Fig. 2-E. 11. Pure cultured organism test fixture mounted in vacuum chamber

After placement of the fixture, the backside of the LN_2 cold wall was mounted and the vacuum cycle, begun. Due to the time requirements for execution of the vacuum cycle, and to provide for equilibrium of the test organisms to the thermal-vacuum environment; the inoculated fixture was loaded into the vacuum chamber and the vacuum cycle commenced the afternoon prior to the day (morning) of actual irradiation.

Temperature control of the test fixture is accomplished by Kapton film heaters bonded to the dark side and/or the GN_2 - LN_2 system of the vacuum chamber. For tests to date requiring below ambient temperatures, the fixture temperature has been controlled by the latter. This has necessitated activation of the LN_2 cold wall well in advance of irradiation (approximately 12 h for -125°C tests and approximately 6 h for -15°C).

Once the fixture had equilibrated to the required temperature under a vacuum of approximately 2×10^{-6} torr, a shutter mechanism (Fig. 2-E.3) was activated thereby irradiating the fixture. After a timed exposure at a specified dose rate (solar constant), the shutter was closed. The fixture was then brought to ambient conditions, removed from the chamber, and transported (in a GN_2 environment) to the microbiology laboratory for assay.

4. Assay of Test Samples. The fixture, upon arrival in the microbiology laboratory after test exposure, was removed from the GN_2 box and assayed in a rapid, consistent manner. Stages were removed from the fixture, placed individually into tubes containing 10 ml of 0.1% sterile peptone water, and exposed to ultrasonic treatment (25 kHz for 12 min) in an ultrasonic bath. Upon removal from the bath the tube contents were thoroughly mixed prior to 10-fold serial 1.0 ml dilutions and triplicate 1.0 ml platings of designated dilutions with TSA. Vegetative organisms were incubated at 37°C for 48 hours; sporeformers at 32°C for the same period (with the exception of Bacillus subtilis var. niger which was incubated at 37°C). All incubations were performed under dark conditions.

5. Microbiological Data. Dilution plates with 30 to 300 colony forming units (CFU) were enumerated for survivors after the incubation period. Survival fractions were computed for each organism. This was accomplished by ratioing the bacterial population recovered from the three sun side stages

to that, from the three dark side stages (controls). In the formulation of a survival fraction, dark and sun side populations were expressed as geometric means. Results were expressed as "percent survivors."

Initial studies of the effect of SER on microorganisms were conducted with an irradiance level of 0.1 sun at temperatures of -125°C and -15°C . Since temperature did not appear to be a significant factor in these tests, the resultant data shown in Table 2-E.2 are expressed as a function of dose and organism type. The objective of these tests was to scope the sensitivity of the test species to the SER. The first series of tests was run at doses of 2, 4, 6, and 8×10^2 ergs mm^{-2} and found sporeforming populations to have a minimum percent survival of approximately 1% at 800 ergs mm^{-2} while, at the same dose, nonsporeformers exhibited a 0.02% survival. A second series of tests was conducted at doses of 2, 4, 6 and 8×10^3 ergs mm^{-2} . These doses showed reduction in the percent survival of sporeformers to 0.3 at 4000 ergs mm^{-2} however, increasing the dose to 6 and 8×10^3 levels produced no additional reduction in the test populations. A similar situation was evident for nonsporeformers with a percent survival on the order of 10^{-2} exhibited at 2000 ergs mm^{-2} ; remaining for the three higher doses.

Table 2-E.2. Percent Survival of Pure Culture Populations Exposed to Solar Electromagnetic Radiation at 0.1 Sun Irradiance

Dose, ergs mm^{-2}	Sporeformers	Nonsporeformers
200	15	1.1
400	5	0.3
600	1.5	0.2
800	1.1	0.02
2,000	1.1	0.04
4,000	0.3	0.02
6,000	0.4	0.05
8,000	0.4	0.03

The inability to reduce the test populations beyond a certain level, irrespective of dose, seemed to point to the possibility that the fraction of the population surviving irradiation was in fact shielded from the lethal spectra by organisms, and/or, impurities remaining in the suspensions after washing. The former situation appeared to be the predominant case as evidenced by scanning electron micrographs (SEM) of inoculated stage surfaces. It was observed that instances of organism clumping, and hence possible shielding, did occur. The SEM depiction of the surface offers a physical corroboration of the proposed shielding effect. This explanation of the loss of dose effect will be pursued with the objective of estimating that fraction of the test population occluded from the beam by one or more cells, and correlating it with the point on the survivor curve where increasing doses have no further effect on the percent survival.

Preliminary tests were also run at 0.5 sun with doses of 2 and 4×10^3 ergs mm^{-2} which yielded percents survival of 2.1 and 0.2, respectively, for sporeformers, and 0.03 and 0.02 for nonsporeformers.

Although physical measurements indicated a highly uniform beam, they lacked specificity with regard to biologically significant spectra (e.g., far ultraviolet). Therefore, the percent survival data were examined as a function of stage position on the test fixture. Statistical analysis of the data by the Kruskal-Wallis test, an analysis of variance by ranks for two or more independent samples, indicated that at the 1% level of significance ($P = 0.01$) the position of the stage on the fixture had no effect on the percent survival observed (Ref. 3).

Selected data were subjected to linear regression analysis. The results indicated, for most cases, a fair agreement with a logarithmic death model.

2.5.3.3 Future Activities. Additional tests on pure cultured organisms will be performed under 1.0 sun, +70°C and 0.5 sun, -15°C conditions. These tests will provide information preparatory to, and supportive of, the naturally occurring population studies. For the naturally occurring studies, populations will be collected from spacecraft assembly environments on Viking-type solar

cells and exposed to SER under high vacuum conditions without any prior laboratory treatment. Survivors will be estimated in a manner analogous to that used for the pure culture studies.

In light of the plateau phenomenon observed for pure cultured organisms at high doses, efforts will be directed to physically estimating that fraction of the population unavailable to the SER.

2.5.4 References

1. Wang, J., personal communication.
2. Phillips, K. L., "Buffing Aluminum Alloys - Detail Specification for, "Specification No. FS500627, Revision B, Jet Propulsion Laboratory, 1967.
3. Ball, G., personal communication.

2.5.5 Presentations and Publications

None.

SECTION III

POST LAUNCH RECONTAMINATION STUDIES
(NASA No. 193-58-62-03)

Contents

Title and Related Personnel

Subtask A
para. 3.1

POST LAUNCH RECONTAMINATION STUDIES

Cognizance: J. Barengoltz

Associate

Personnel: D. Edgars (Bionetics)

3.1 POST LAUNCH RECONTAMINATION STUDIES

3.1.1 Introduction

The objective of the task is the development of an analytical technique for the evaluation of the probability of the relocation of particles from nonsterile to sterile areas on a spacecraft. The recontamination process is important for all multiple missions with separate microbiological burden allocations for various major spacecraft systems, and critical for life detection experiments that risk contamination from nonsterile components.

The approach has been threefold. The previously developed computer models have had their coding modified such that the thin plate surface effect model (YANG1) after J. Yang's analysis (Ref. 1) and the particle release model (RELEAS) after J. Barengoltz-C. Bauerle (Ref. 2) have been combined into a single unit capable of generating output data distributions for the surface velocity, acceleration, particle removal fraction, particle clearing radii, and velocity probabilities which correspond to the input micrometeoroid parameters. The initial spacecraft geometric description (Ref. 1) has been revised to yield calculational simplifications. The new geometry has been included into the general particle transport computer program. This program combines the YANG1 and RELEAS routines with the new coding that traces the trajectory of released contaminant grains to determine the likelihood of spacecraft recontamination.

3.1.2 Significant Accomplishments

3.1.2.1 Model Geometry Modification. The philosophy of the particle transport has been substantially altered from the geometric discussion begun in Reference 1, where the typical spacecraft/lander was represented as a combination of polygonal sections. The present approach utilizes a combination of truncated right circular cones for the body and plane sections for the solar panels.

Figure 3-A.1 denotes the cross-sectional configuration of the typical spacecraft, with the new model drawn as heavy lines around the spacecraft structure. This approximation to a realistic geometry lends itself to analytical computer techniques more readily than the previous model. Except for the solar panel regions which are treated as finite plane sections, the radial symmetry in the x-y coordinate plane enables closed form approximations for the force fields and grain localization algorithms.

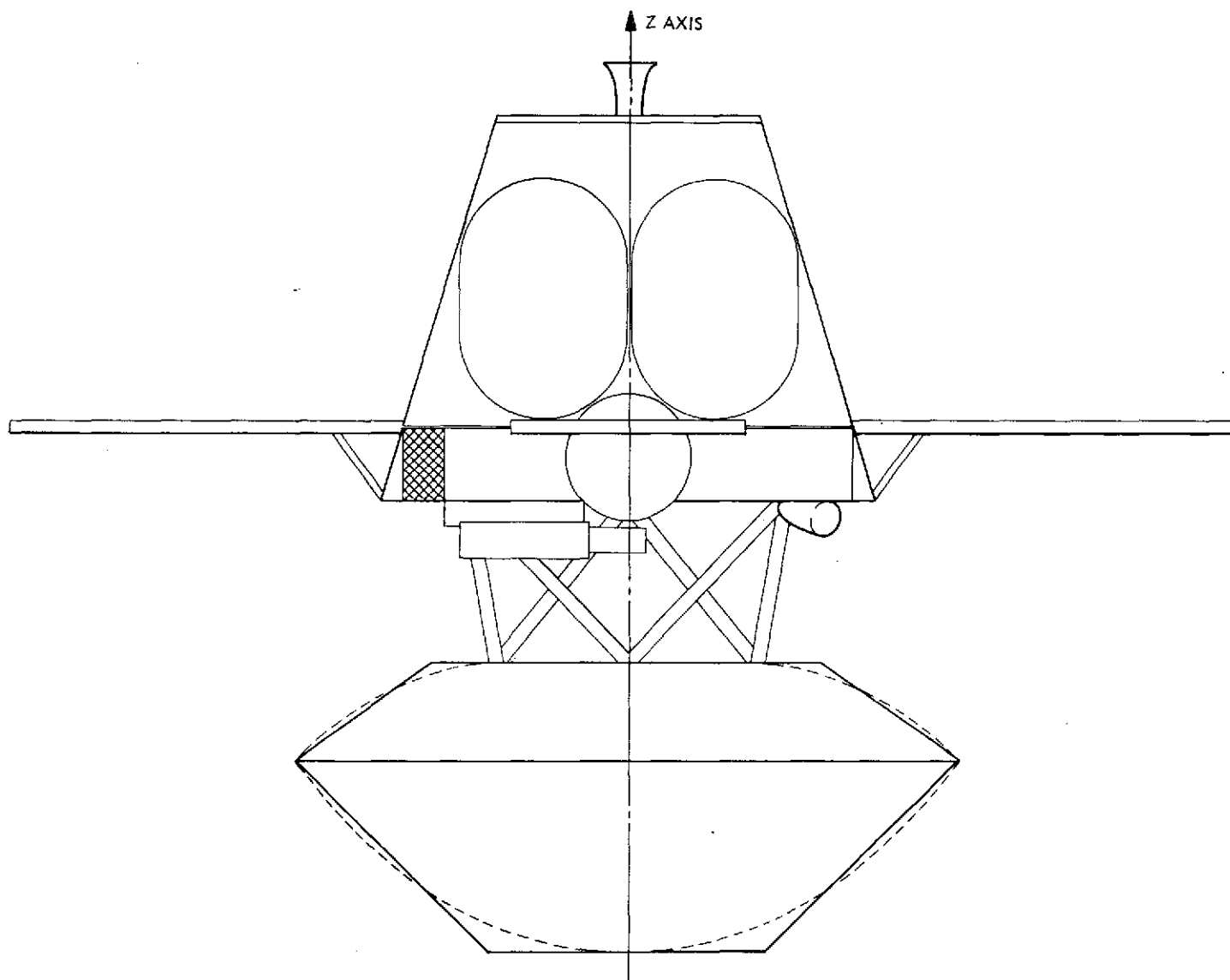


Fig. 3-A.1. Typical spacecraft cross-sectional geometry with cone spacecraft model superimposed

We have represented the spacecraft in quarter sections (Fig. 3-A.2). The assumption has been made that the z-axis maintains parallel tracking with the sun vector. Therefore, from geometric symmetry, motion in the first octant is sufficient to fully define three dimensional motion for free particles in the vicinity of the spacecraft.

3.1.2.2 Overall Model Integration. The recontamination analysis is well suited for a Monte Carlo statistical treatment. Monte Carlo is a semi-sophisticated computer coin flipping session where random combinations of the necessary input parameters are selected and each of the many subensembles are analyzed with a record kept of the results. The purpose of the randomness in these selections is aimed at extracting useful information from the statistical trends which evolve as the overall ensemble increases. For example, the use of Monte Carlo relates to the fact that, although the kinematics of particulate motion is well known, we must consider the ensemble of combinations or distributions in mass, velocity, location of impact, etc. The approach is that of a nested (or double) Monte Carlo (MC). The graphical representation in Fig. 3-A.3 outlines the conceptual computer logic flow within the general surface effect-particle transport model. Three of these block elements contain the coding previously developed (Ref. 2) and have the symbol (JBB) on their label.

The outer MC loop operates on the surface effect subroutine (YANG1-THINPL) by choosing a meteoroid mass and velocity from the presently accepted distributions (Ref. 3). The data then causes the YANG1-THINPL code groups to generate the surface response distributions for the peak acceleration (over time) vs. range from meteoroid impact and the velocity of the surface at peak acceleration for the same ranges.

Subroutine RELEAS calculates the removal fractions for the corresponding range values, the effective clearing radius and velocity distribution as a function of grain size.

The outer MC loop generates a sufficiently large set of possible parameter combinations to warrant an inner MC loop that operates repetitively on this ensemble. In this loop, the initial location of the ejected grain (equivalently, the meteoroid impact), the grain size and its initial velocity are selected.

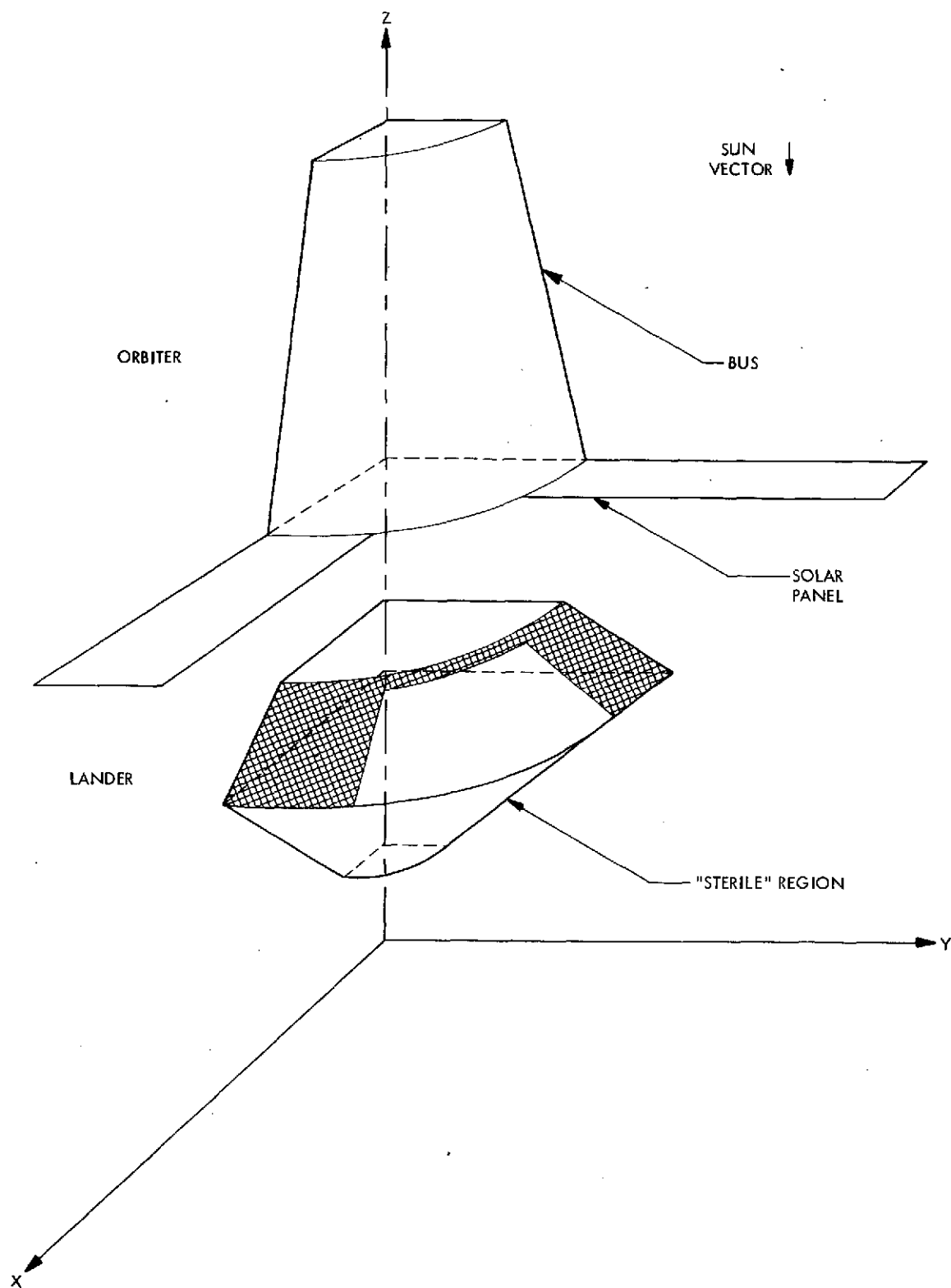


Fig. 3-A.2. Conceptual view of cone spacecraft model in the first octant (x, y, z all positive) with illuminated and shaded areas indicated

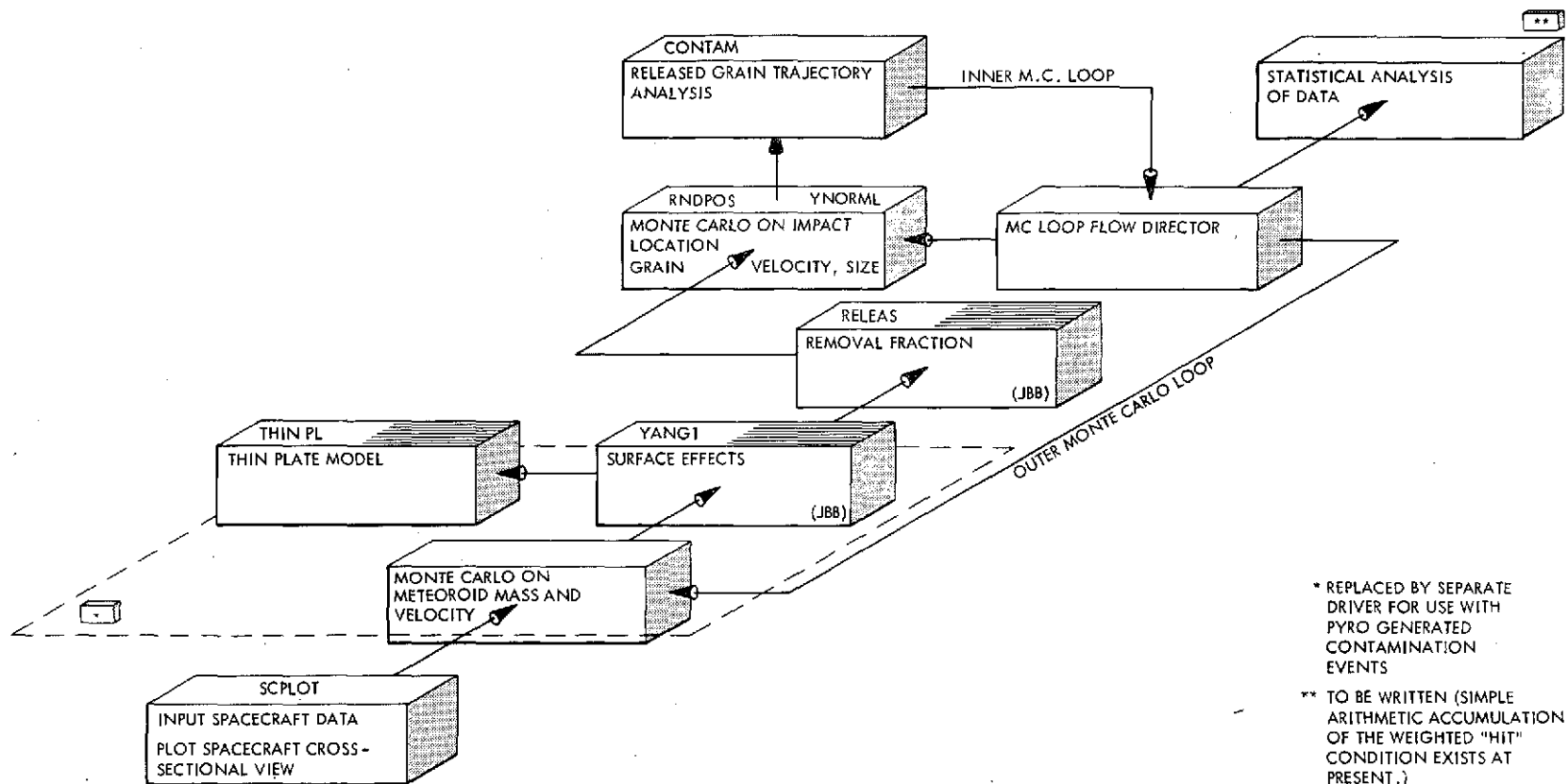


Fig. 3-A.3. Conceptual block diagram of the recontamination software

The approximately isotropic nature of the micrometeoroid flux existing in the interplanetary space (Ref. 3) traversed by the spacecraft allows the correlation of the thin plate analysis and the surface of the spacecraft. Except for the lander region of the chosen spacecraft geometry, all points on the surface are equally likely to be selected as the initial ejecta location. The present model does not permit trial cases where the initial impact location is on the "sterile" spacecraft areas, and omits the interconnecting superstructure between the spacecraft subsections. Eventually, a cylindrical surface enclosing this latter region will be included.

Once the position has been randomly specified (RNDPOS) for the particular trial, another section of computer coding determines the surface outward normal vector (VNORML) and presumes that the grain is ejected along this direction vector. The Monte Carlo selection from YANG1 and RELEAS produces a likely initial velocity magnitude for the grain size selected, allowing the stepwise trajectory analysis to commence. The physical kinematics are straightforward, requiring the calculation of the significant force terms which alter the straight line paths for the ejecta, such as electric fields. The trajectory analysis is accomplished with the code group named CONTAM.

The velocity and position of the particle are traced incrementally on each MC pass until a definite conclusion may be inferred, with attention given to: sun/shade conditions, whether the particle escapes from the vicinity of the spacecraft, whether the particle leaves the first octant (in which case the position and velocity are translated back to this coordinate region), and whether it recontacts any part of the spacecraft. The position is monitored in order to determine whether the particle recontacts any portion of the spacecraft, which would be considered a recontaminating event.

3.1.3 Future Activities

The development of the electric field algorithm will be further tailored to conform to the newly adapted spacecraft geometry.

The statistical post-processor will be written to interpret the output results of the present Monte Carlo herein described.

The program integration will be continued.

The present computer model will be adapted to account for the recontamination events due to pyro firing events.

An activity to assess the applicability of the present recontamination analysis to space shuttle and sample return missions will continue. Identification of new areas requiring analysis will continue.

3.1.4 References

1. Planetary Quarantine Annual Review, Space Technology and Research, July 1971 - July 1972, JPL Document 900-597, February, 1973.
2. Planetary Quarantine Semi-Annual Review, Space Research and Technology, July 1973-December 1973, JPL Document 900-655, April, 1974.
3. "Meteorite Environment Model - 1970 (Interplanetary and Planetary)," NASA Monograph SP8038, October, 1970.

SECTION IV

SPACECRAFT CLEANING AND DECONTAMINATION TECHNIQUES
(NASA No. 193-58-63-02)

Contents

Title and Related Personnel

Subtask A
para. 4.1

PHYSICAL REMOVAL OF SPACECRAFT
MICROBIAL BURDEN

Cognizance: H. W. Schneider

Associate
Personnel: E. Roos (Bionetics)

Subtask B
para. 4.2

EVALUATION OF PLASMA CLEANING
AND DECONTAMINATION TECHNIQUES

Cognizance: S. Fraser (Boeing)
D. Taylor

Associate
Personnel: R. Olson (Boeing)
W. Leavens (Boeing)

4.1 PHYSICAL REMOVAL OF SPACECRAFT MICROBIAL BURDEN

4.1.1 Subtask A Introduction

Present planetary quarantine constraints for flyby and orbiter vehicles require maintaining the microbial burden on the spacecraft below a certain critical level. State-of-the-art clean room facilities and contamination control techniques do not assure that this critical level can be maintained throughout necessary assembly and test operations.

Previous activities under this task concentrated on the study of vacuum techniques with and without the use of a brush, and on blow cleaning by means of extra dry, high-purity nitrogen. A test device was developed that would allow for the simulation and evaluation of these techniques under controllable conditions with an observation of the behavior of the test particulates under a 100X microscope. Studies to establish the mechanical properties of candidate brush-materials were conducted in the JPL materials test laboratory. As described in detail in JPL documents 900-597 and 900-636, the following problems were identified.

- 1) Brushes efficiently detach particles of the smallest detectable size ($2-3\mu\text{m}$) but entrainment into the flow is extremely poor. The flow resistance across the bristles is very high, and flow velocities near the surface are too low to accomplish entrainment and transport of the detached particles into the vacuum system. Consequently, the bristles quickly become saturated with particles and the brush becomes a particle source rather than a cleaning tool. To avoid this, frequent cleaning of the brushes during or between uses would be necessary. For biological applications periodic biological decontamination may be appropriate.
- 2) Vacuum flow alone (without the aid of a brush) efficiently detaches and removes particles larger than $10\mu\text{m}$ size if, a) the surface is dry, b) flow velocities are near critical (choked flow) and, c) the nozzle stand-off distance from the surface is not larger than $150-200\mu\text{m}$. The removal efficiency drops off sharply at larger stand-off distances.

- 3) Blow cleaning efficiently removes particles greater than $5\mu\text{m}$ in size from normally dry (i. e., $\leq 50\%$ RH) surfaces at pressures on the order of 30 psig across the blow nozzle. Pressures on the order of 50 to 80 psig are necessary to efficiently remove particulate matter smaller than $50\mu\text{m}$ from oily (fingerprinted) surfaces.
- 4) The cleaning of moist surfaces was very inefficient under all of the conditions tested.
- 5) Natural sable hair (presently used in spacecraft cleaning brushes) has a very low fatigue resistance and tends to break up and to shed during use. Dupont Felor fiber was found to have the most acceptable properties as a substitute material for cleaning brushes, particularly in regard to a utilization of the fiber material on motorized (rotary or oscillating) brushes.

4.1.2 Approach

The primary objective during this reporting period was to reduce the blow pressures required for efficient blow cleaning. Because of the encouraging results obtained in earlier tests, emphasis was given to the evaluation of "jet-blocking" techniques by means of a rotary mask. Investigated also were methods that would induce pulse flow and jet oscillation by means of resonating transfer tubes, by blowing against wedges and vibrating rods, as well as the application of sonic and ultrasonic waves. The test apparatus was essentially the same as the one described in earlier reports, modified to accommodate additional components as needed to produce the described pulse effects in a controllable and repeatable manner. The various set-ups used are shown and explained in Figs. 4-A.1 through 4-A.7.

As before, all tests were conducted with glass beads and with standard test dust, GM 1543637, seeded on 5×5 cm optical glass, fogged by chilling (where indicated) to simulate accidental moisture condensation of the surface. The room environment was controlled and varied between $25\text{-}28^\circ\text{C}$ and $45\text{-}55\%$ RH. A newly designed seeding apparatus was used which allowed a more controllable preparation of the test samples in the desired size ranges and concentration (see Fig. 4-A.8).

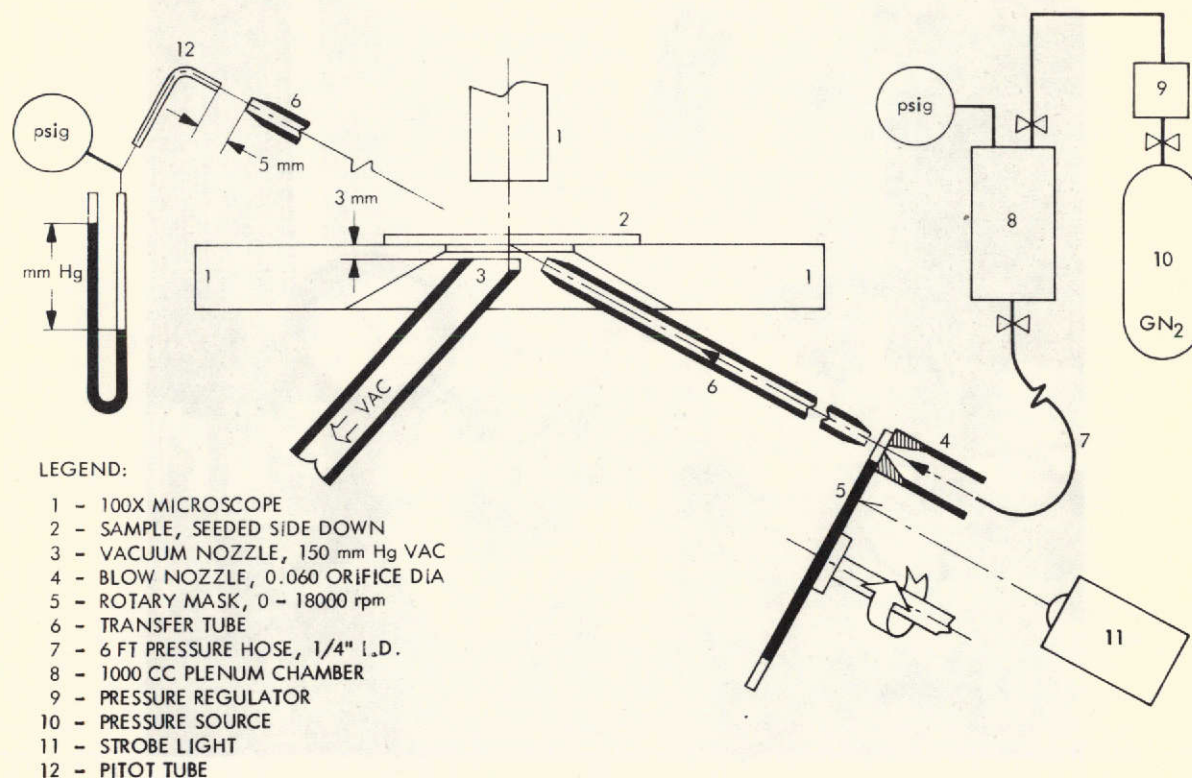
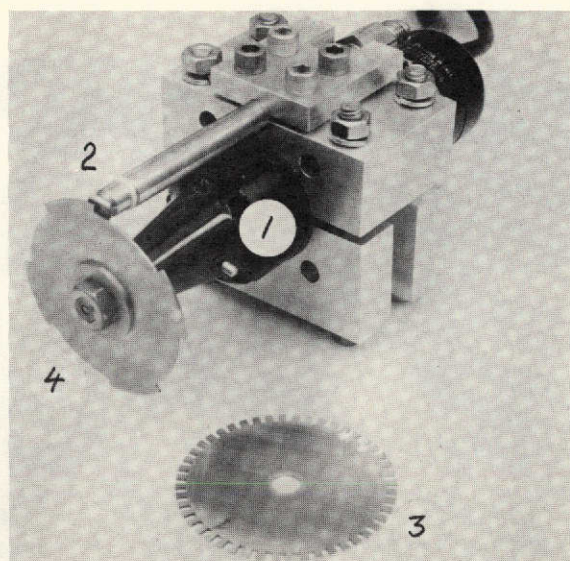


Fig. 4-A.1. Schematic of rotary mask test set up



- | | |
|----------------|------------------------|
| 1. Motor | 3. 48 Slot Rotary Mask |
| 2. Blow Nozzle | 4. 4 Slot Rotary Mask |

Fig. 4-A.2. Rotary mask pulse generator assembly

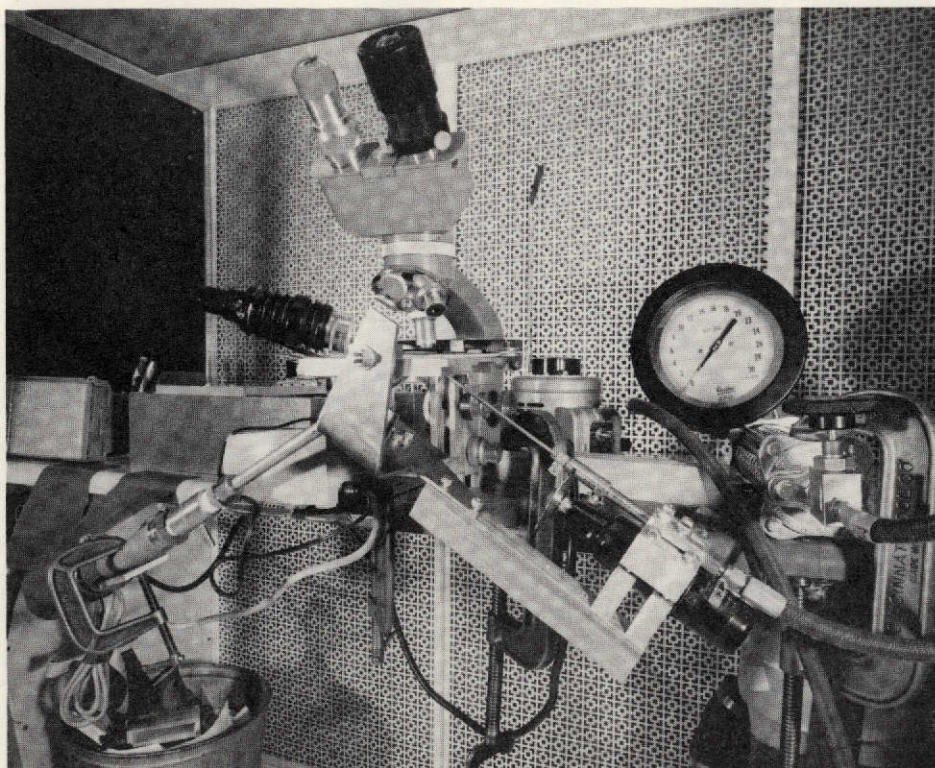


Fig. 4-A.3. Pulse blow test set up (shown with 12 inch transfer tube installed between pulse generator and sample)

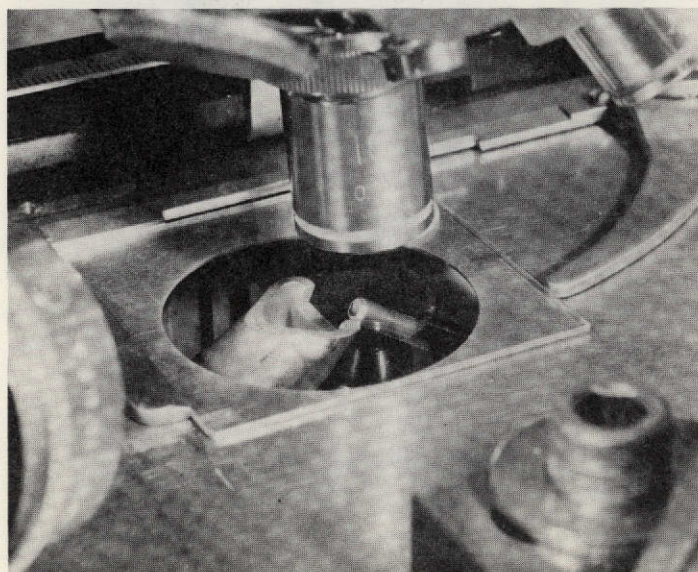


Fig. 4-A.4. Pulse blow nozzle arrangement as viewed through sample plate. Left: vacuum nozzle; Right: transfer tube from generator

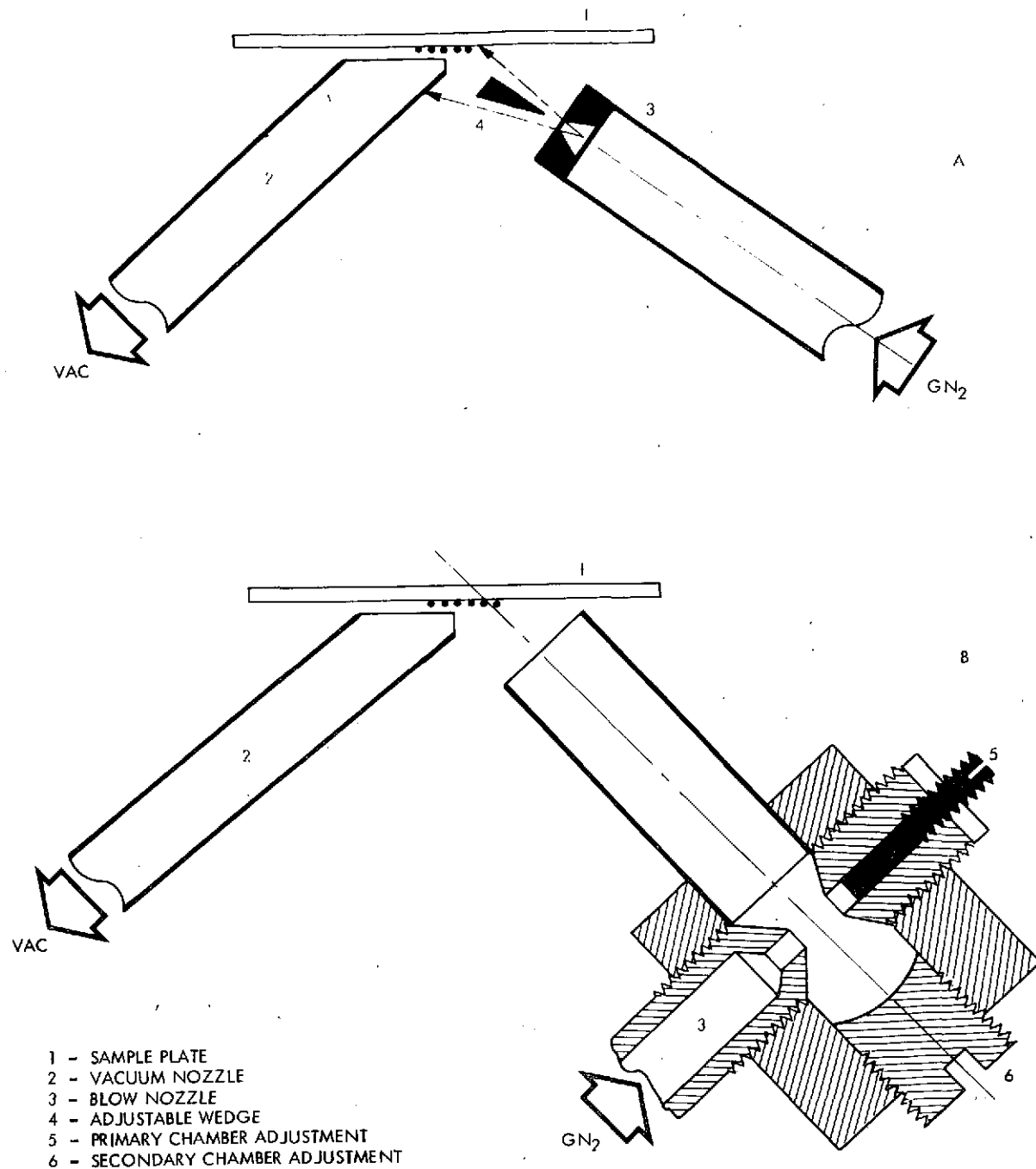


Fig. 4-A.5. Schematic of ultrasonic generator set up

A Wedge generator
 B Hartmann generator } *

*Goldman, R., Ultrasonic Technology, 1962.

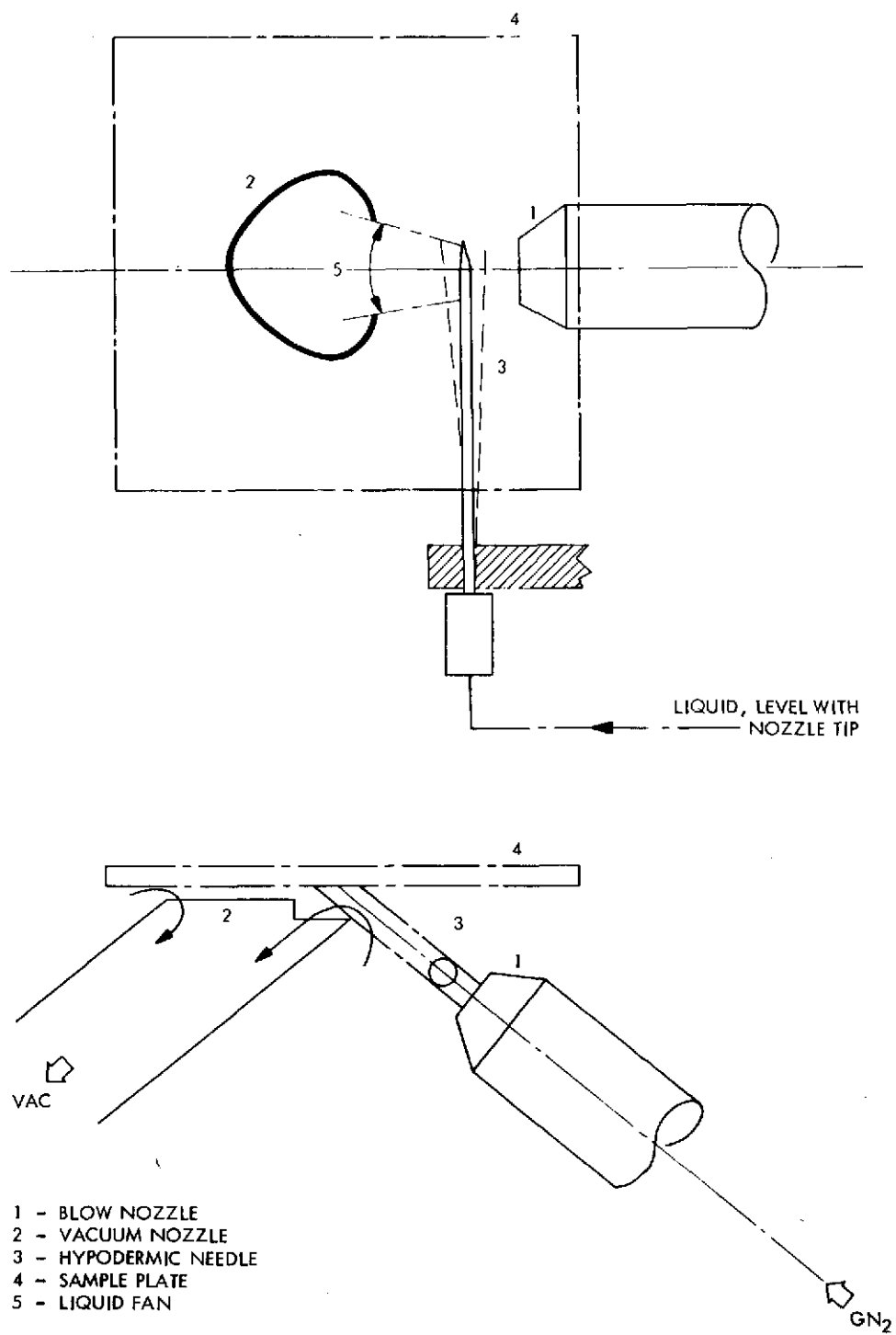


Fig. 4-A. 6. Schematic of oscillating rod set up

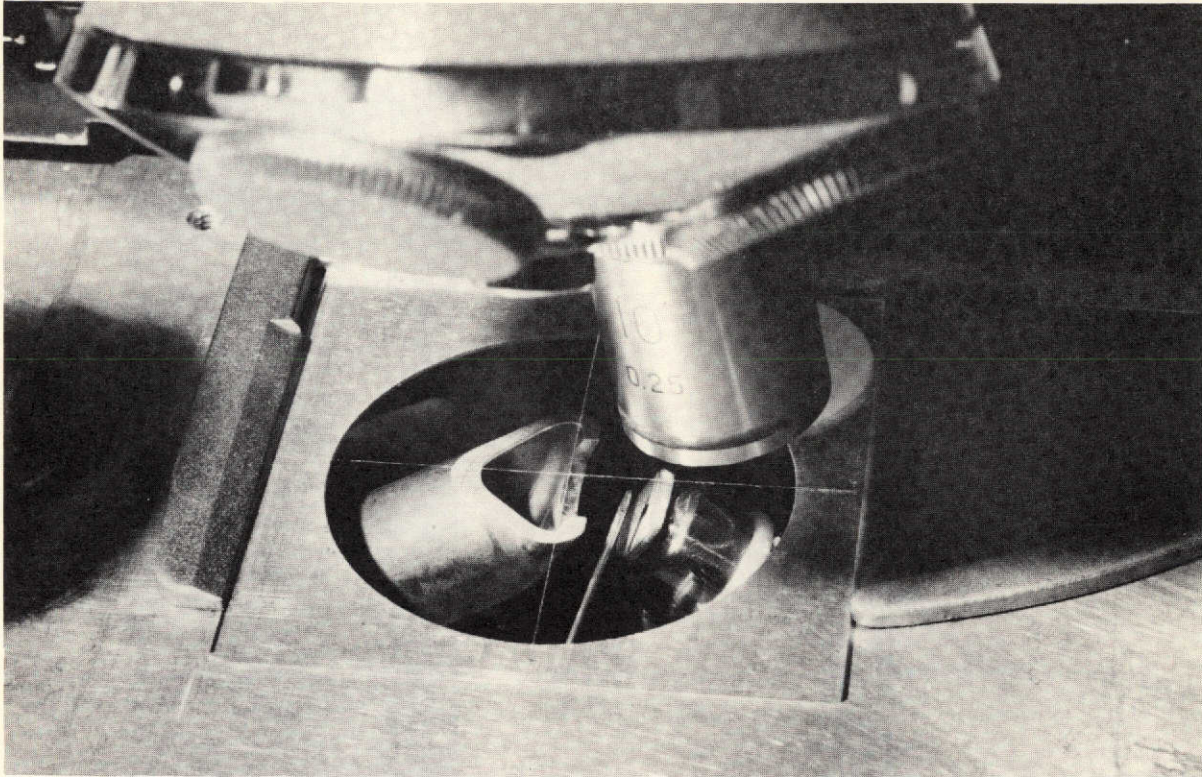


Fig. 4-A. 7. Oscillating rod set up. In experiment shown, hypodermic needle is used as the rod.

The tests were accomplished by laterally sweeping the sample normal to the impinging jet. The data discussed represent removal efficiencies, η , in terms of particles present after the test, in relation to the original count taken prior to the test from the same $1/2 \times 1/2 \text{ mm}^2$ control area in the sample center. Variations between samples were accounted for by means of a correction factor obtained from a reference vacuum sweep over the sample prior to use. Unless indicated otherwise, two determinations per data point were made, and a new sample was prepared for each test. The blow angle was 32 degrees against the sample plane for all tests.

4.1.3 Significant Accomplishments

4.1.3.1 Jet Blocking Techniques. Initial observations made during tests with a 48 slot rotary mask indicated that a certain number of particles not

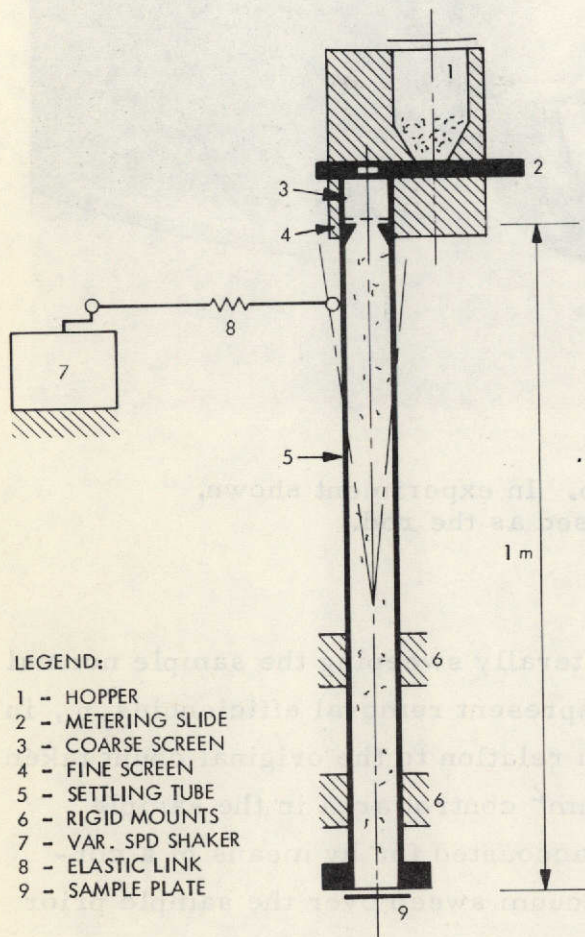


Fig. 4-A.8A. Schematic
seeding apparatus

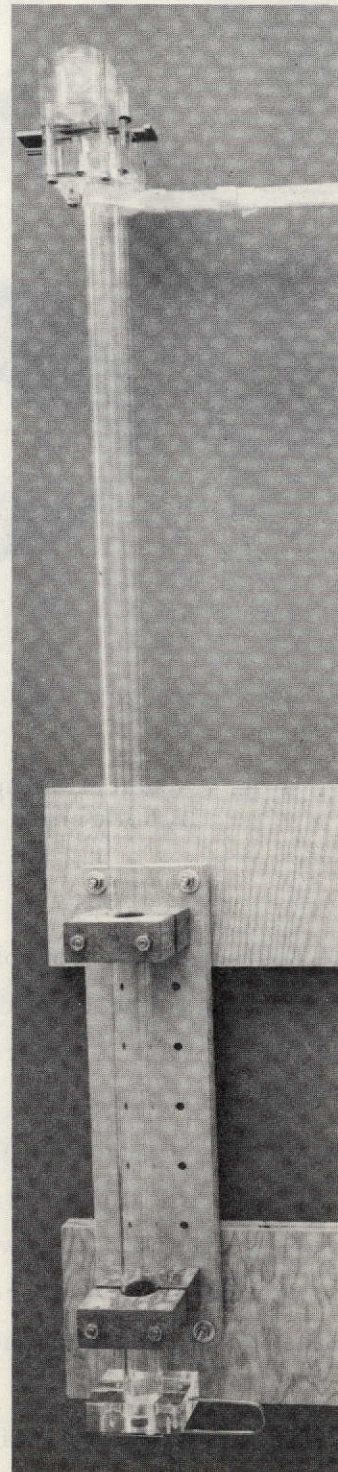


Fig. 4-A.8B. Dust seeding
apparatus

removed by a steady state jet would detach whenever the jet flow was temporarily blocked. Particle detachment would stop after a few pulses regardless of frequency and duration of flow. If the sweep was started from the highest producible frequency (15,000 Hz) and swept down, only a very few particles would detach, which was mainly attributed to mechanical systems vibrations. No further motion could be observed on the sample surface until shortly before the mask came to a stop (motor stalling point). This was in contrast with earlier conclusions which expected best removal efficiencies (if any) to occur at frequencies that would produce highest sound pressure levels (Fig. 4-A. 9). Due to this phenomenon a 4 slot mask was manufactured which would allow a more accurate control of the frequencies below 1,000 Hz.

The data obtained from a series of efficiency tests at critical nozzle pressure (15 psig) conducted with the 4-slot mask on 5-10 μ m glass beads (see Fig. 4-A. 10) substantiated the above observation in a quantitative manner. Best efficiencies were achieved at the lowest possible blocking frequency which could only be produced by slowly turning the mask by hand, and at a frequency about 40 Hz, which is the breaking point of the motor.

Figure 4-A. 11 shows the effect of plenum pressure on the removal efficiency of 5-10 μ m glass beads for the minimum pulse frequencies producible with the 4 and the 48 slot mask. It can be seen that the previous statement still holds. The lower frequencies are more efficient. In either case, marked improvement of pulse blow over steady state blow at the surface is evident. The peaks shown for the low frequency (dashed curve) between 10 and 15 psig, and for the high frequency (solid curve) test about 5 psig, are believed induced by system pressure resonances typical for the set up used (see Fig. 4-A. 1).

The reason why slow pulses produce better removal efficiencies can be explained with the fact that it takes time (a) to build up a boundary layer (it is the initial pulse that produces most of the drag on the particle before the boundary layer has been formed), (b) to accelerate the nozzle flow and (c) to replenish the gas in the pressure hose between pulses. As can be seen from Fig. 4-A. 12 (top), at a given plenum pressure, the mean impingement pressure (pitot pressure) of the jet drops rapidly as the pulse frequency goes up. Due to these considerations all further tests were made with the 4-slot mask at the minimum producible stable pulse frequency just above the motor breaking point.

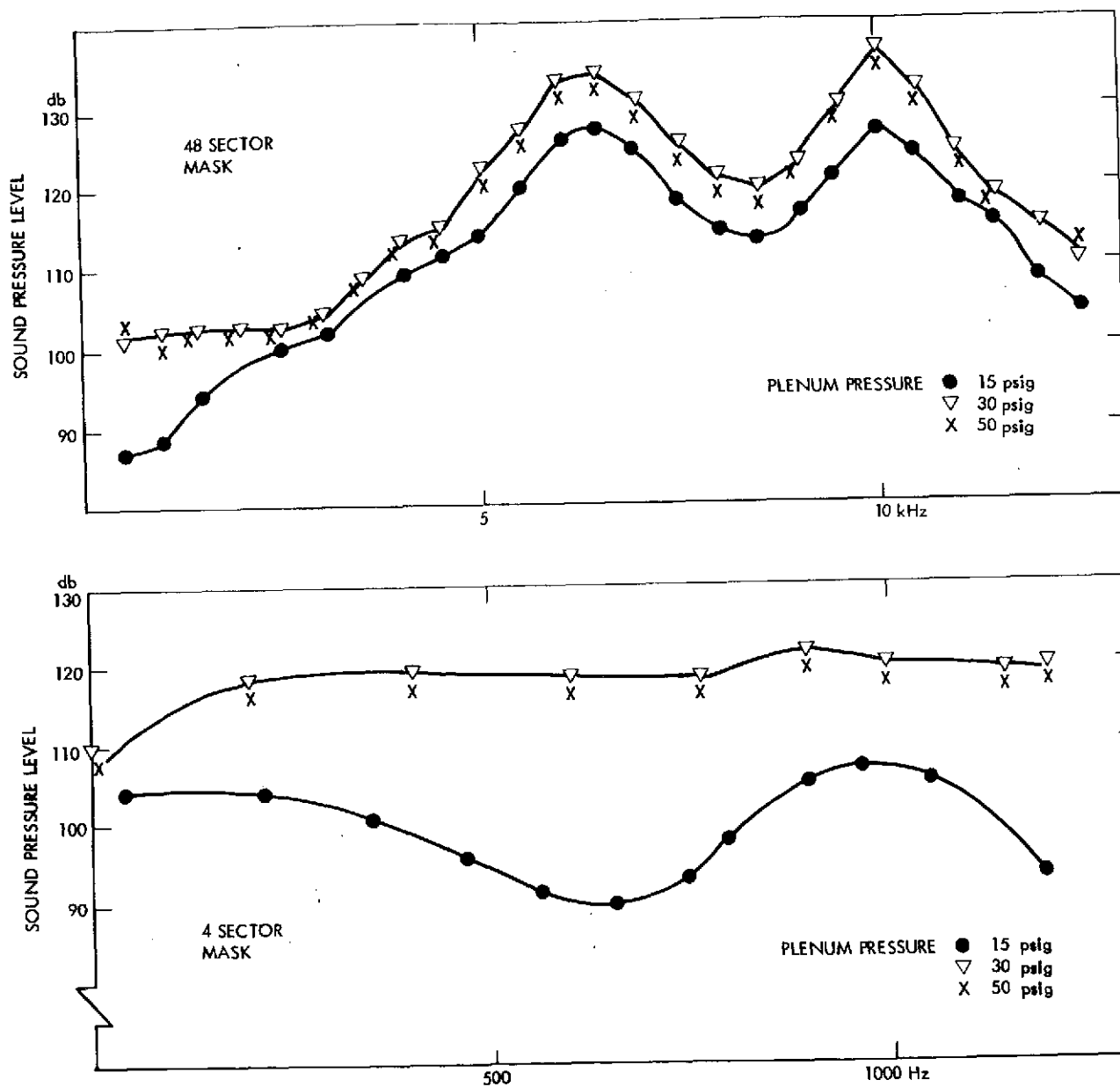


Fig. 4-A.9. Pulse frequency vs sound pressure level, 5 mm from mask

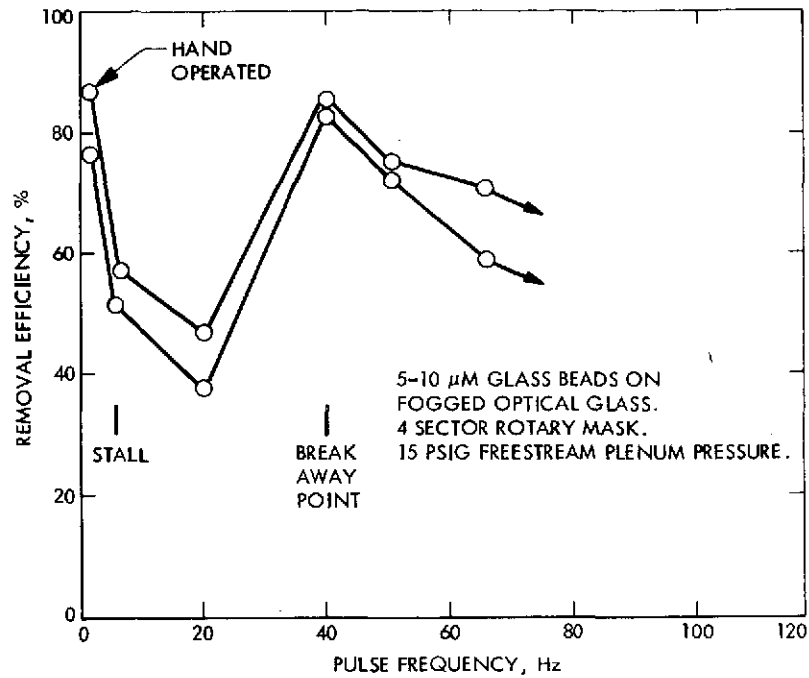


Fig. 4-A. 10. Effect of pulse frequency on removal efficiency

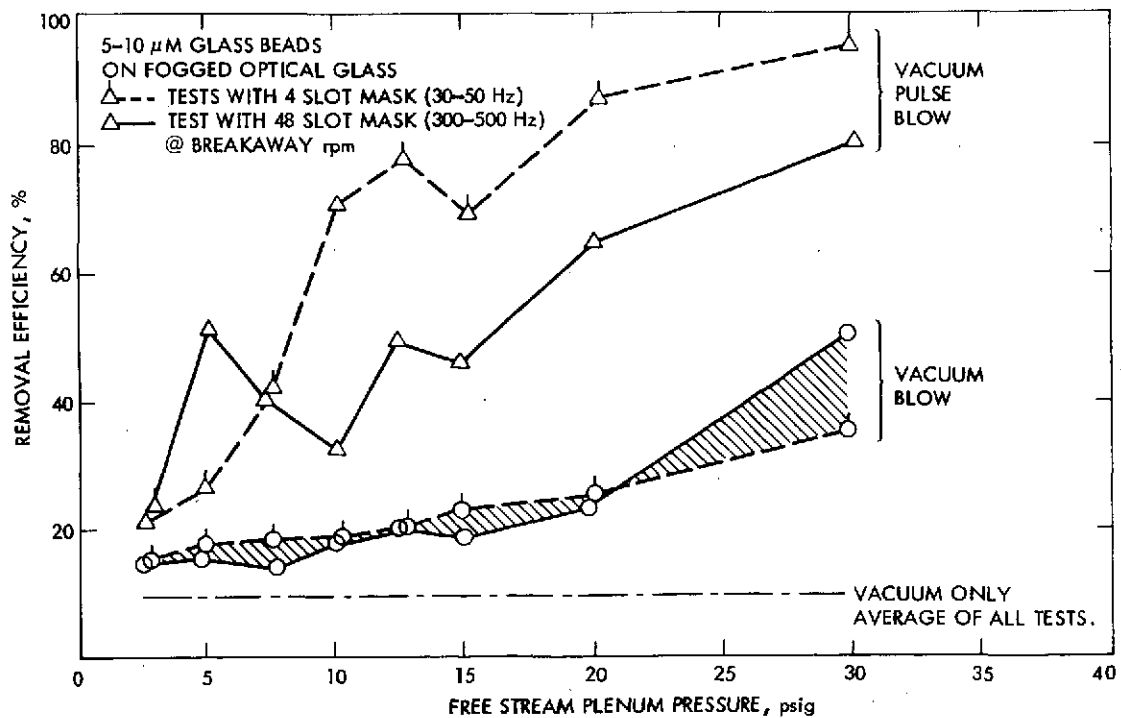


Fig. 4-A. 11. Effect of plenum pressure on removal efficiency comparison of 4 and 48 sector mask at breakway RPM

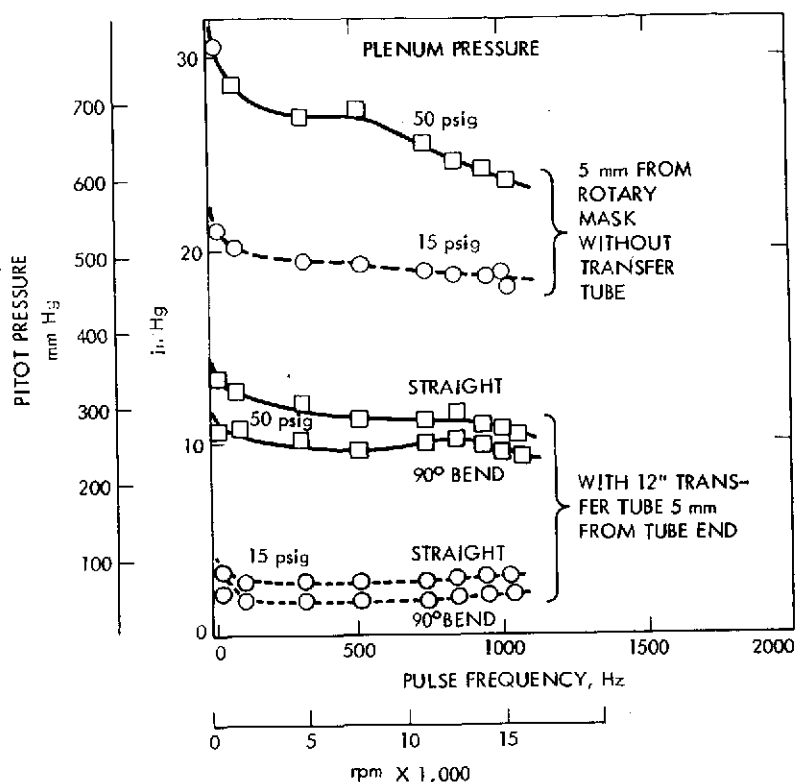


Fig. 4-A.12. Effect of pulse frequency on impingement pressure

Figure 4-A.13 shows removal efficiency data obtained with GM No. 1543637 standardized test dust on fogged optical glass selectively seeded for the indicated size ranges. The efficiency improvement that can be achieved with pulse flow is not as strong as indicated for glass beads, but is evident for all particle sizes tested. A plenum pressure of no more than 15 psig (critical expansion) appears to be the logical choice for cleaning because, as can be seen from Fig. 4-A.14, higher pressures do not improve the mean impingement (pitot) pressure when periodically blocked. Disintegration of the jet and boundary layer growth on the surface are believed the main reasons for this.

As described in Para. 4.1.2, a new sample was prepared for each test. Each test consisted of a succeeding application of one vacuum sweep, followed by a steady state or pulse blow. To eliminate the potential effects of the reference vacuum sweep on the succeeding test (repeated cleaning), a series of tests were conducted at a constant nozzle pressure of 15 psig, where each sample was only tested once, using the indicated method. These tests

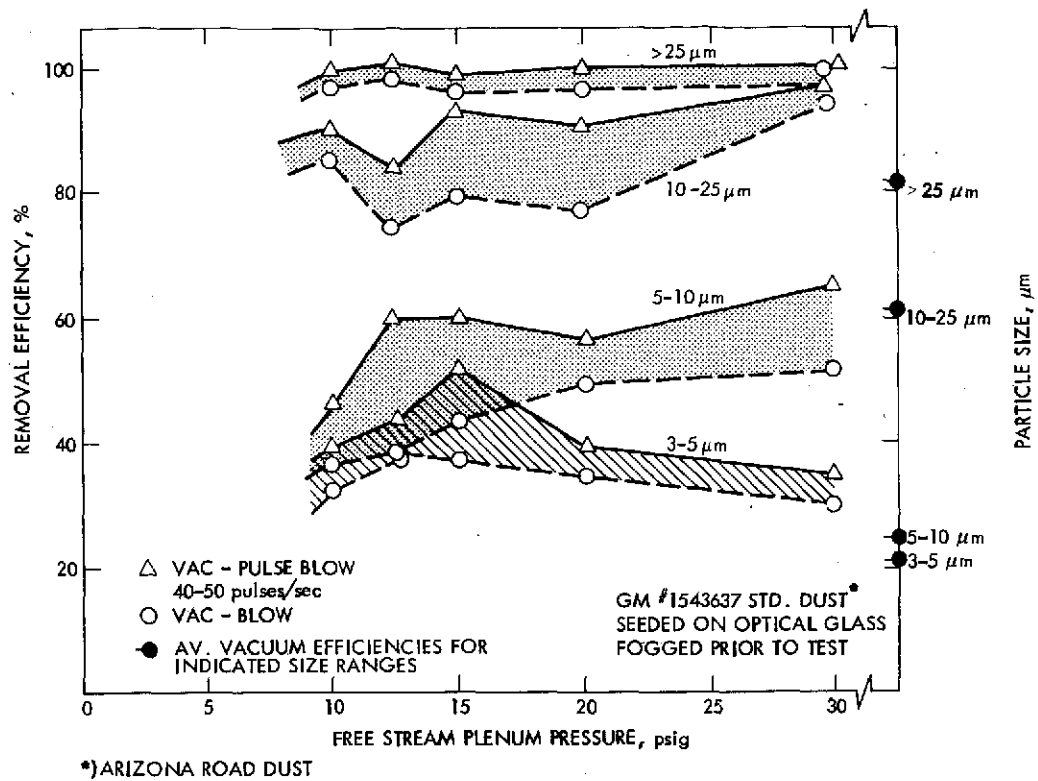


Fig. 4-A.13. Removal efficiencies vs plenum pressure and particle size

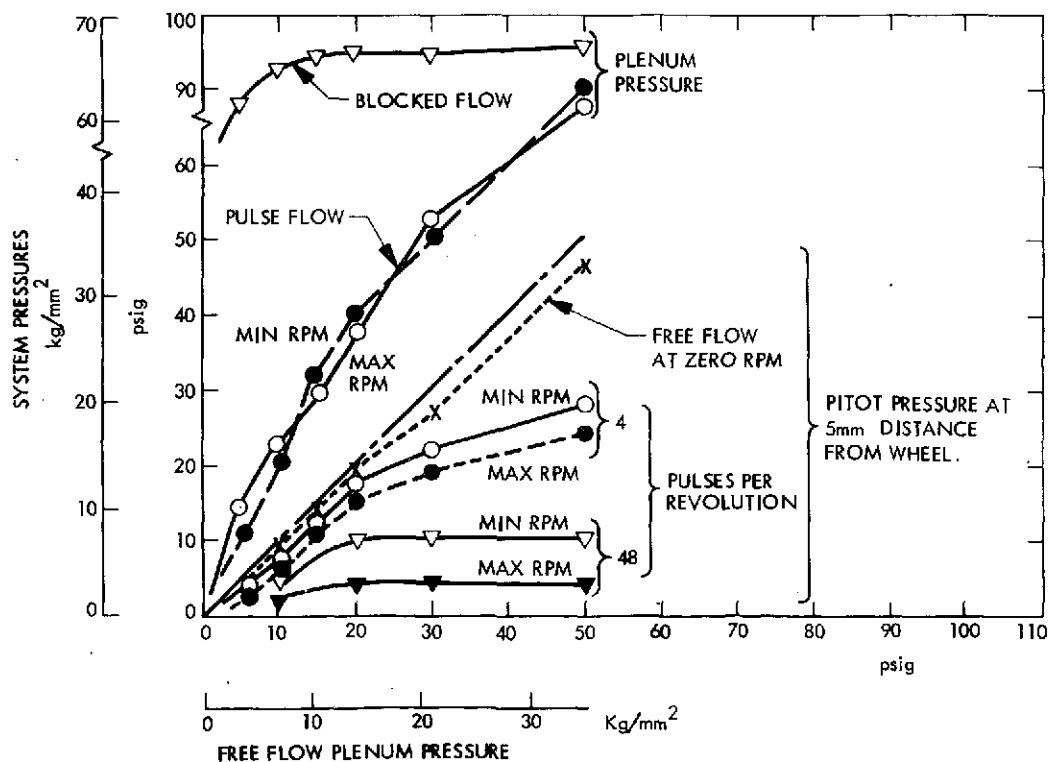


Fig. 4-A.14. Typical pressure characteristics of test apparatus without transfer tube

were conducted on fogged and on dry samples at normal and at relatively high, relative humidity conditions, with and without the use of a 12 inch long transfer tube. The results are shown in Fig. 4-A.15 and 4-A.16. It can be seen from Fig. 4-A.15 that the conclusions made from the preceding tests still hold. The improvement in removal efficiency of the pulse over a steady state blow is pronounced for all conditions tested.

The efficiencies achieved with the 12 inch transfer tube are 30 to 50 percent lower than the ones obtained without it. This was attributed to typical drawbacks of the existing test set up which, originally, was not designed to be used with a transfer tube. As can be seen from Fig. 4-A.12 and 4-A.14, the resonance response of the tube is very flat and the pitot pressure at the tube outlet could not be raised above 10 psig. This is attributed to the pressure losses caused by the normal shock at the tube inlet as well as by frictional attenuation inside the tube.

Figure 4-A.16 shows the results obtained from an identical series of tests conducted specifically to demonstrate the effect of surface conditions. On dry samples, pulsing did not noticeably enhance detachment except for the smaller particles below 5 μm . The efficiency improvement due to pulsing,

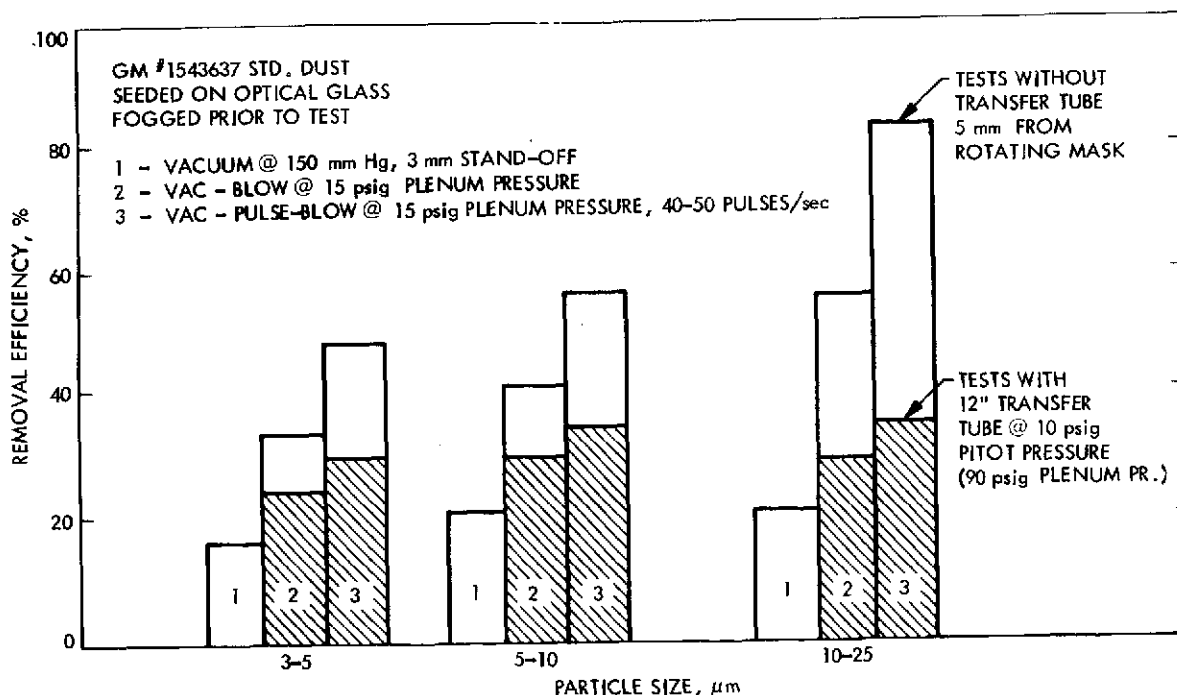


Fig. 4-A.15. Removal efficiency vs particle size with and without transfer tube

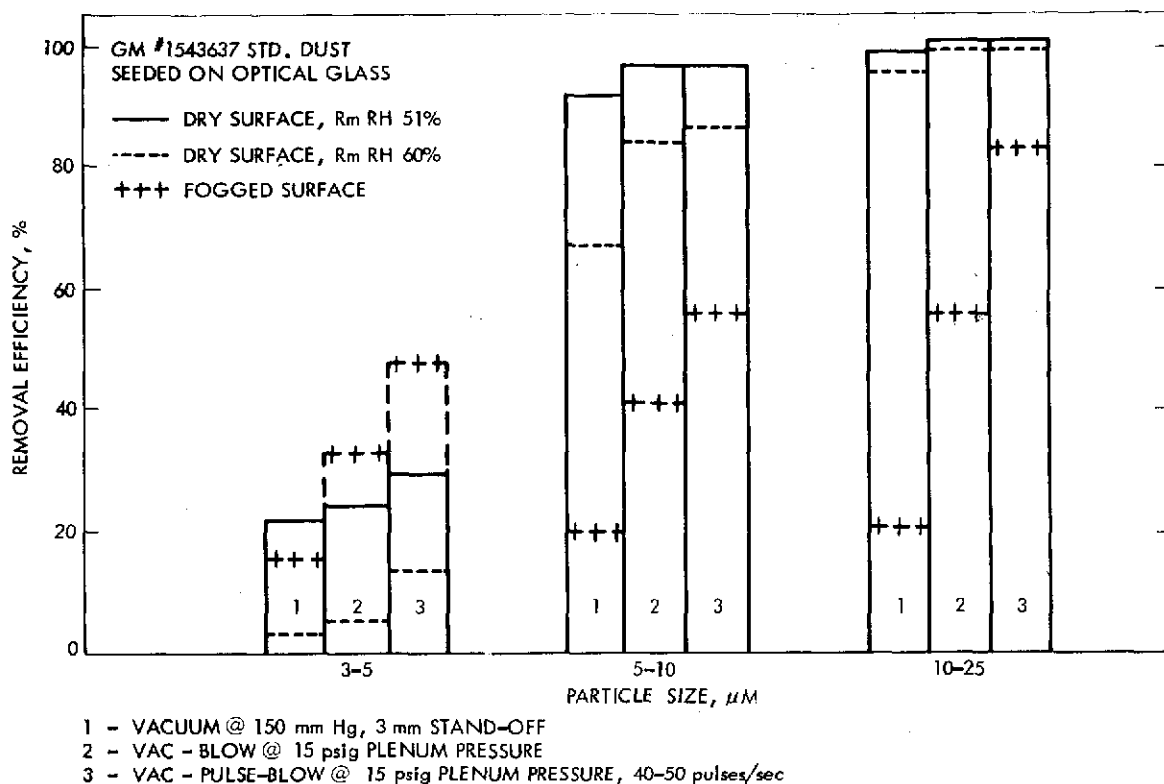


Fig. 4-A.16. Removal efficiency vs particle size for practically dry surface

however, becomes increasingly pronounced as the humidity goes up. The relatively high removal efficiencies achieved with the $\leq 5 \mu\text{m}$ particles on a fogged surface (if compared to the dry-data) can be explained with the fact that after fogging, the surface film contracts into individual droplets. As the droplets dry, the tendency is to flush the particles toward the center of the droplets, where they form lumps. The sizes $\geq 5 \mu\text{m}$ are too heavy to follow the surface film and usually remain where they were seeded. This has been also observed on earlier tests conducted with glass beads and dust, using steady state vacuum flow and/or jet blow techniques.

It is concluded from the test data that the incorporation of a slow pulse feature into cleaning tools that utilize flow effects alone (vacuum and blow) to detach and to remove particulates from surfaces would improve its efficiency.

4.1.3.2 Jet Deflection Techniques. According to the literature (see Fig. 4-A.5) periodic jet deflection can be induced by blowing against a

wedge. This method proved to be impractical for this task. The tolerances for flow and angular adjustments necessary to achieve resonance conditions were very narrow and were hard to sustain. Tests with this device, therefore, were dropped from the program.

Blowing over a cantilevered rod represented here by a 2 inch long hypodermic needle rigidly clamped to the test apparatus (see Fig. 4-A.6 and 4-A.7) produced jet oscillation over a fairly wide range of nozzle pressures (see Fig. 4-A.17). No increase in particle detachment capability could be observed when compared to steady state blow. Very efficient removal was found when isopropyl alcohol was introduced through the needle tip which was adjusted in such a manner that the nozzle jet would pass just through the needle axis where it intersected with the oblique plane of the open end. Under these conditions (see Fig. 4-A.6) the needle would oscillate in a rotary motion periodically fanning a thin liquid film onto the surface, in a similar way as frequently done with a garden hose to detach leaves from a concrete surface. This would instantly flush all particles (glass beads and dust) into the vacuum system (See Table 4-A.1).

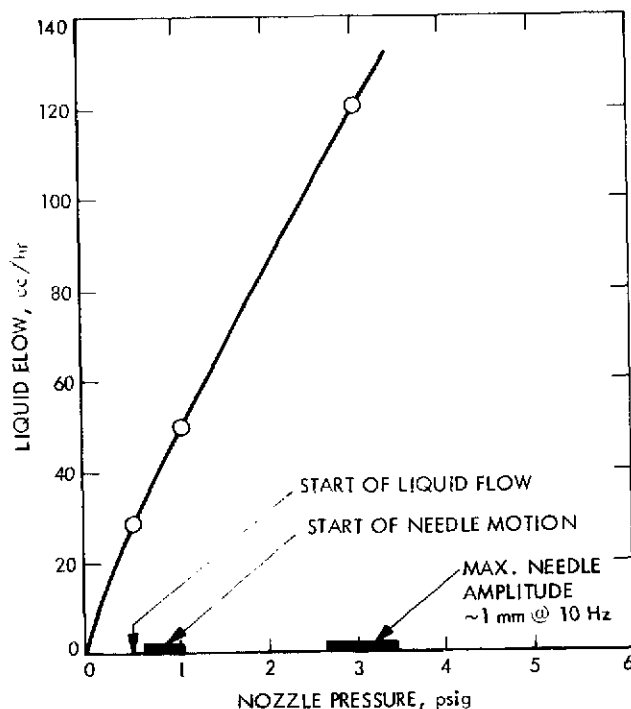


Fig. 4-A.17. Flow rates and dynamic behavior of spray-rod vs nozzle pressure

Table 4-A.1. Particle Counts For Oscillating Rod Test

Counts From 1/2 × 1/2 mm Control Surface	Particle Size, μm								Nozzle Pressure psig
	3 - 5		5 - 10		10 - 25		> 25		
Original	53	43	45	53	112	72	6	12	0.5
Vacuum	53	43	38	41	60	60	2	6	
Spray	0	3	0	0	0	0	0	0	
Original	76	41	40	73	63	106	7	11	1.0
Vacuum	76	41	40	69	44	97	1	11	
Spray	0	0	0	0	0	0	0	0	
Original	62	72	162	102	182	112	13	17	3.0
Vacuum	62	72	100	80	70	50	0	0	
Spray	0	0	0	0	0	0	0	0	

GM # 1543637 Standard Dust
Fogged Optical Glass
Needle Standoff - 1 mm from Blow Nozzel
2.8 mm Pressure Vacuum Nozzle

In contrast to earlier tests with spray into high velocity vacuum flow, there was no particle pile-up noticeable on the samples after the test. Figure 4-A. 18 shows the flow pattern of the liquid film during a 3 psig GN_2 blow at 150 mmHg vacuum flow through the nozzle. It can be seen that the liquid is fanning out upon impacting the surface, but the film flows within and does not spill beyond the contour of the vacuum nozzle.

Although greatly improvised, this experiment indicates the potential of the concept for a combined particulate cleaning and/or biological decontamination tool, where the use of liquids is acceptable. However, as mentioned in earlier reports, an item of great concern in spacecraft operations is the possible capillary entrapment of liquids between hardware interfaces, and the potential hazards resulting from the vapors (fire and explosion, degradation of printed electronics circuits). It is believed at this point that the discussed method could be developed to meet stringent requirements pertaining to the above indicated hazards. While a hypodermic needle was used in this experiment the physics of an oscillating impingement of a liquid fan can

Table 4-A.18. Particle Counts for Oscillating Rod Test

Particle Size, μ m	Particle Size, μ m				Control Surface
	10-25	25-50	50-100	100-250	
10-25	12	0	0	0	Original Vacuum Spray
25-50	11	11	0	0	Original Vacuum Spray
50-100	17	0	0	0	Original Vacuum Spray
100-250	0	0	0	0	Original Vacuum Spray

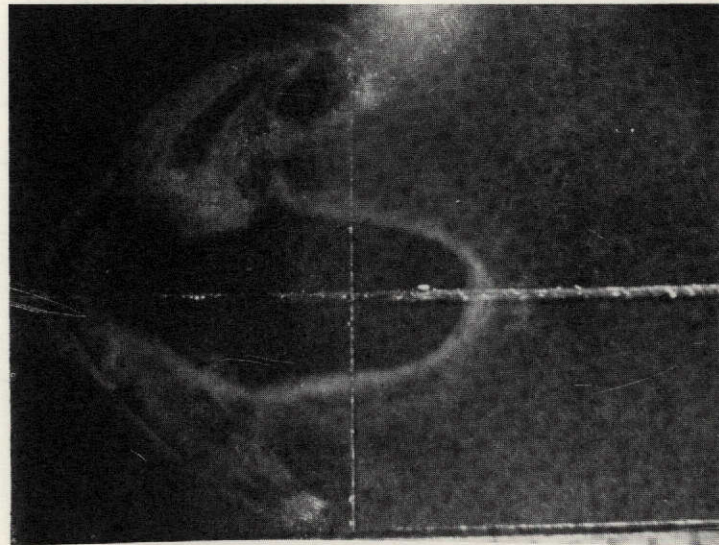


Fig. 4-A.18. Flow pattern of liquid surface film during oscillating spray-rod test

conceivably be better accomplished with an array of oscillating spray tubes that are designed specifically for this purpose.

4.1.3.3 Sonic Wave. The application of sonic pressure waves in a synergistic mode with flow did not produce any improvement over what could be accomplished with flow alone. The Hartmann generator (see Fig. 4-A.5) produced a maximum of 135 db on the surface at a relatively low frequency of 11,000 Hz at 50-60 psig, which was different from published characteristic data of the device (see Reference Fig. 4-A.5). Because of limited time it was not possible to provide the proper electronic equipment necessary to thoroughly survey the device, and to tune it for maximum performance. The results obtained therefore are not fully conclusive at this point.

4.1.4 Summary and Conclusions

In regard to the overall task objective (guidelines for particulate cleaning tools) the following conclusions can be made from the study efforts during this reporting period:

4.1.4.1 Jet Blocking.

- a) A periodic blocking of the jet noticeably enhances removal efficiency (on the order of 20-30%) where otherwise relatively low removal efficiencies (<50%) are achieved. This is observed for particle sizes < 5 μ m, and for larger sizes on surfaces that have been exposed to humidity conditions > 60% RH.
- b) Best results are obtained at blow pressures between 10 and 15 psig (critical expansion) across the blow nozzle, and at pulse frequencies below 50 Hz. An equally efficient cleaning with a steady state jet would require pressures 15 to 20 psig higher.
- c) The pulse can be transferred to the surface through a straight or bent transfer tube (in this case 12 inches). However, removal efficiencies are greatly impaired (30 to 50%). To eliminate inlet shock losses and to minimize frictional attenuation, instead of blocking a jet impinging the tube inlet, the mask should block the flow expanding into the tube from a pressurized plenum, such as for example shown in Fig. 4-A.21.
- d) System typical parameters such as the length and the volume of the feed line, the plenum chamber volume, pressure regulator characteristics, mask window dimensions, etc., have certain effects on the performance of the device. The data obtained, therefore, hold only for the particular set up tested, (see Fig. 4-A.1), and do not represent optimum conditions. This set up was chosen as the result of practical consideration pertaining to typical spacecraft cleaning operations.

4.1.4.2 Jet Deflection Techniques. Jet deflection induced by blowing over a wedge or oscillating rods did not improve detachment. Efficient (nearly 100%)

removal of particulates of all sizes could be produced by feeding liquid (isopropyl alcohol) through a hollow rod blown across its open end at pressures between 1 and 3 psig. The method appears to have the potential for a combined particulate cleaning and biological decontamination tool, and should be investigated further.

4.1.4.3 Ultrasonic Techniques. The effectiveness of ultrasonic techniques in a synergistic mode with flow cleaning is still inconclusive. The results obtained were negative, which might be attributed to the insufficient power output of the existing apparatus (Hartman generator).

4.1.5 Future Activities

4.1.5.1 Brush Cleaning. Many irregularly shaped areas exist on present generation spacecraft which depend entirely on brush cleaning. Future activity under this task, therefore, will concentrate on determining the basic characteristics (pick-up capability, shedding and cleanability) of Felor fiber, using a new test apparatus that simulates the cleaning cycle of a self-cleaning rotary brush in linear motion. The data obtained from these tests will serve as a baseline for the design of a one inch wide experimental self-cleaning rotary brush. Tests will then be conducted with the rotary brush to verify the results, and to finally establish guidelines for the design of prototype operational cleaning brushes. Figure 4-A.19 and 4-A.20 are diagrams of conceivable designs.

4.1.5.2 Flow Cleaning. There are no further tests with flow cleaning planned at this point. A few selected tests with existing hardware on surfaces other than optical glass may potentially be necessary to support final conclusions. The flow cleaning effort will then be essentially concluded by establishing guidelines for the design of blow-vacuum cleaning tools. It appears at this point that flow cleaning will be the preferred method in areas that are hard to reach, and do not allow for the use of brushes because of space. Figure 4-A.21 shows a concept of a cleaning tool based upon the conclusions drawn on Para. 4.1.4.1 (c).

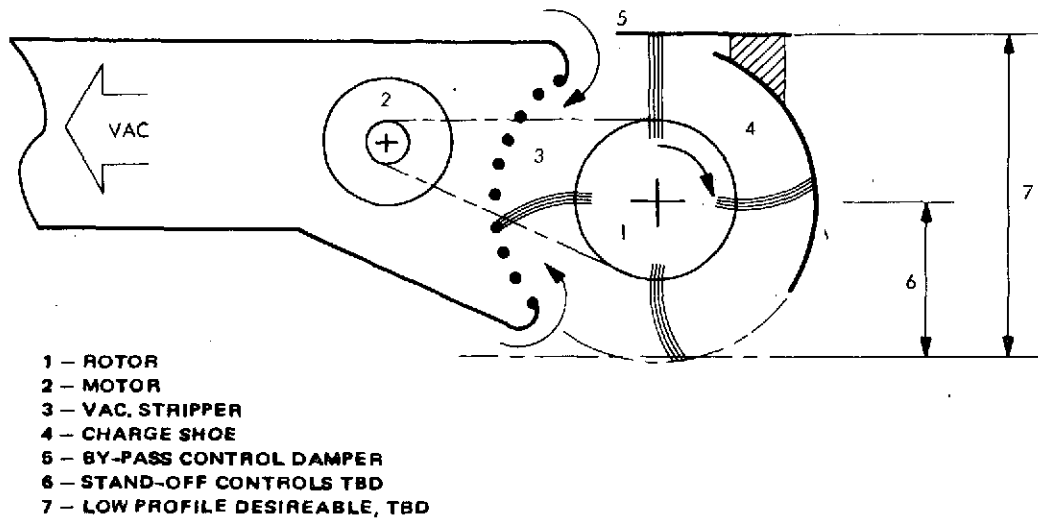


Fig. 4-A.19. Concept for a rotary self cleaning brush

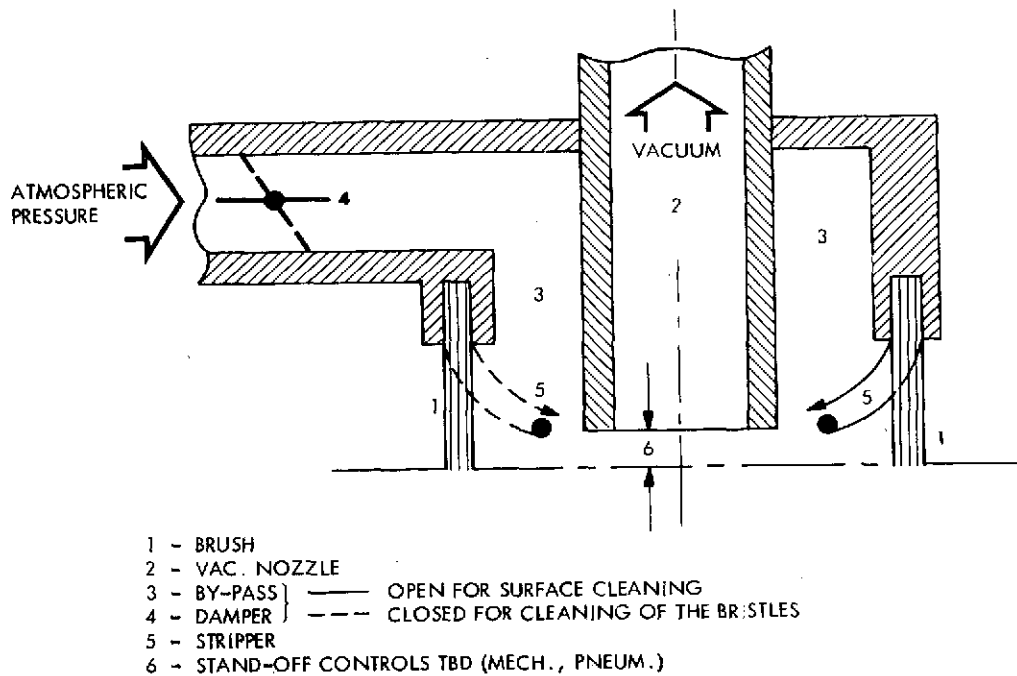


Fig. 4-A.20. Concept for an intermittently cleanable vacuum brush

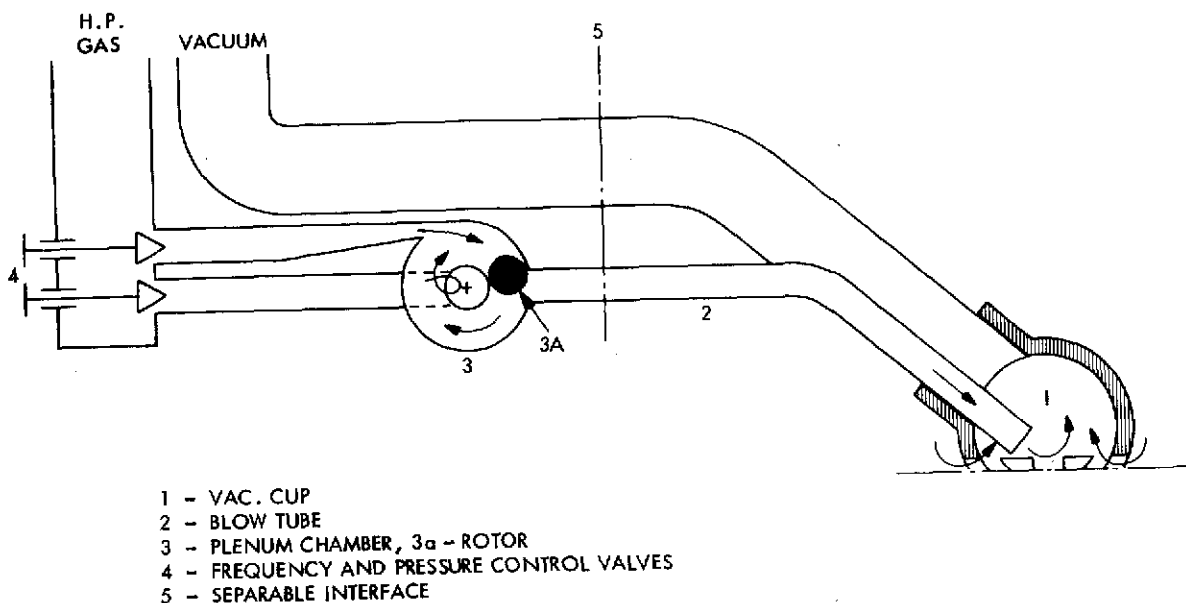


Fig. 4-A.21. Concept of a pulsating blow - vacuum, spot cleaning tool

4.1.5.3 Quantitative Data on Particle Adhesion. Fundamental tests will be conducted to establish the adhesion of glass-beads and of GM standard dust under atmospheric and high vacuum conditions, using a Lourdes centrifuge. The fabrication of the test hardware is in progress. The set up will allow generation of 30,000 g's in the sample plane and normal to the sample surface, at atmospheric and at vacuum conditions. The data obtained will be used to support the final evaluation of flow cleaning tests, and for post launch re-contamination analysis work.

4.1.6 Open Areas

A number of open areas still exist that, besides cleaning efficiency, are also important for the design of operational cleaning tools. These are the problems of surface compatibility and the stand-off control of the tool from the

surface. Both of these problems are linked together, and are spacecraft dependent. Investigations pertaining to these problems, therefore, have not been within the scope of the present task.

4.2 EVALUATION OF PLASMA CLEANING AND DECONTAMINATION TECHNIQUES

4.2.1 Subtask B Introduction

The overall program objective is to develop and apply plasma gas sterilization technology to problems associated with planetary quarantine. This program consists of three phases. Phase I was concerned with defining the effective sterilizing ranges for different single gas plasmas as related to power and pressure. Also formulation pertaining to the theoretical nature of plasmas was begun. The results of this phase was reported in JPL Document 900-655.

Phase II concentrated on utilizing the data obtained during Phase I to expand the range of biological testing. Measurements for diagnosing the lethal constituents of a plasma environment were developed. In addition, plasmas of mixed gases were studied. These results are presented in this report.

Phase III efforts will be primarily directed towards ascertaining spacecraft materials and plasma compatibility and determining the effectiveness of plasma gas for sterilizing surfaces of various configurations. The program approach will result in data applicable for use in development of preliminary design concepts for plasma sterilizers for space or terrestrial applications.

Previous preliminary Boeing data showed the feasibility of using an argon plasma, at low pressures, to inactivate Bacillus subtilis var. niger spores. RF power values were also shown to affect the rate of spore death. Phase I was designed to define, via specific test matrices, optimum rf power, and the "best" single gas and chamber pressure required for plasma sterilization. In addition, both theoretical and experimental plasma physics' functions were performed.

Experiments completed during Phase I indicated that the combination of a low chamber pressure (0.2 mm Hg), an ionization power input of 300 watts, and the gas helium were the most efficient for killing B. subtilis spores. These parameters were the operating conditions for plasma tests in Phase II.

In addition, Phase I data indicated that ultraviolet irradiation was the dominant kill mechanism in plasma.

4.2.2 Approach

The approach of Phase II was to obtain additional information on the biological range of effectiveness of helium plasma, develop plasma environmental diagnostics, and modify the operating parameters to obtain the optimum conditions for sterilization.

The design of experiments for Phase II was based on data obtained during Phase I. The primary gas for plasma production was helium. Operating conditions were 300 watts rf, 0.2 mm Hg chamber pressure, and 20 cc/minute gas flow. These conditions had been established as those resulting in the quickest spore kill.

4.2.2.1 Task 1 - Death Rates of Microorganisms. The lethal effect of plasma gas on a variety of organisms was investigated. Test organisms were selected to represent a typical spacecraft population upon which the range and effectiveness of the plasma process would be tested (Table 4-B.1). A controlled number of organisms were exposed to the plasma and analysis for survivors conducted. Operating parameters of the plasma tests equipment were established from data obtained during Phase I tests. These conditions provided the greatest overall spore death (Table 4-B.2).

The test configuration consisted of locating the samples at three positions within the chamber (Fig. 4-B.1). A glass ring, on which six test samples and two sterile controls were attached, was placed at each chamber position. A timed exposure consisted of 18 test samples, 6 replicates at each position, and 6 sterile controls, 2 located at each position. Test samples were inoculated stainless steel planchets.

Appropriate ambient die-off and procedural test controls were conducted for each test. Analyses of the exposed samples and controls were performed per standardized microbial recovery procedures. These procedures were adapted from NASA Standard Procedures for the Microbial Examination of Space Hardware, NHB 5340.1A and included sample inoculation and drying in a

Table 4-B.1. Test Organisms

Organism	Selection Rationale
JPL-1	Spore, spacecraft isolate
JPL-2	Spore, spacecraft isolate
JPL-16	Spore, spacecraft isolate
<u>Bacillus subtilis</u> var. <u>niger</u> , WCR-8	Spore, comparative control for sporeformers
JPL-5	Nonsporeformer, spacecraft isolate
<u>Staphylococcus</u> <u>epidermidis</u> ATCC 17917	Nonsporeformer, comparative control for JPL-5
<u>Aspergillus niger</u>	Fungus (spores)

Table 4-B.2. Operating Parameters

RF Power	300 watts
Gas	Helium, 20 cc/min. flow
Pressure	0.2 mm Hg
Time	5, 10, 15, 30 minutes

Class 100 clean bench, microbial removal by sonication, and enumeration with Trypticase Soy Agar pour plates.

1. Comparison of Plasma Sensitivity Between Two Bacillus Subtilis var. Niger Spore Types. The influence of the spore suspending medium upon the subsequent plasma susceptibility of the microorganism was investigated. B. subtilis var. niger, WCR-8 spores (JPL) and B. subtilis var. niger spores ATCC 9372 (Boeing) were the test organisms compared. The JPL spore, prepared at JPL, was originally suspended in ethyl alcohol. It was observed in Task 1 that the JPL B. subtilis spore was killed at a significantly slower

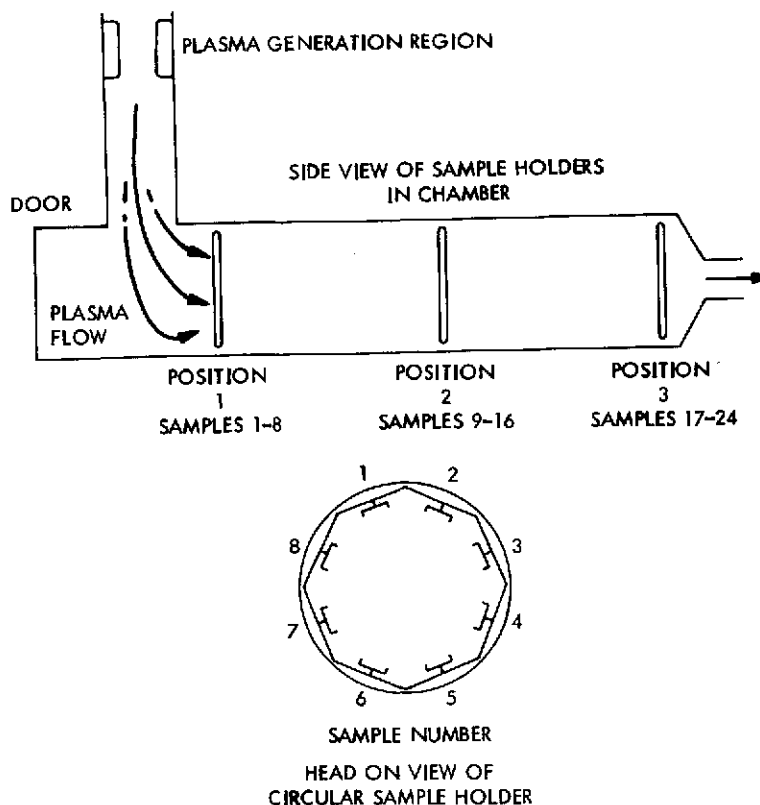


Fig. 4-B. 1. Test configuration

rate than the Boeing B. subtilis spore. Since the suspending medium in the latter case was water, the type of suspending medium was suspect. Aliquots of both spore types were suspended in water and alcohol, and test samples prepared. Test parameters were the same as Task 1.

2. Effect of Plasma Chamber Position on Microorganisms.

B. subtilis var. niger spores were exposed to helium plasma close to the ionization region. The plasma density in this region exceeded the plasma density in the chamber. Sterility of the test samples was the objective. (The test rationale of Phase I was to avoid sterility so that statistical comparisons of surviving numbers would be possible.)

Operating parameters were those of Task 1. Test configuration consisted of locating the samples in the plasma generation tube and exposing for 15 and 30 minutes (Fig. 4-B. 2). Analyses for survivors followed standardized procedures.

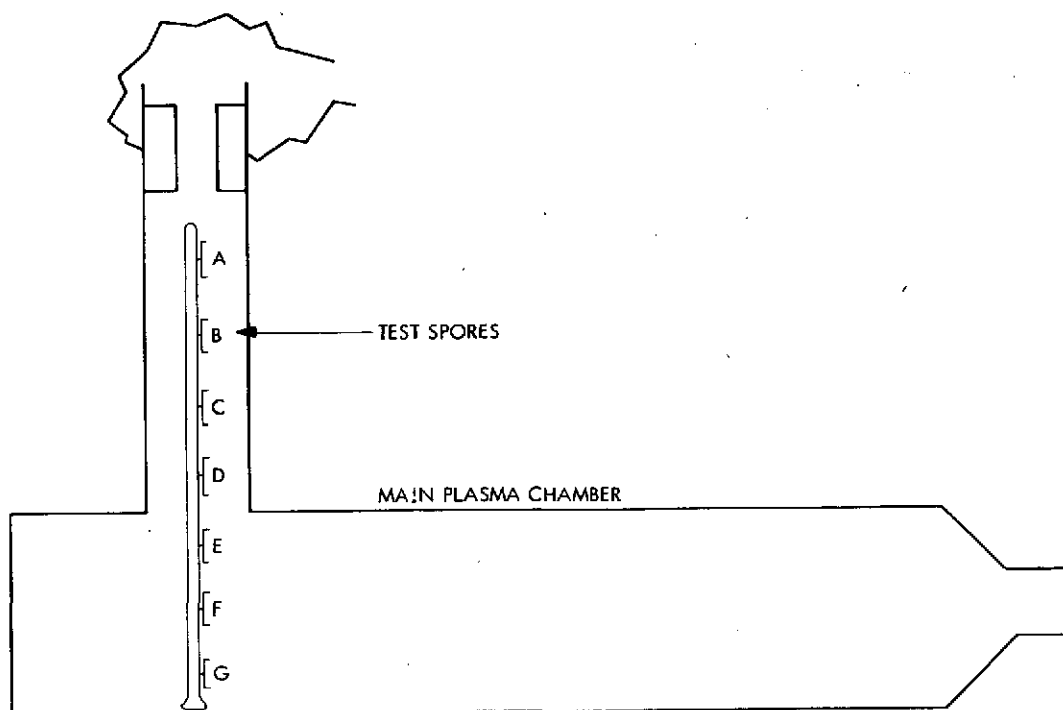


Fig. 4-B.2. Test sample arrangement

4.2.2.2 Task 2 - Plasma Gas Kill Mechanisms. The two most likely microbial kill mechanisms in plasmas are ultraviolet irradiation from the recombining plasma, and sputtering of the cell wall by ion bombardment. Experiments were performed to obtain data on these two possible mechanisms.

1. Ultraviolet Irradiation. The ultraviolet (UV) properties of plasma with respect to spore lethality were investigated.

The UV spectra of plasmas was separated with filters such that wavelengths below 140, 220, and 360 nanometers were not transmitted. Spores of B. subtilis var. niger were exposed to the various spectral fractions of argon, helium and oxygen plasmas by covering the samples with filters. The test matrix is shown in Table 4-B.3 and the operating parameters are given in Table 4-B.4.

Table 4-B.3. Test Matrix

Filter	Beginning Spectral Transmission, Nanometers	Plasma Gas		
		Argon	Helium	Oxygen
Glass	340	9*	9	9
Corning 9-54	220	9	9	9
Sapphire Window	140	9	9	9
No Filter		9	9	9

* = Number of replicates, 6 for biological analysis, 3 for electron scan.

Table 4-B.4. Operating Parameters

RF Power	150 watts
Gas	Argon, Helium, Oxygen
Flow	20 cc/min.
Pressure	0.2 mm Hg
Time	15 minutes
Organism	<u>B. subtilis</u> spores
Chamber Position	2

2. Electron Scanning Microscope. Electron scanning photomicrographs of spores exposed to plasma were performed. Spores, exposed to the different UV fractions of argon, helium, and oxygen plasmas were examined for physical change. Untreated spore samples were used as comparative controls.

4.2.2.3 Task 3 - Plasmas of Mixed Gases. The sterilizing efficiency of mixed gases for plasma production was evaluated. Argon, helium, and oxygen were mixed in various proportions and the resulting plasmas compared with respect to spore killing properties. Operating parameters are shown in Table 4-B.5.

Table 4-B.5. Operating Parameters

Power, rf	300 watts
Gases	Argon, Helium or Oxygen
Flow	20 cc/min. total
Pressure	0.2 mm Hg

B. subtilis var. niger spores were exposed to the plasmas for 15 minutes at Chamber Position 1. Analysis for survivors proceeded per standardized methods.

4.2.2.4 Task 4 - Plasma Gas Diagnostics. The likely mechanisms for plasma sterilization - ultraviolet irradiation and possibly sputtering - depend directly on the properties of the plasma. The readily controlled parameters, such as rf power and gas flow rates, will also control the kill rate, but only indirectly, and the relationship is confused by any irregular behavior of the plasma generator arising from surface contaminants and other factors which are difficult to monitor and analyze.

Of the variables which should directly affect rates for the kill processes, the most important are the gas pressure and species and the plasma density. The UV radiation flux from recombination is proportional to the square of the plasma density, and the UV flux from neutral gas excitation by the plasma electrons is directly proportional to the plasma density. The UV spectrum is determined by the species and the gas pressure, with a transition from a line spectrum to a less energetic continuum occurring at a pressure on the order of several mm of Hg. Electron temperature and gas pressure both influence the recombination and excitation rates strongly.

Sputtering rates should be directly proportional to the plasma density, and are extremely sensitive to the energy of the bombarding ions which is in turn proportional to the effective electron temperature. Consequently, systematic sterilization experiments require monitoring of those important fundamental variables, specifically plasma density and electron temperature, which are not

susceptible to direct control. The objective of this task was a discussion of the relevant plasma properties and phenomena, a description of various probe experiments conducted in the test chamber, and a tabulation of results.

4.2.2.5 Task 5 - Electrode Placement and Design. The objective of this phase was to produce a more dense plasma by modifications in electrode placement and electrode design. The criteria for evaluating improvement was to produce a more lethal plasma. Secondly, Langmuir probe measurements of the plasma density were compared to spore survival data. RF powers of less than 200 watts were used. Two modifications of electrodes were studied and are diagrammed in Fig. 4-B.3. Modification A was employed for 10 and 50 watts, while 50 and 150 watts were tested with Modification B. Also, Modification B was tested with helium and argon gases whereas Modification A was only helium.

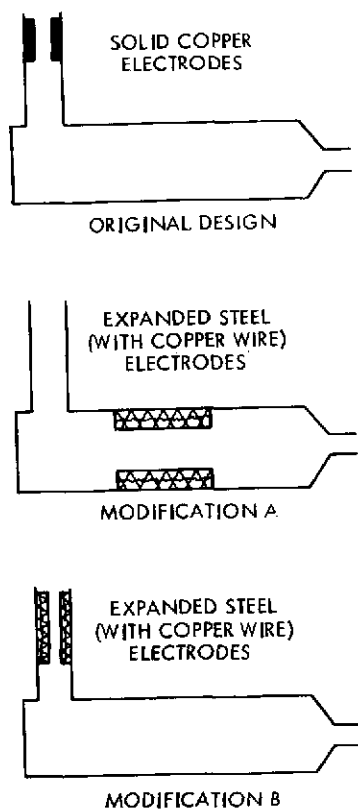


Fig. 4-B.3. Electrode placement and design

4.2.3 Significant Accomplishments

4.2.3.1 Task 1 - Death Rates of Microorganisms. Seven different types of microorganisms were exposed to helium plasma. Analysis for survivors was performed. Table 4-B.6 presents the results of these analyses. Percent survival calculations were conducted for these data and are shown in Table 4-B.7. The figures for B. subtilis var. niger, ATCC 9372, have been included for comparisons with phase I data.

Table 4-B.6. Mean Number of Microorganisms Surviving Helium Plasma Exposure^a

Test Organism	Chamber Position	Helium Plasma Exposure, Minutes				
		0	5	10	15	30
<u>Bacillus subtilis</u> WCR-8, Spore	1	4.6×10^5	2.8×10^{3b}	1.3×10^3	1.8×10^3	4.9×10^2
	2		7.8×10^3	2.7×10^3	2.2×10^3	2.2×10^3
	3		2.0×10^4	8.4×10^3	5.1×10^3	2.5×10^3
JPL-1, Spore	1	6.5×10^5	1.6×10^5	9.0×10^4	2.9×10^4	6.3×10^3
	2		2.0×10^5	1.3×10^5	4.5×10^4	1.7×10^4
	3		2.3×10^5	2.2×10^5	9.8×10^4	1.4×10^4
JPL-2, Spore	1	6.0×10^5	1.5×10^4	1.1×10^4	1.1×10^4	5.3×10^3
	2		2.2×10^4	1.5×10^4	1.5×10^4	6.8×10^3
	3		4.1×10^4	3.8×10^4	2.4×10^4	1.3×10^4
JPL-16, Spore	1	2.0×10^5	2.0×10^3	2.3×10^3	1.5×10^3	7.6×10^2
	2		1.7×10^4	4.7×10^3	1.9×10^3	1.3×10^3
	3		1.5×10^4	6.5×10^3	6.0×10^3	3.7×10^3
JPL-5, Non Sporeformer	1	5.3×10^{5c} (2.4×10^6)	6.2×10^2	1.4×10^2	1.2×10^2	3.3×10^0
	2		2.0×10^3	5.0×10^2	4.1×10^2	7.5×10^0
	3		1.3×10^4	1.6×10^3	5.9×10^2	8.8×10^1
<u>Staphylococcus Epidermidis</u> , Non Sporeformer	1	6.5×10^{4c} (5.0×10^5)	0	0	0	0
	2		0	0	0	0
	3		0	0	0	0
<u>Aspergillus niger</u> , Fungal Spore	1	2.7×10^4	1.5×10^2	6.6×10^1	1.5×10^1	9.0×10^0
	2		6.7×10^2	1.0×10^2	5.6×10^1	1.7×10^1
	3		1.9×10^3	4.6×10^2	1.8×10^2	4.3×10^1
a300 watts, 0.2 mm Hg pressure, 20 cc/minute gas flows						
bMean of 6 replicates						
cCorrected for vacuum effects						

Table 4-B.7. Percent Survival of Microorganisms After Exposure to Helium Plasma

Test Organism	Chamber Position	Helium Plasma Exposure, Minutes			
		5	10	15	30
<u>Bacillus subtilis</u> var. <u>niger</u> , ATCC 9372, Spore, Boeing ^a	1 2 3	0.03 0.12 0.36	0.01 0.02 0.12	0.00 0.01 0.06	b
<u>Bacillus subtilis</u> var. <u>niger</u> , WCR-8, Spore, JPL	1 2 3	0.61 1.70 4.35	0.28 0.59 1.83	0.39 0.48 1.11	0.11 0.48 0.54
JPL-1, Spore	1 2 3	24.62 30.77 35.38	13.85 20.00 33.85	4.46 6.92 15.08	0.97 2.62 2.15
JPL-2, Spore	1 2 3	2.50 3.67 6.83	1.83 2.50 6.33	1.83 2.50 4.00	0.88 1.13 2.17
JPL-16, Spore	1 2 3	1.00 8.50 7.50	1.50 2.35 3.25	0.75 0.95 3.00	0.38 0.65 1.85
JPL-5, Nonsporeformer	1 2 3	0.12 0.38 2.45	0.03 0.09 0.30	0.02 0.08 0.11	0.00 0.00 0.02
<u>Staphylococcus epidermidis</u> , Nonsporeformer	1 2 3	0.00 0.00 0.00	0.00 0.00 0.00	0.00 0.00 0.00	0.00 0.00 0.00
<u>Aspergillus niger</u> , Fungal Spore	1 2 3	0.56 2.48 7.04	0.24 0.37 1.70	0.06 0.21 0.67	0.03 0.06 0.16
^a Phase-1 Data ^b Not in Phase-1 Test Matrix					

It is noted that: (1) differences existed between the two strains of B. subtilis var. niger spores with respect to plasma susceptibility, and (2) the three spacecraft sporeforming isolates (JPL-1, JPL-2, JPL-16) were overall more resistant to plasma than B. subtilis.

1. Plasma Sensitivity of Two Bacillus Subtilis Spores. Comparison of the plasma susceptibility of B. subtilis var. niger WCR-8 spores (JPL) and ATCC 9372 spores (Boeing) was made. Also, a comparison of water versus alcohol as spore suspending media was conducted. Table 4-B.8 presents the number of spores surviving helium plasma exposure.

Calculations for percent survival are shown in Table 4-B.9. These data show that the B. subtilis spores prepared by JPL are more resistant to plasma effects than Boeing prepared spores. Also, spores suspended in alcohol prior to test sample preparation are more resistant to plasma than spores suspended in water.

Communications with C. Hagen, JPL, revealed that JPL utilized a modified sporulation medium that was purposely designed to produce an especially thick spore coat not only for B. subtilis, but also the spacecraft isolates, JPL-1, JPL-2 and JPL-16. Evaluation of the biological variation due to the cultural conditions will be needed in future investigations.

2. Influence of Chamber Position on Sterility. Organisms were exposed to helium plasma near the ionization region. Analysis for sterility of the samples was conducted and the results are shown in Table 4-B.10. Samples A through E were sterilized during the thirty minute plasma exposure. Temperatures in the region of E-F-G samples remained under 50°C during plasma production.

Table 4-B.8. Mean Number of Spores Surviving Helium Plasma Exposure^a

Organism	Spore Suspending Medium	Helium Plasma Exposure, Minutes				
		0	5	15	30	60
Bacillus subtilis var. niger, WCR-8, Spore, JPL	Alcohol	5.6×10^4 ^b	1.9×10^3	3.6×10^2	2.4×10^2	2.5×10^2
	Water	6.1×10^4	1.6×10^2	3.8×10^1	8.3×10^0	2.2×10^0
Bacillus subtilis var. niger, ATCC 9372, Spore, Boeing	Alcohol	7.7×10^3	0.5×10^0	1.0×10^0	1.3×10^0	0
	Water	1.1×10^4	0	0	0	0

^a300 watts, 0.2 mm Hg pressure, 20 cc/minute gas flow, Chamber Position 1

^bMean of 6 replicates

Table 4-B.9. Mean Percent Survival of Spores to Helium Plasma

Organism	Spore Suspending Medium	Helium Plasma Exposure, Minutes			
		5	15	30	60
<u>Bacillus subtilis</u> var. <u>niger</u> , WCR-8, JPL	Alcohol	3.39 ^a	0.64	0.43	0.04
	Water	0.26	0.06	0.01	0.00
<u>Bacillus subtilis</u> var. <u>niger</u> , ATCC 9372, Boeing	Alcohol	0.01	0.01	0.02	0.00
	Water	0.00	0.00	0.00	0.00
^a Mean of 6 replicates					

Table 4-B.10. Total Number of Bacillus subtilis var.
niger Spores Surviving Helium Plasma
Exposure^{a, b}

Chamber Position	Plasma Exposure, Minutes	
	15	30
A	0 ^c	0
B	2	0
C	0	0
D	0	0
E	0	0
F	0	0
G	21	15
^a 1.1 × 10 ⁵ at 0 time ^b 300 watts, 0.2 mm Hg pressure, 20 cc/min. gas flow ^c Total of 3 replicates		

4.2.3.2 Task 2 - Plasma Kill Mechanisms.

1. Ultraviolet Irradiation. Experimentation on the ultraviolet properties of argon, helium, and oxygen plasmas, with respect to spore survival was performed. The results are shown in Table 4-B.11. Percent survival calculations are given in Table 4-B.12.

The spores that experienced the total plasma environment, i. e., no filter, also exhibited the least percent survival.

2. Electron Scan Microscopy. Helium, argon, and oxygen plasma treated spores of B. subtilis were examined with an electron scanning microscope. Photomicrographs were obtained and are reproduced in Figs. 4-B.4 through 4-B.9. Visual comparison of the nontreated versus plasma treated spores suggest physical damage. However, the spores protected from the various spectral fractions of the plasmas with filters do not appear to show such damage. Although physical change in these spores is not apparent, the data presented in Table 4-B.12 showed that spore death at these conditions did occur.

4.2.3.3 Task 3 - Plasmas of Mixed Gases. Table 4-B.13 presents spore survival percentages obtained from exposing spores to plasmas of mixed gases. Using Position 3 as a reference point (farthest from plasma generation area), the argon and helium combination resulted in less spore survival than the plasmas of argon combined with oxygen or oxygen combined with helium.

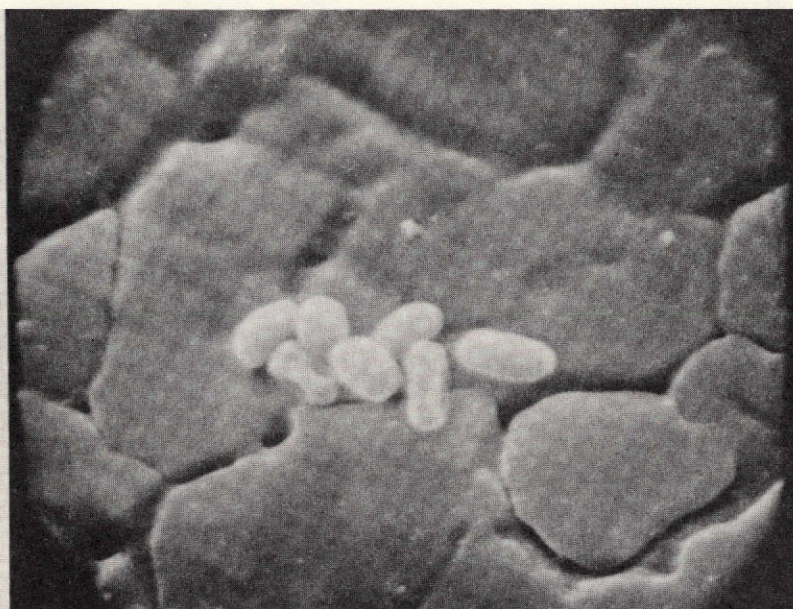
4.2.3.4 Task 4 - Plasma Gas Diagnostics. The purpose of this section is to introduce the fundamental aspects of plasma behavior which pertain to plasma sterilization and diagnostics. The plasma used in the experiments is, nominally, a "flowing rf generated afterglow plasma." Gas is admitted at one end of the system and pumped out the other end by a vacuum pump. Pressure is controlled by the flow rate. Near the gas inlet is a pair of electrodes used to apply a strong rf electric field which causes rf breakdown in the gas, creating a plasma by ionizing about one part in a million of the flowing gas. The plasma is carried through the system by the gas flow, decaying by recombination as it goes.

Table 4-B.11. Mean Number of Bacillus subtilis var.
niger Spores Protected from Plasma
Environment with Filters^{a, b}

Filter	Beginning Spectral Transmission, Nanometers	Argon Plasma	Helium Plasma	Oxygen Plasma
Glass	340	1.7×10^5 ^c	1.2×10^5 ^c	1.8×10^5 ^d
Corning 9-54	220	7.4×10^2	3.4×10^3	9.5×10^4
Sapphire Window	140	1.6×10^2	3.8×10^2	1.0×10^5
No Filter	-	2.3×10^1	4.4×10^1	0
^a 150 watts, 0.2 mm Hg pressure, 20 cc/min. gas flow, Position 1, 15 minutes exposure ^b Mean of 6 replicates ^c 2.0×10^5 at 0 time ^d 2.2×10^5 at 0 time				

Table 4-B.12. Percent Survival of Bacillus subtilis var.
niger Spores Protected from Plasma
Environment with Filters

Filter	Spectral Transmission, Nanometers	Argon Plasma	Helium Plasma	Oxygen Plasma
Glass	340	60.00	85.00	81.82
Corning 9-54	220	1.70	0.37	43.18
Sapphire Window	140	0.19	0.08	45.45
No Filter	-	0.02	0.01	0.00

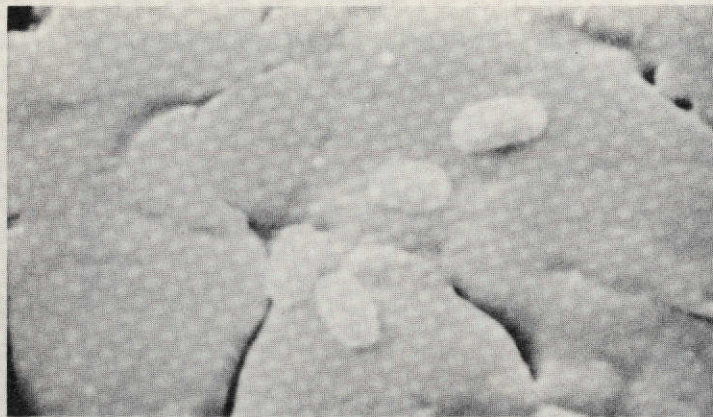


NO PLASMA

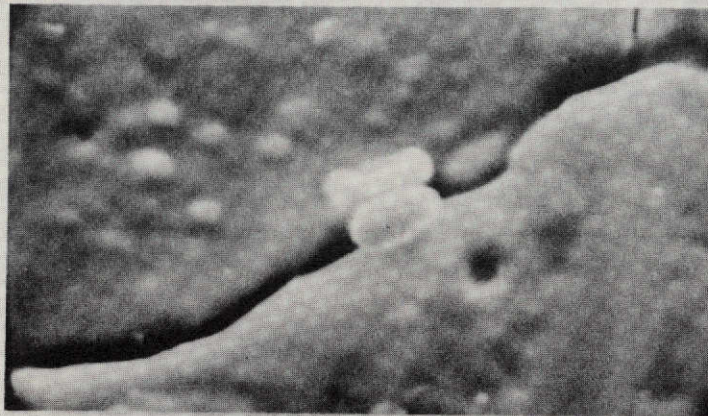


ARGON PLASMA

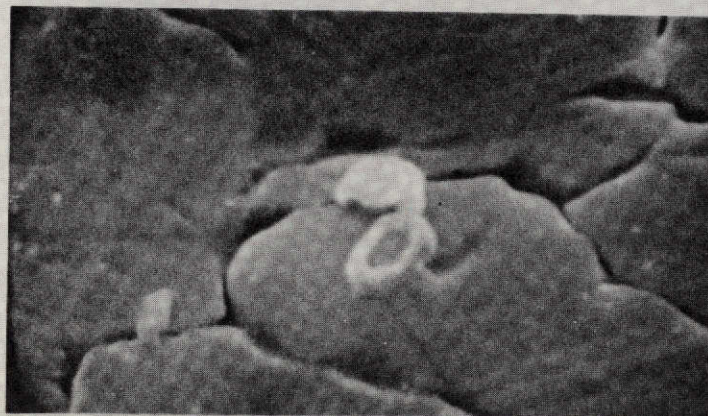
Fig. 4-B.4. Bacillus subtilis var. niger spores exposed to argon plasma, 9000X



GLASS FILTER, 340 NANOMETERS

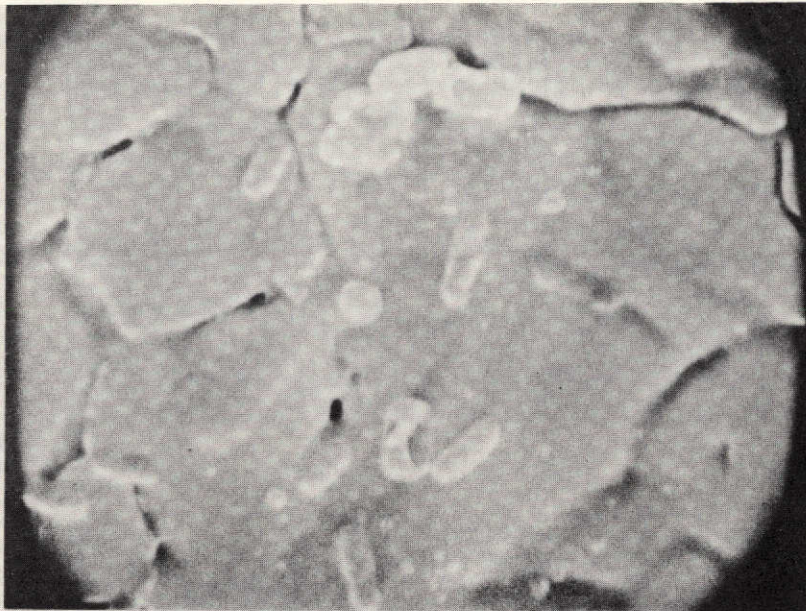


CORNING #9-54 FILTER, 220 NANOMETERS

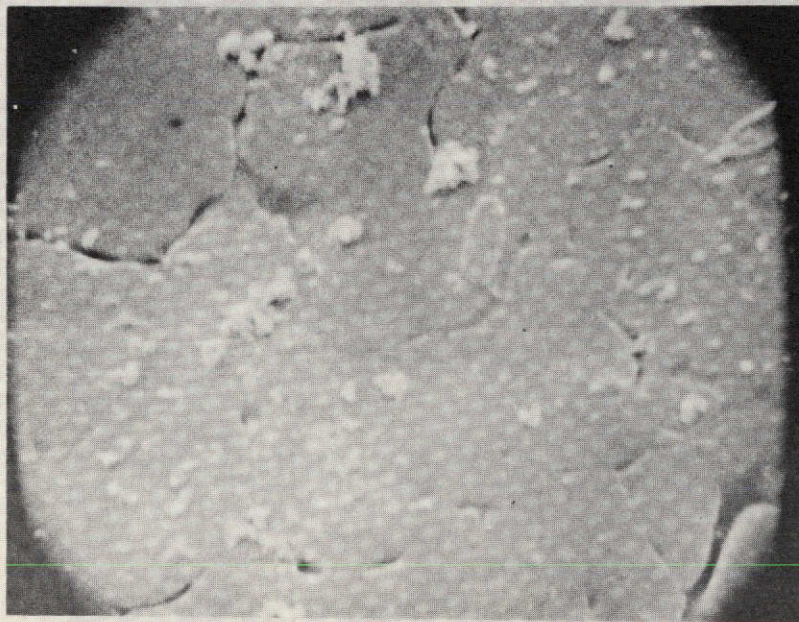


SAPPHIRE WINDOW, 140 NANOMETERS

Fig. 4-B.5. Bacillus subtilis var. niger spores exposed to argon plasma, 9000X

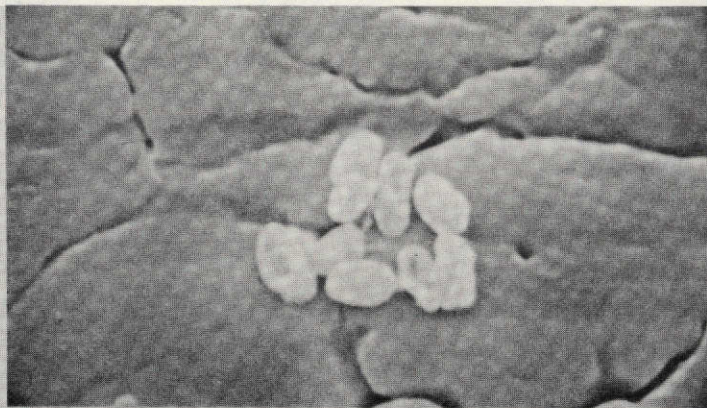


NO PLASMA



HELIUM PLASMA

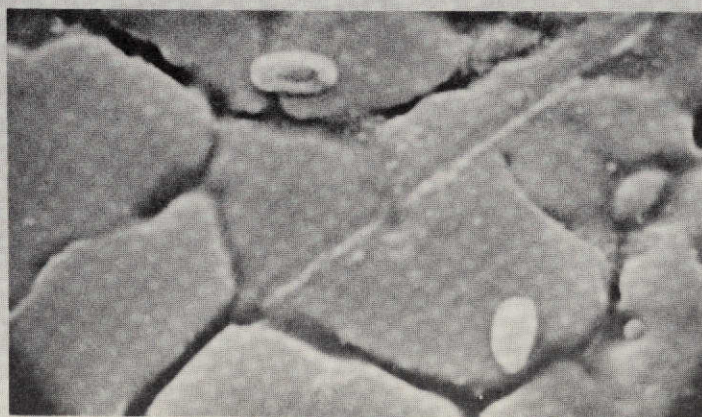
Fig. 4-B.6. Bacillus subtilis var. niger spores, 8000X



GLASS FILTER, 340 NANOMETERS

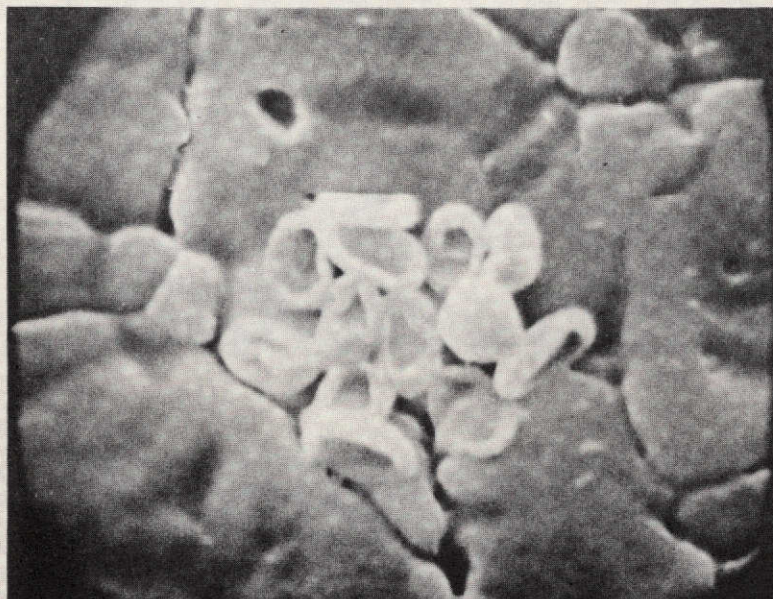


CORNING #9-54 FILTER, 220 NANOMETERS

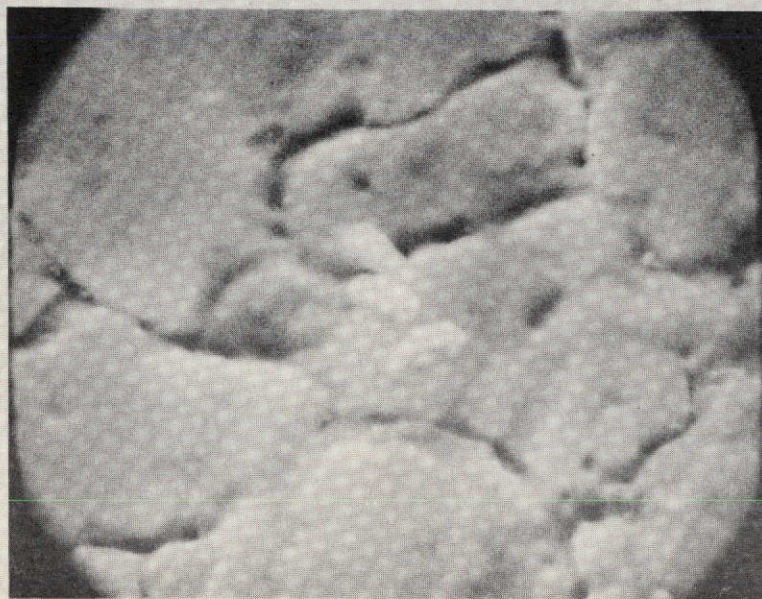


SAPPHIRE WINDOW, 140 NANOMETERS

Fig. 4-B. 7. Bacillus subtilis var. niger spores exposed to
helium plasma, 8000X

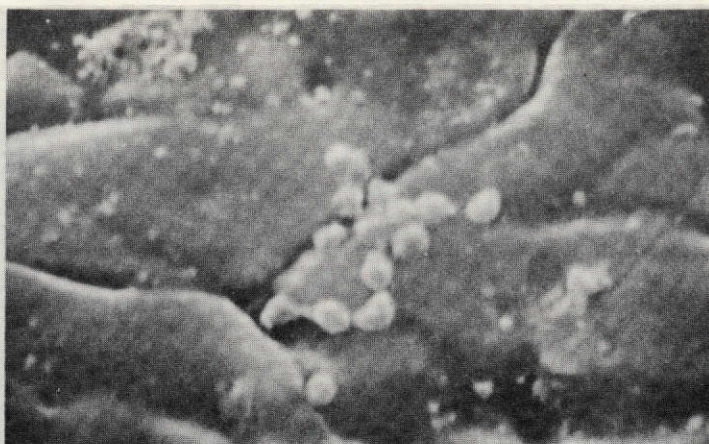


NO PLASMA

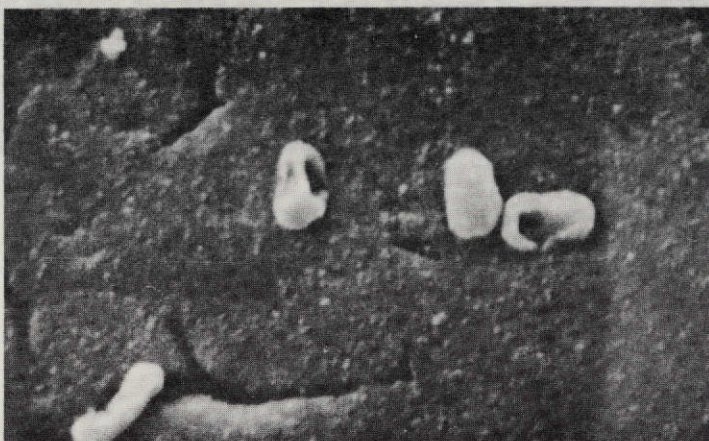


OXYGEN PLASMA

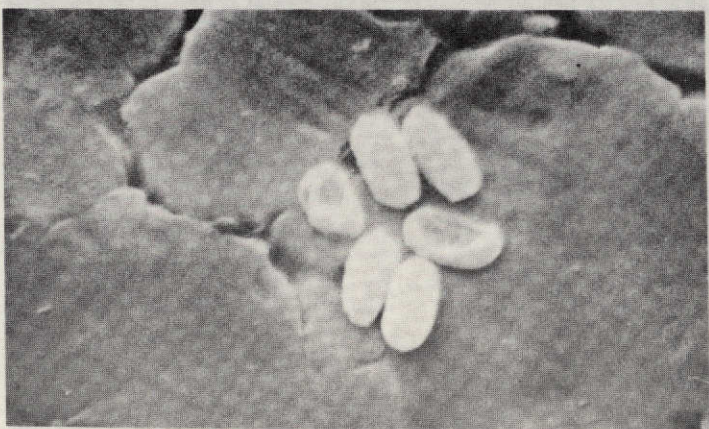
Fig. 4-B.8. Bacillus subtilis var. niger spores, 10,000X



GLASS FILTER, 340 NANOMETERS



CORNING #9-54 FILTER, 220 NANOMETERS



SAPPHIRE WINDOW, 140 NANOMETERS

Fig. 4-B.9. Bacillus subtilis var. niger spores, 140, 220, 340, nanometers

Table 4-B.13. Percent Survival Bacillus subtilis var. niger Spores Exposed to Mixed Gas Plasmas^a

Gas - CC/Minute	Chamber Position		
	1	2	3
Helium - 20	0.00	0.01	0.06
Argon - 20	0.08	0.01	65.31
Oxygen - 20	0.00	9.70	64.50
Argon - 18 + Oxygen 2	0.00	0.80	70.59
Argon - 10 + Oxygen 10	0.00	4.63	84.21
Argon - 18 + Helium 2	0.01	0.03	10.59
Argon - 10 + Helium 10	0.00	0.01	0.05
Oxygen - 18 + Helium 2	0.00	0.64	81.82
Oxygen - 10 + Helium 10	0.00	1.35	76.47
Oxygen - 10 + Argon 10	0.00	5.18	94.12
^a 300 watts, 0.2 mm Hg pressure, 15 minutes			

This Boeing developed rf plasma system, however, has a special feature in that rf current is allowed to leak out of the electrode region, and tends to follow the flowing plasma. This guided rf current will heat the electrons in the "flowing afterglow" plasma, and if it maintains an electron temperature of more than one or two electron volts, will cause further ionization, thus maintaining a denser plasma farther from the source.

RF heating is the dominant electron heating mechanism, and the electrons are cooled primarily by inelastic collisions with the cold neutral gas. These processes occur much more rapidly than the gradual changes as the plasma flows through the system. Consequently, the electron gas is in local

equilibrium, with its temperature determined by the balance between heating and cooling. The heating rate is:

$$P_{in} = \frac{ne^2 E^2}{m} \frac{\nu}{\omega^2 + \nu^2} \quad (1)$$

where: n is the plasma density (number of electrons per cubic meter), e is the charge on the electron in coulombs; E is the magnitude of the rf electric field associated with the rf current, in volts per meter; m is the mass of the electron, in kilograms; ν is the frequency with which a typical electron collides with neutral gas molecules, in seconds⁻¹; and ω is the angular frequency of the rf field, $\omega = 2\pi \times 13.7 \text{ MHz} = 8.6 \times 10^7 \text{ sec}^{-1}$, which is constant in these experiments.

The cooling rate is:

$$P_{out} = \nu ne \left[T_e \left(\frac{m}{M} \right) + \epsilon_I \left(\frac{\sigma_I}{\sigma_0} \right) e^{-\epsilon_I/T_e} \right] \quad (2)$$

where: T_e is the electron temperature, in electron volts; M is the mass of the neutral atom, in kilograms; ϵ_I is the mean energy lost in inelastic collisions with neutral gas molecules, in electron volts; σ_0 is the cross-section for momentum exchanging collisions between electrons and neutrals; and σ_I is the mean cross-section for inelastic collisions. In the conditions found in the sterilization plasma, the first term, representing cooling by elastic collisions, is small compared to the cooling by inelastic collisions. This latter term represents a significant fraction of the power supplied to the system. The electron-neutral collision frequency is conveniently expressed as:

$$\nu = 6 \times 10^7 P_c p T_e^{1/2} \quad (3)$$

where p is the gas pressure, in mm of Hg, and P_c is the collision probability¹. Balancing the power flowing into the electron gas with the cooling rate, assuming that $\nu \gg \omega$, expressing the rf electric field in kilovolts per meter, and using Eq. (3) for ν , gives a transcendental equation for the electron temperature.

$$T_e = \epsilon_I / \ln (A \times B), \quad (4)$$

where

$$A = 3.6 \times 10^{15} m \epsilon_I P_c^2 p^2 T_e / e E^2, \quad (5)$$

and

$$B = \sigma_I / \sigma_o.$$

The constants are:

$$m = 9 \times 10^{-31} \text{ kg}$$

$$e = 1.6 \times 10^{-19} \text{ coul},$$

and

$$P_c = 10 \text{ (He)}$$

Most measurements have been done at $p = 0.2$ mm, and E is observed to be on the order of 3 kilovolts/meter. For helium the metastable level is at $E_m = 19.80$ eV, the resonance line is at 21.21 eV, and the ionization potential is 24.58 eV, so that

$$\epsilon_I \simeq 20 \text{ eV}. \quad (6)$$

The cross-sections in He are

$$\sigma_I \simeq 10^{-16} \text{ cm}^2$$

and

$$\sigma_o \simeq 2.8 \times 10^{-16} \text{ cm}^2.$$

Using these numbers and solving Eq. (4) either graphically or by iteration determines T_e ,

$$T_e \approx 31 \text{ eV} \quad (7)$$

Electron temperatures on the order of tens of electron volts are sufficient to increase the ionization, so that plasma decay will be deferred. Anticipating later results, the plasma density is on the order of 10^{15} m^{-3} , i.e.,

$$n \approx 10^{15} \text{ m}^{-3}. \quad (8)$$

With the density, temperature, and pressure known, most of the important characteristic parameters of the plasma can be estimated. From Eq. (3), the collision frequency in helium is

$$\nu \approx 2 \times 10^8 \text{ sec}^{-1}, \quad (9)$$

verifying the assumption in Eq. (4) that $\nu \gg \omega$.

The other important characteristic frequency is the plasma frequency

$$\omega_p = 2\pi \times 10 \times n^{1/2} = 2 \times 10^9 \text{ sec}^{-1}, \quad (10)$$

so that the characteristic frequencies form a sequence,

$$\omega_p \gg \nu \gg \omega. \quad (11)$$

For the conditions expressed in Eq. (11), the skin-depth for rf current in the plasma is

$$\delta \approx \frac{c}{\omega_p} \approx 15 \text{ cm}, \quad (12)$$

where c is the speed of light in vacuum.

Then the skin depth is comparable to the diameter of the plasma so that the rf heating current will be distributed throughout the plasma.

Another important length is the Debye length

$$\lambda_D = 7 \times 10^5 (T_e/n)^{1/2} \quad (13)$$

which is the characteristic length for electrostatic space-charge effects in the plasma. For $T_e = 31$ eV, $n = 10^{15} \text{ m}^{-3}$, we have $\lambda_n = 0.1$ cm. The Debye length is important for plasma penetration; normally plasma will not penetrate holes much smaller than one λ_D . In order to penetrate holes smaller than 0.1 cm, it may be necessary to ground out the rf heating current with a grounded ring electrode around the plasma. The downstream plasma should then become a true afterglow with a typical temperature of about 0.1 eV, and a Debye length of as little as 0.007 cm.

One other important length is the electron mean-free-path between momentum randomizing collisions with the neutral gas molecules,

$$\lambda_c = \frac{1}{n_o \sigma_o} = \frac{1}{P_{cp}} \approx 0.5 \text{ cm}, \quad (14)$$

where n_o is the density of the neutral gas in atoms per cubic meter.

The plasma density and electron temperature are determined by Langmuir probe techniques (Refs. 2, 3, 4, and 5). This method involves several difficulties because of the unusual characteristics of this plasma. But alternative techniques - microwave cavities; low current, high voltage electron beam probes; laser interferometry; resonance probes; thermionic emission probes; double probes; and spectroscopy; would encounter similar or greater problems.

A Langmuir probe is a small metallic collector inserted into the plasma and connected to an adjustable DC power supply. The current from the plasma to the probe is measured as a function of the voltage applied to the probe. For stable, DC plasmas with low background gas pressure (long mean-free-path), the theory and practice of Langmuir probes has been worked

out in great detail. There are even apparatus which will automatically record probe data and reduce it to a plot of the kinetic energy distribution of the electrons.

The rf field and high electron temperature in this plasma prevent such a detailed interpretation. But the main features of probe analysis are still present and can be used to determine the electron temperature. The DC electric field applied to the plasma by the probe is on the order of

$$E_p \approx T_e / e\lambda_D \approx 240 \text{ V/cm}, \quad (15)$$

for the example of the plasma characteristics given above. Since this is about seven times greater than the typical rf field, the rf field is a relatively small perturbation on the electron orbits near the probe.

The characteristic time during which electrons are affected by the probe is the plasma period, $2\pi/\omega_p$. Eq. (11) shows that this time is short compared to the period by the rf field, which is $2\pi/\omega$.

Consequently, the rf field does not affect an electron orbit during the time the electron is being influenced by the probe. The resulting probe curves are the same as would be obtained in the same plasma without any rf field, except for being smoothed over a range.

$$\Delta V \approx E\lambda_D \approx 1 \text{ volt}. \quad (16)$$

The characteristic voltage for significant changes in the probe curve is the electron temperature, $T_e \approx 10 \text{ eV}$, so that the "rf smoothing" has relatively little effect on the probe curve.

Insulating walls and other objects drawing zero net current from the plasma are charged to a negative potential, called the floating potential.

$$V_f \approx - \frac{T_e}{e} \frac{1}{2} \ln (m_+/m_-), \quad (17)$$

where T_e is the electron temperature in eV, m_+ is the ion mass, and e and m_- are the charge and mass of the electron. (The term "temperature" is used

merely to denote the average electron energy, and does not necessarily imply a Boltzmann distribution, although Eq. (17) is most accurate for a Boltzmann distribution.

The floating potential given by Eq. (17) is not measured with respect to ground potential but instead with respect to the potential of the nearby plasma, called "space potential" or "plasma potential." In most plasmas, space potential is close to ground potential, and floating potential, when measured with respect to ground, is given by Eq. (17).

In this plasma, however, space potential is high, and floating potential, although properly negative with respect to space potential, is positive with respect to ground.

Space potential is usually very close to the potential of the most positive electrode exposed to the plasma. The high positive space potential results from the lack of a good reference electrode, and is easily modified by any apparatus which tends to supply such a reference. Consequently, plasma experiments must be conducted and interpreted carefully.

Figure 4-B.10 shows one of our first Langmuir probe curves, recorded in nitrogen plasma using a planchet as the probe. This has the usual feature of plasma probe curves, and we use it to illustrate both the standard interpretation and some of the dangers. At the lowest voltages there is a nearly constant positive current, called the ion saturation current, labeled (1) on the plot.

At (2) on the probe curve the positive current starts to decrease as a few of the most energetic electrons get through to the probe surface. The zero current point (3), is floating potential, here at 70 V above ground. The discontinuity in the curve just above floating potential is due to a change of instrument scale.

At (4) on the curve, the electron current is rising rapidly as the probe approaches space potential and more electrons can overcome the repulsive potential barrier. At space potential (5), all electrons can reach the probe, and the curve flattens somewhat, the continuing increase being due to the slow growth of the region from which the probe attracts electrons. At (7) the probe voltage is so high that the probe is causing breakdown, and the current increases rapidly again.

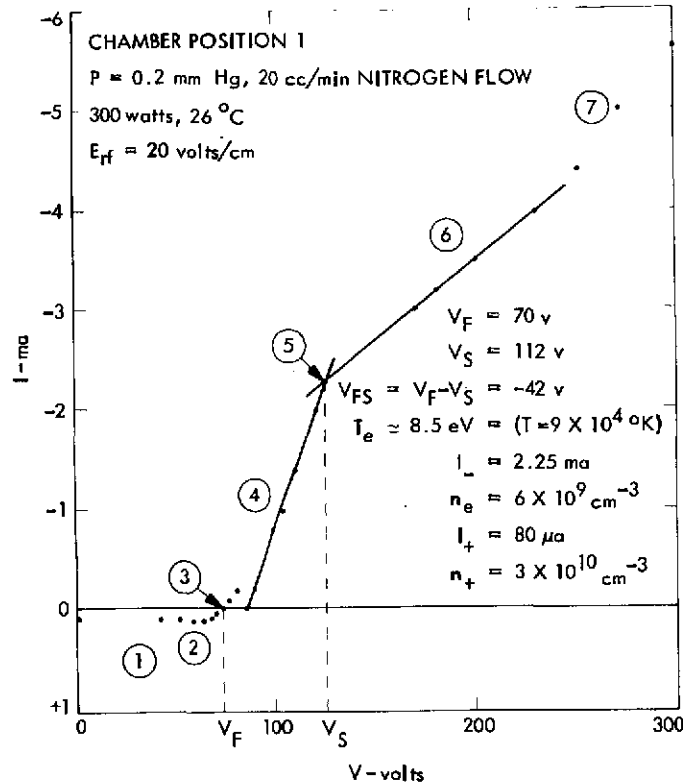


Fig. 4-B.10. Nitrogen plasma probe curve

Knowing space potential and floating potential, we can obtain T_e from Eq. (17). The current at space potential then gives the electron density as $n_e \approx 6 \times 10^9 \text{ cm}^{-3}$.

But these results from Fig. 4-B.10 can only be correct if there is a high density of negative ions ($\approx 2.4 \times 10^{10} \text{ cm}^{-3}$) in the nitrogen plasma. The ratio of ion saturation current to electron saturation current should just be $(m_-/m_+)^{1/2}$ (Ref. 3). The ion current in Fig. 4-B.10 is much larger than would be expected from the electron saturation current. Either there is actually a large difference between the electron density and the ion density, with space charge balanced by negative ions (which is possible in nitrogen), or else the data in Fig. 4-B.10 is distorted.

One common form of distortion is using too large a probe, which draws so much current that the plasma is depleted. Figure 4-B.11 shows another early probe curve, in helium, which is a clear example of this artificial saturation. Again, the ratio of ion saturation current to electron

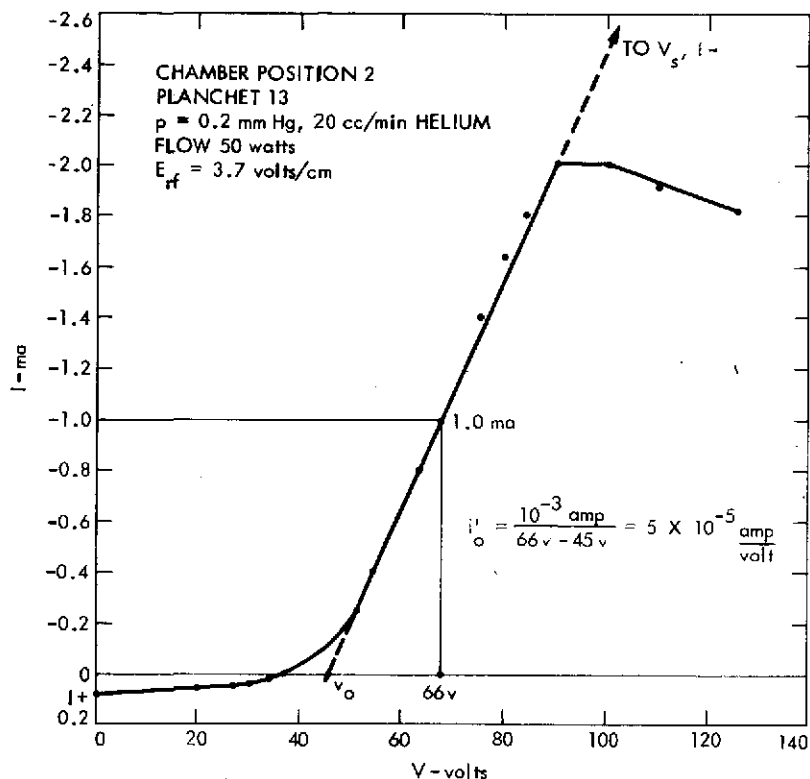


Fig. 4-B. 11. Helium plasma probe curve

saturation current is surprisingly large. As in several other probe curves using planchets for probes, the electron saturation is extremely flat, even decreasing somewhat. What is really happening was learned by monitoring the floating potential on another nearby probe while recording this data. Variations in floating potential simply follow equal variations in the space potential. Correcting the voltages in Fig. 4-B. 11 for these space potential variations shows that, at the higher probe voltages, the plasma potential is following the probe potential, and the voltage difference between the plasma and the probe changes very little when the probe voltage changes. This implies that the probe must be the best reference electrode available to the plasma. Consequently, probe curves like Fig. 4-B. 10 may be misleading, and those like Fig. 4-B. 11 are definitely wrong.

To obtain useful information from Fig. 4-B. 11 we use the fact, mentioned above, that electron and ion saturation currents to a probe differ by the square root of the mass ratio. This is based on a subtle phenomenon

observed by D. Bohm, and known as the "Bohm criterion" (Ref. 3). The result of the Bohm criterion is that ion current to a probe is given by the plasma density times the ion thermal speed calculated at the electron temperature (not the ion temperature, which is probably only on the order of 10^3 °K). Thus the electron current at the knee should be

$$I_- = (m_+/m_-)^{1/2} I_+ \quad (18)$$

in helium, with $(m_+/m_-)^{1/2} = 86$, the knee of Fig. 4-B.11 should be at $I_- \approx 6.9$ ma, which is off the graph.

The lower, linearly rising, part of the probe curve in Fig. 4-B.11 is not distorted and can be used to extrapolate to the correct space potential. Let I_o' be the slope of that part of the curve, and let V_o be the intercept of the continued straight line with the zero current axis (see Fig. 4-B.11). The electron saturation current is

$$I_- = I_o' * (V_s - V_o) , \quad (19)$$

Using Eqs. (18) and (19) the true knee is at a space potential of

$$V_s = V_o + \left(\frac{m_+}{m_-} \right)^{1/2} I_+ / I_o' . \quad (20)$$

From probe theory (Ref. 3), floating potential differs from space potential by

$$V_s - V_f = \ln (m_+/m_-) (kT_-/e) , \quad (21)$$

which determines the electron temperature,

$$\frac{kT_-}{e} = \frac{(V_s - V_f)}{1/2 \ln (m_+/m_-)} . \quad (22)$$

With the electron temperature and either the electron or the ion saturation current we can determine the plasma density

$$n = 6 \times 10^{18} I_- / A_p v_- \text{ cm}^{-3} \quad (23)$$

where A_p is the probe area and

$$v_- = 6 \times 10^7 (kT_-)^{1/2} \text{ cm/sec}, \quad (24)$$

where kT_- is in electron volts.

Carrying through this procedure for Fig. 4-B.11, we find

$$kT_- \equiv T_e = 22 \text{ eV},$$

and

$$n = 2 \times 10^7 \text{ cm}^{-3}. \quad (25)$$

These results are obtained from parts of the probe curve which show no sign of distortion, and, so far as we know, the data is reliable. The extrapolation to floating potential along a straight line, however, is not very accurate, since the correct probe curve would not be straight. The error is almost certainly less than 50%.

The above discussion shows the problems involved using large probes in this plasma. Small probes would draw less current, and might not drive the plasma potential, thus avoiding the artificial saturation. A series of development tests and diagnostic runs have been made with small probes. The probe curves are collected in Fig. 12 through 17. The small probe revealed a new problem. Since a small probe is driven to higher voltages than a large probe without depleting the plasma, it can, and does, increase the plasma ionization. Consequently, small probe curves have no distinguishable knee, but instead show a continuous current increase right up to breakdown. The small probe curves are reduced by the extrapolation technique given in Eqs (19) through (24). With this technique there are no great differences between

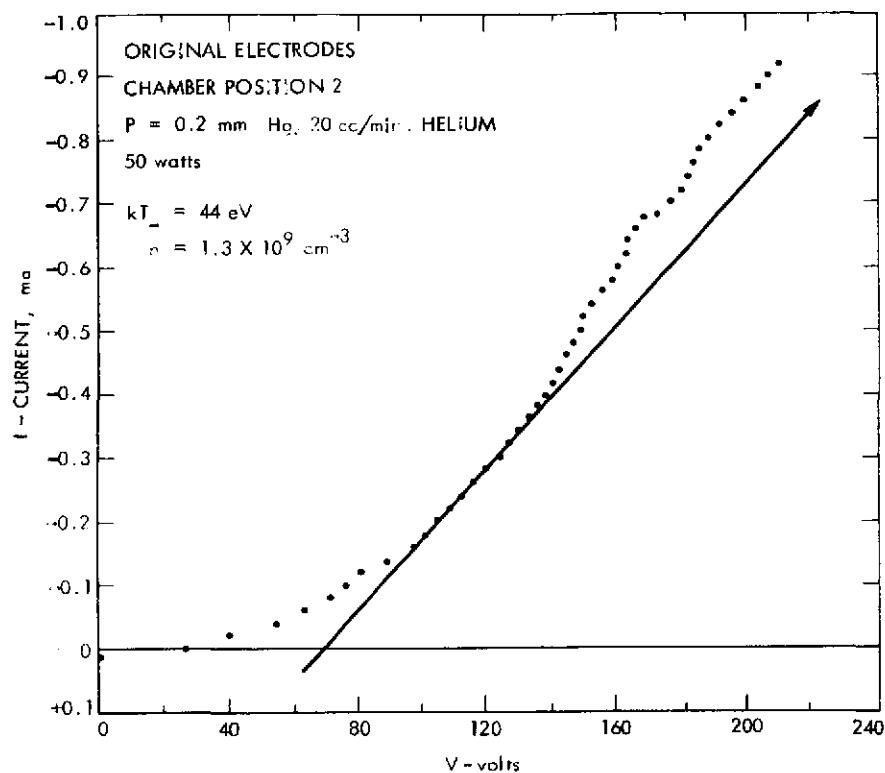


Fig. 4-B.12. Helium plasma probe curve

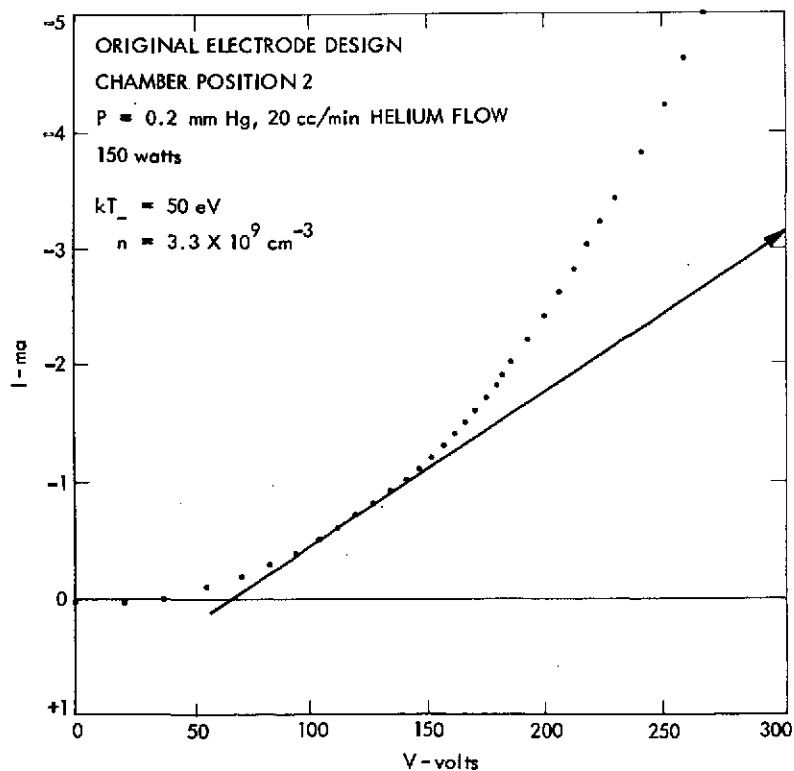


Fig. 4-B.13. Helium plasma probe curve

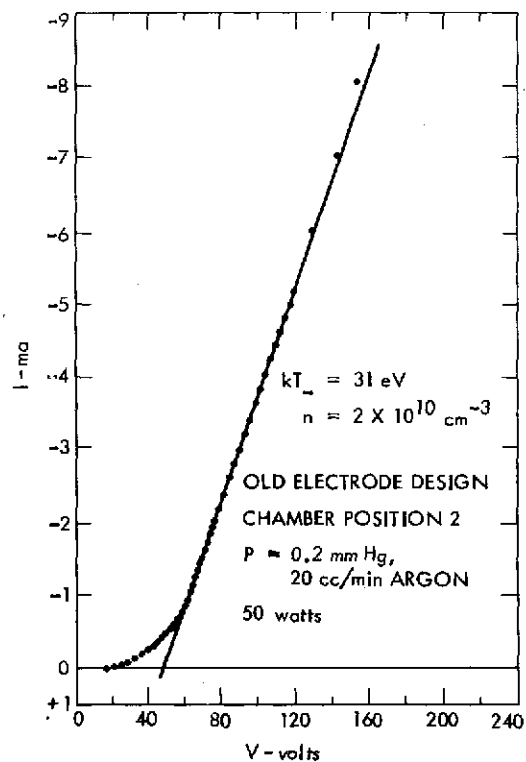


Fig. 4-B. 14. Argon plasma probe curve

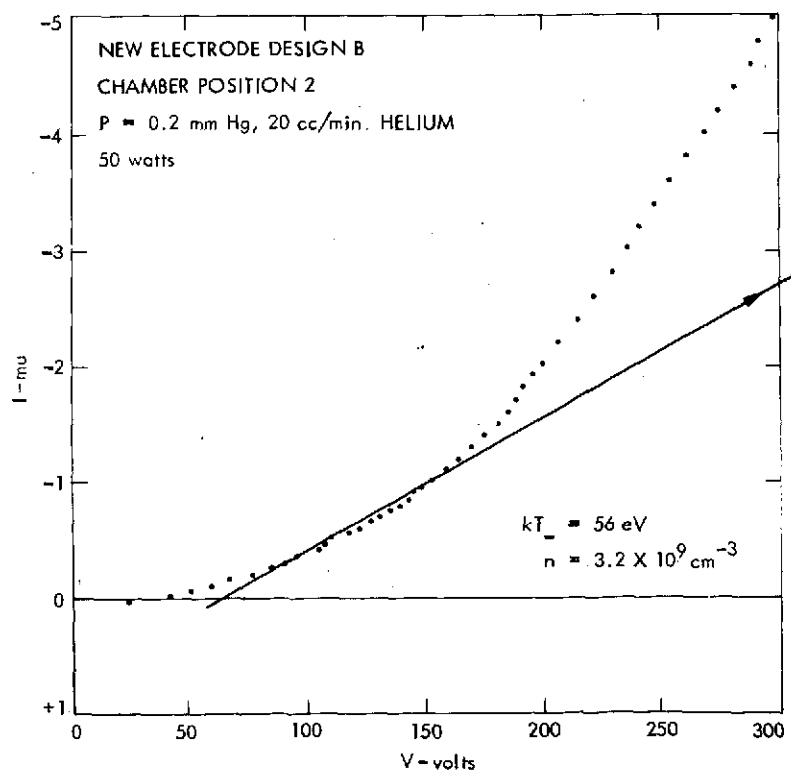


Fig. 4-B. 15. Helium plasma probe curve

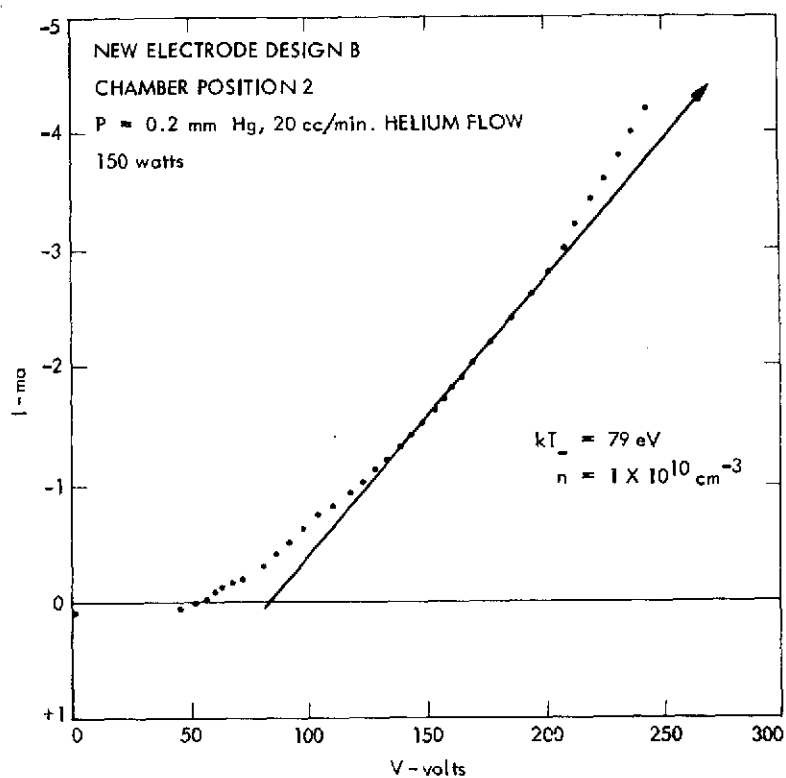


Fig. 4-B.16. Helium plasma probe curve

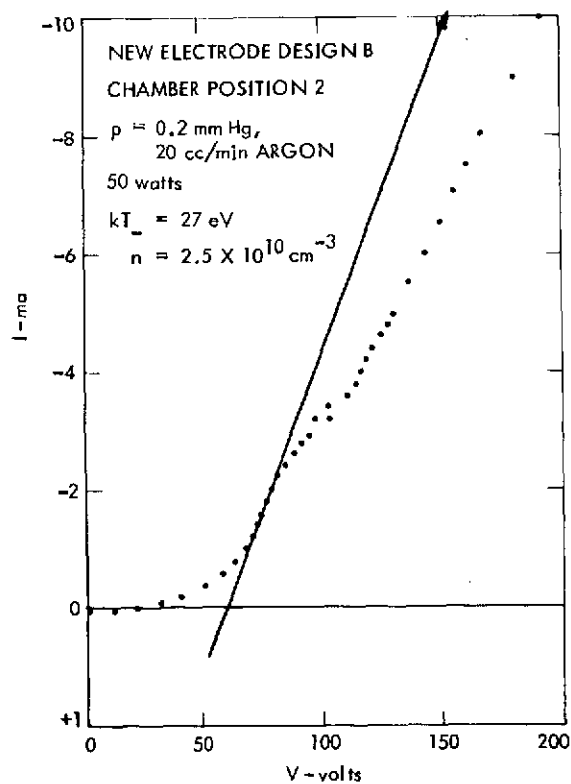


Fig. 4-B.17. Argon plasma probe curve

using small probes and large probes, except that the extrapolation is easier with large, flat probes.

4.2.3.5 Task 5 - Electrode Placement and Design. Percent spore survival calculations for organisms exposed to helium plasma generated by Modification A electrodes is presented in Table 4-B.14. Spore reduction was noted at even the lowest power of 10 watts. Although it is difficult to compare lethality due to this modification with lethality of the original electrode placement, this type of configuration (A) may provide a means of sterilizing at lower powers than so far envisioned.

A comparison of the calculations of percent spore survival for Modification B electrodes with the original electrodes (Phase I) are shown in Table 4-B.15. The most apparent improvement in plasma lethality, i.e., spore death, is seen with 50 watts for both helium and argon. The new electrode design accounted for a two log reduction in spore survival.

In addition to spore survival analyses, Langmuir probe measurements were made during each of the tests (see Figs. 4-B.12, 4-B.14, 4-B.15 and 4-B.17). Calculations, obtained from these plots for electron temperature and plasma density, are compared in Table 4-B.16. In addition, spore survival percentages are included.

Table 4-B.14. Mean Percent Survival of Bacillus subtilis Spores in Helium Plasma^a

RF Power, Watts	Chamber Position		
	1	2	3
10	0.217 ^b	0.314	0.134
50	0.049	0.019	0.008
^a 20 cc per minute, 0.2 mm Hg pressure, 15 minutes exposure ^b Mean of 8 replicates			

Table 4-B.15. Mean Percent Survival of Bacillus subtilis Spores in Plasma^a

Plasma Gas, 20 cc/Minute	RF Power Watts	Electrode Configuration	
		Phase I	Modification B
Argon	50	3.877 ^b	0.043
	150	0.049	0.077
Helium	50	22.143	0.160
	150	0.031	0.017
^a 15 minutes exposure, 0.2 mm Hg pressure, Position 2 ^b Mean of 6 replicates			

In the case of helium plasma, the increase in spore lethality may be explained by an increase in electron temperature of 44 eV to 56 eV. However, the same ease of interpretation is not noted for the argon data. Calculations show apparent physical similarities in the two plasmas produced by the two electrode designs, but dissimilarities in spore survival. Also, visual observation of the appearance of the two plasmas detected a readily noted difference. The color of the plasma produced with electrode Modification B was more intense and extended much further down into the chamber. The inability of the Langmuir probe measurements to detect this apparent difference for argon plasma is as yet unaccounted for.

4.2.4 Summary and Conclusions

The following preliminary conclusions of Phase II have been reached based on the data available to date. In some cases these conclusions must be substantiated during the remainder of the program.

- 1) Microorganisms are killed by plasma gas. Death rates vary between microbial types.

- 2) Energetic ultraviolet radiation appears to be the primary kill mechanism (with the possible exception of oxygen) which causes disruption of the physical integrity of the cell.
- 3) Helium gas, or a combination of helium and argon, yield plasmas which are the most efficient for sterilization.
- 4) Plasma density and electron temperature measurements were developed that provide plasma diagnostics for comparison with microbial kill data.
- 5) Modification of equipment electrodes improved the ionization of gases, i. e., increased the plasma density, which increased organism death.

4.2.5 Future Activities

Efforts will be primarily directed towards ascertaining spacecraft materials and plasma compatibility and determining the effectiveness of plasma gas for sterilizing surfaces of various configurations. The program approach will result in data applicable for use in development of preliminary design concepts for plasma sterilizers for space or terrestrial applications.

4.2.6 References

1. E. W. MCDaniel in "Collision Phenomena in Ionized Gases," John Wiley, 1964, p. 115.
2. I. Langmuir and H. Mott Smith, Gen. Elec. Review 27, 449, 538, 616, 762, 810 (1924).
3. D. Bohm, E.H.S. Burhop, and H. S.W. Massey, in A. Guthrie and R. K. Wakerling, Eds., "The Characteristics of Electrical Discharge in Magnetic Fields," NNES, Div. 1, Vol. 5, McGraw-Hill Book Co., Inc., 1949, p. 13.
4. J. E. Allen, R.L.F. Boyd, and P. Reynolds, Pro. Phys. London, B70, 297 (1953).
5. D. B. Bernstein and I. N. Rabinowitz, Phys. Fluids 2, 112 (1959).

Table 4-B.16. Comparison of Plasma Environment with Spore Survival^a

Plasma Gas	RF Power Watts	Original Electrode Design			New Electrode Design (B)		
		Mean % Survivors	Electron Temp.	Plasma Density	Mean % Survivors	Electron Temp.	Plasma Density
Argon	50	3.88 ^b	31 eV ^c	$2 \times 10^{10} \text{ cm}^{-3}$	0.04	27 eV	$2.5 \times 10^{10} \text{ cm}^{-3}$
Helium	50	22.14	44 eV	$1.3 \times 10^9 \text{ cm}^{-3}$	0.16	56 eV	$3.2 \times 10^9 \text{ cm}^{-3}$
^a 0.2 mm Hg pressure, 20 cc/min. gas flow, 15 minute exposure, Position 2 ^b Mean of 6 replicates ^c Extrapolation of Langmuir probe measurements							

SECTION V

PLANETARY QUARANTINE LABORATORY - RESEARCH ACTIVITIES
(NASA No. 193-58-63-06)

Contents

Subtask A
para. 5.1

Title and Related Personnel

TEFLON RIBBON EXPERIMENTS

Cognizance: J. R. Puelo

Associate
Personnel: G. Oxborrow
N. Fields
S. Lindsey

5.1 TEFLON RIBBON EXPERIMENTS

5.1.1 Subtask A Introduction

The objective of this study is to characterize the thermal resistance profiles of naturally occurring bacterial spores associated with assembly facilities at Kennedy Space Center.

The validity of the currently accepted sterilization cycle should be confirmed. The cycle, to be valid, should be effective against bacterial spores associated with spacecraft in residence at Kennedy Space Center, Florida.

5.1.2 Significant Accomplishments

5.1.2.1 Results. The details of the thermal apparatus and experimental test procedures were described in para. 5.1.2.1 of Jet Propulsion Laboratory (JPL) Doc. No. 900-655, April 1974. Naturally occurring airborne bacterial spores were collected on Teflon ribbons exposed to the intramural environment of the Vehicle Assembly Building (VAB), Kennedy Space Center (KSC), Florida. Table 5-A.1 shows the results obtained when the spores were subjected to a water concentration of 0.01 mg/liter (R.H. 0.001%) at the 113°C high thermal inertia cycle. With the exception of five experiments, heat survivors were recovered from all thermal experiments. The initial spore concentration (N_0) for twenty-eight experiments were found to be 10^3 spores per teflon ribbon. In four experiments, the N_0 was 10^4 , and in one experiment, the N_0 dropped to a spore concentration of 10^2 .

In each mixed spore population there exists a number of spores with varying thermal resistance. To measure this portion of the population, a "Survivor Fraction" of the hardest spores was derived. The "Survivor Fraction" is the total number of "hardy" organisms surviving a sterilization cycle, N_H , divided by the total initial population N_0 , (i.e. N_H/N_0). In short, the "Survivor Fraction" is the ratio of the Most Probable Numbers (MPN) per Teflon ribbon number to the N_0 per Teflon ribbon number. The data show that this fraction was 10^{-5} for this set of experiments.

Table 5-A.2 shows the results when the overall water concentration in the oven was increased to 1.2 mg/liter (R.H. 0.133%) at the 113°C high thermal

Table 5-A.1. Thermal Resistance of Spores Collected on Teflon Ribbons — VAB — KSC

TEMP. 113°C

0.01 mg/Liter water

Experiment number	N ₀ spores	Positive/Total	MPN for ribbon	Survivor Fraction N _H /N ₀
4	6.4 × 10 ³	4/24	0.182	2.9 × 10 ⁻⁵
5	4.5 × 10 ³	5/24	0.234	5.2 × 10 ⁻⁵
6	6.1 × 10 ³	5/24	0.234	3.8 × 10 ⁻⁵
7	7.3 × 10 ³	3/24	0.134	2.7 × 10 ⁻⁵
8	3.0 × 10 ³	0/24	0.00	0
9	4.7 × 10 ³	0/24	0.00	0
10	7.5 × 10 ²	0/24	0.00	0
11	1.3 × 10 ³	1/24	0.042	3.1 × 10 ⁻⁵
12	2.2 × 10 ³	4/24	0.182	8.3 × 10 ⁻⁵
13	3.8 × 10 ³	5/24	0.234	6.2 × 10 ⁻⁵
14	1.4 × 10 ³	0/24	0.00	0
15	1.7 × 10 ³	4/24	0.182	1.1 × 10 ⁻⁴
16	2.2 × 10 ³	6/24	0.287	1.3 × 10 ⁻⁴
17	3.5 × 10 ³	7/24	0.345	9.7 × 10 ⁻⁵
18	1.4 × 10 ⁴	4/24	0.182	1.3 × 10 ⁻⁵
19	7.5 × 10 ³	7/24	0.345	4.6 × 10 ⁻⁵
20	1.1 × 10 ⁴	1/24	0.042	3.8 × 10 ⁻⁶
21	7.6 × 10 ³	4/24	0.182	2.4 × 10 ⁻⁵
22	7.6 × 10 ³	0/24	0.0	0
23	3.4 × 10 ³	1/24	0.042	1.2 × 10 ⁻⁵
24	6.2 × 10 ³	4/24	0.182	2.9 × 10 ⁻⁵
25	4.6 × 10 ³	8/24	0.406	8.9 × 10 ⁻⁵
26	2.2 × 10 ³	2/24	0.087	3.9 × 10 ⁻⁵
27	7.2 × 10 ³	4/24	0.182	2.5 × 10 ⁻⁵
28	7.5 × 10 ³	7/24	0.345	4.6 × 10 ⁻⁵
29	5.5 × 10 ³	4/24	0.182	3.3 × 10 ⁻⁵
30	5.4 × 10 ³	3/12	0.287	5.3 × 10 ⁻⁵
31	3.4 × 10 ³	3/12	0.287	8.5 × 10 ⁻⁵
32	6.7 × 10 ³	3/12	0.287	4.3 × 10 ⁻⁵
33	5.7 × 10 ³	2/12	0.182	3.2 × 10 ⁻⁵
35	4.8 × 10 ³	4/12	0.406	8.5 × 10 ⁻⁵
37	2.6 × 10 ³	2/24	0.087	3.3 × 10 ⁻⁵
39	1.0 × 10 ⁴	19/24	1.569	1.5 × 10 ⁻⁴

Table 5-A.2. Thermal Resistance of Spores Collected
on Teflon Ribbons - VAB - KSC

TEMP. 113 C
1.2 mg/Liter water

Experiment number	N ₀ spores	Positive/Total	MPN for ribbon	Survivor Fraction N _H /N ₀
49	3.5 × 10 ³	11/24	0.613	1.8 × 10 ⁻⁴
50	2.0 × 10 ³	10/24	0.539	2.7 × 10 ⁻⁴
51	3.0 × 10 ³	8/24	0.406	1.4 × 10 ⁻⁴
52	2.4 × 10 ³	9/24	0.470	2.0 × 10 ⁻⁴
53	1.6 × 10 ³	2/24	0.087	5.3 × 10 ⁻⁵
56	1.7 × 10 ³	7/24	0.345	2.0 × 10 ⁻⁴
58	5.2 × 10 ³	8/24	0.406	7.8 × 10 ⁻⁵
59	4.9 × 10 ³	9/24	0.470	9.5 × 10 ⁻⁵
60	5.9 × 10 ³	8/24	0.406	6.9 × 10 ⁻⁵

Table 5-A.3. Thermal Resistance of Spores Collected
on Teflon Ribbons - VAB - KSC

TEMP. 111.7 C
1.2 mg/Liter water

Experiment number	N ₀ spores	Positive/Total	MPN for ribbon	Survivor Fraction N _H /N ₀
41	6.0 × 10 ³	23/24	3.179	5.3 × 10 ⁻⁴
42	5.5 × 10 ³	24/24	∞	—
43	4.9 × 10 ³	22/24	2.485	5.1 × 10 ⁻⁴
45	6.8 × 10 ³	21/24	2.080	3.1 × 10 ⁻⁴
46	2.3 × 10 ³	6/24	0.288	1.3 × 10 ⁻⁴
54	1.8 × 10 ³	7/24	0.345	1.9 × 10 ⁻⁴
55	3.8 × 10 ³	12/24	0.693	1.8 × 10 ⁻⁴
61	9.8 × 10 ³	12/23	0.651	6.6 × 10 ⁻⁵
62	3.3 × 10 ³	4/24	0.182	5.6 × 10 ⁻⁵
63	1.3 × 10 ⁴	10/24	0.539	4.3 × 10 ⁻⁵

inertia cycle. Survivors were recovered from all nine thermal experiments. The data show that at these experimental conditions, the survivor fraction was 10^{-4} .

Table 5-A.3 shows the results when the Teflon ribbons were subjected to a water concentration of 1.2 mg/liter and the 111.7°C high thermal inertia cycle. A maximum temperature of 111.7°C was used because this will be a more realistic temperature the spacecraft will be exposed to during final sterilization. An increase in the number of thermal survivors were noted under these experimental conditions than were obtained using the same water concentration (1.2 mg/liter) but a higher oven temperature (Table 5-A.2). This effect was reflected in higher MPN.

A summary of all the Teflon ribbon experiments completed to date at the varying water concentrations and temperatures of 111.7°C and 113°C is shown in Table 5-A.4. A comparison of the results obtained in the thermal experiments performed under identical conditions, i. e. same water content and temperature, in the Manned Spacecraft Operations Building (MSOB) and the VAB, revealed a larger survivor fraction in the MSOB experiments but higher MPN values in the VAB experiments.

Teflon ribbon experiments were conducted in the Spacecraft Assembly Facility (SAF) clean room at JPL, Pasadena, California. No heat survivors were recovered from these thermal experiments. The Teflon ribbons were subjected to the same experimental conditions (i. e. temperature 113°C, 1.2 mg/liter water) as those experiments conducted at KSC. Low levels of spore concentrations (low 10^2) found on the Teflon ribbons might have been a factor. Heat survivors were isolated and identified. With the exception of two Teflon ribbons, the survivors from each positive ribbon were found to be the same species.

Three isolates, each with a different series of biochemical test reactions, were recovered from one of the Teflon ribbons after exposure to the thermal sterilization cycle of 113°C and a water content of 0.01 mg/liter. Two organisms recovered from the second ribbon, had the same biochemical test reactions and were identified by the computer as the same Bacillus species. These organisms were separated solely on the basis of morphology and growth characteristics on solid media.

Table 5-A.4. Summary of Thermal Teflon Ribbon Experiments
Conducted in MSOB and VAB

Number of experiments	Location	Temperature C°	Water concentration mg/Liter	Total Teflon ribbons	MPN	Survivor Fraction
18	MSOB	113	0.01	431	0.017	1.2×10^{-4}
11	MSOB	113	1.2	262	0.109	3.5×10^{-4}
5	MSOB	113	2.4	60	0.105	1.6×10^{-3}
33	VAB	113	0.01	732	0.189	3.7×10^{-5}
9	VAB	113	1.2	216	0.406	1.4×10^{-4}
3	VAB	113	2.4	36	1.500	1.9×10^{-4}
10	VAB	111.7	1.2	239	0.882	1.6×10^{-4}
1	VAB	111.7	2.4	24	∞	-

Table 5-A.5. Biochemical Test Reactions of Heat-Stressed
Environmental IsolatesTEMP. 113°C
0.01 mg/Liter water

Organism	No. of Isolates	Mannitol	Tyrosine	Phenylalanine	Casein	Starch	Voges-Proskauer	Citrate	Nitrate	Anaerobic Growth
<u>B. brevis</u>	2	-	-	-	+	-	-	-	-	-
	9	-	-	-	-	-	-	-	+	-
<u>B. circulans</u>	1	-	-	-	-	+	-	-	-	+
<u>B. lentus</u>	48	-	-	-	-	+	-	-	-	-
	4	+	-	-	-	+	-	-	+	-
	2	+	-	-	-	+	-	-	-	-
	1	+	-	-	+	+	-	-	-	-
	1	+	-	-	-	-	-	-	-	-
	1	+	-	-	-	-	-	-	-	-
<u>B. sphaericus</u>	4	-	-	+	-	-	-	-	-	-
Atypical Bacilli	2	-	-	-	+	+	-	-	-	-
	41	-	-	-	-	-	-	-	-	-
	12	-	-	-	-	+	-	-	+	-
	3	-	-	-	-	-	-	-	-	+

Although only five Bacillus species were isolated and identified, variations in biochemical tests within a species did occur. These distinct test sequences are characterized in Table 5-A.5. The number of isolates and frequency of isolation of each species is listed below:

<u>Organism</u>	<u>Number of isolates</u>	<u>Percent</u>
<u>B. brevis</u>	11	8.5
<u>B. circulans</u>	1	0.7
<u>B. lentus</u>	56	43.1
<u>B. sphaericus</u>	4	3.1
Atypical bacilli	58	44.6
Total	130	

A larger number of Bacillus species with a greater number of positive biochemical test reactions were isolated when the maximum temperature attained was 111.7°C and the water content was increased to 1.2 mg/liter. Because of the increase in the number of survivors obtained at the above experimental conditions, including a significant increase in the number of multiple isolates, only selected isolates were picked for identification. These isolates and their biochemical test reactions are shown in Table 5-A.6. The total number of each species identified and its frequency of isolation is listed below:

<u>Organism</u>	<u>Number</u>	<u>Percent</u>
<u>B. brevis</u>	1	2.2
<u>B. circulans</u>	1	2.2
<u>B. coagulans</u>	9	19.5
<u>B. lentus</u>	25	54.4
<u>B. pumilus</u>	1	2.2
Atypical bacilli	9	19.5
Total	46	

A total of 732 Teflon ribbons, exposed to airborne microbial fallout and subsequently exposed to the thermal sterilization cycle previously described, yielded 130 heat-stressed survivors (Table 5-A.5). The maximum temperature attained on this profile was 113°C, and the water content was at a level of 0.01 mg/liter. All of these organisms were identified by computer and classified in

Table 5-A.6. Biochemical Test Reactions of Heat-Stressed Environmental Isolates

TEMP. 111.7°C
1.2 mg/Liter water

Organism	No. of Isolates	Mannitol	Tyrosine	Phenylalanine	Casein	Starch	Voges- Proskauer	Citrate	Nitrate	Anaerobic Growth
<u>B. brevis</u>	1	-	-	-	-	-	-	-	+	-
<u>B. circulans</u>	1	+	-	-	-	+	+	-	-	+
<u>B. coagulans</u>	5	-	-	-	-	-	+	-	-	-
	3	-	-	-	-	+	+	-	-	-
	1	-	-	-	-	+	+	-	+	-
<u>B. lentus</u>	4	+	-	-	-	+	-	-	-	-
	19	-	-	-	-	+	-	-	-	-
	1	+	-	-	-	-	-	-	-	-
	1	+	-	-	-	+	+	-	-	-
<u>B. pumilus</u>	1	+	-	-	+	-	+	-	-	-
Atypical Bacilli	1	+	-	-	-	-	-	-	+	-
	6	-	-	-	-	-	-	-	-	-
	2	+	-	-	-	-	+	-	-	-

one of five groups. The majority of these organisms had only one positive test reaction. A few exceptions did occur with as many as three positive reactions being recorded. Only four isolates were capable of growing anaerobically.

Those organisms exposed to a lower temperature (111.7°C) and a higher water content (1.2 mg/liter) revealed a greater diversity of identifiable species. The frequency of isolation of organisms classified as Atypical bacilli decreased significantly while those classified as B. lentus increased (Table 5-A.6). It is interesting to note at this point that almost one-third of the organisms identified produced acetyl-methyl-carbinol for a positive Voges-Proskauer (VP) test; and only one species was capable of anaerobic growth.

5.1.3 Future Activities

Future activities relative to these studies are to develop thermal death curves using different temperatures, water concentrations, and variations in duration of thermal exposure; to complete environmental airborne fallout studies at JPL, Pasadena, California and Martin-Marietta Aerospace, Denver, Colorado in order to determine if spore population concentration and thermal resistance are similar to those found at KSC, Florida; and to complete cooperative Teflon ribbon studies with Hardin-Simmons University. Additionally there will be increased activity in the effort to develop rapid and reproducible methods for computer identification of microorganisms using pyrolysis-gas-liquid chromatographic methods.

5.1.4 Presentations

Puleo, J. R., "Teflon Ribbon Experiments," presented at NASA Spacecraft Sterilization Technology Seminar, San Francisco, California, February 1974.

Puleo, J. R., "Review of Hardy Organisms" Results, Factors of Temperature and Humidity, presented to AIBS Planetary Quarantine Panel, Denver, Colorado, July 1974.